Applied Catalysis B: Environmental 194 (2016) 169–201

Contents lists available at ScienceDirect

Applied Catalysis B: Environmental

journal homepage: www.elsevier.com/locate/apcatb

Review

Generation of sulfate radical through heterogeneous catalysis for organic contaminants removal: Current development, challenges and prospects

Wen-Da Oh[a,b], Zhili Dong[a,c], Teik-Thye Lim[a,b,*]

[a] Nanyang Environment and Water Research Institute (NEWRI), Interdisciplinary Graduate School (IGS), Nanyang Technological University, 1 Cleantech Loop, CleanTech One, Singapore 637141, Singapore
[b] Division of Environmental and Water Resources Engineering, School of Civil and Environmental Engineering, Nanyang Technological University, 50 Nanyang Avenue, Singapore 639798, Singapore
[c] School of Materials Science and Engineering, Nanyang Technological University, 50 Nanyang Avenue, Singapore 639798, Singapore

ARTICLE INFO

Article history:
Received 16 January 2016
Received in revised form 1 April 2016
Accepted 3 April 2016
Available online 16 April 2016

Keywords:
Peroxymonosulfate
Heterogeneous catalysts
Sulfate radical
Hydroxyl radical
Persulfate

ABSTRACT

Sulfate radical-based advanced oxidation processes (SR-AOPs) employing heterogeneous catalysts to generate sulfate radical ($SO_4^{\bullet-}$) from peroxymonosulfate (PMS) and persulfate (PS) have been extensively employed for organic contaminant removal in water. This article aims to provide a state–of–the–art review on the recent development in heterogeneous catalysts including single metal, mixed metal, and nonmetal carbon catalysts for organic contaminants removal, with particular focus on PMS activation. The hybrid heterogeneous catalyst/PMS systems integrated with other advanced oxidation technologies is also discussed. Several strategies for the identification of principal reactive radicals in $SO_4^{\bullet-}$–oxidation systems are evaluated, namely (i) use of chemical probe or spin trapping agent coupled with analytical tools, and (ii) competitive kinetic approach using selective radical scavengers. The main challenges and mitigation strategies pertinent to the SR-AOPs are identified, which include (i) possible formation of oxyanions and disinfection byproducts, and (ii) dealing with sulfate produced and residual PMS. Potential future applications and research direction of SR-AOPs are proposed. These include (i) novel reactor design for heterogeneous catalytic system based on batch or continuous flow (e.g. completely mixed or plug flow) reactor configuration with catalyst recovery, and (ii) catalytic ceramic membrane incorporating SR-AOPs.

Contents

Abbreviations: AC, activated carbon; ACF, activated carbon fiber; CNT, carbon nanotube; DMPO, 5,5-dimethyl-1-pyrroline N-oxide; DMSO, dimethyl sulfoxide; DOM, dissolved organic matter; ESR, electron spin resonance; EtOH, ethanol; GO, graphene oxide; HDBP, halogenated disinfection byproduct; MeOH, methanol; MW, microwave; NB, nitrobenzene; NHE, normal hydrogen electrode; OMS, octahedral molecular sieves; PMS, peroxymonosulfate; PS, persulfate; rGO, reduced graphene oxide; SR-AOPs, sulfate radical-based advanced oxidation processese; $SO_4^{\bullet-}$, sulfate radical; TBA, tert-butyl alcohol; US, ultrasonic; ZVI, zero valent iron; 4-NB, 4-nitrobenzoic; $^{\bullet}OH$, hydroxyl radical.

* Corresponding author at: Nanyang Environment and Water Research Institute (NEWRI), Interdisciplinary Graduate School (IGS), Nanyang Technological University, 1 Cleantech Loop, CleanTech One, Singapore, 637141, Singapore. Tel.: +65 6790 6933; fax: +65 6791 0676.
E-mail address: cttlim@ntu.edu.sg (T.-T. Lim).

http://dx.doi.org/10.1016/j.apcatb.2016.04.003
0926-3373/

1. Introduction

In recent decades, environmental pollution by recalcitrant organics is increasingly becoming a challenging multidisciplinary problem as new chemicals are being introduced continuously into the environment. Water pollution due to recalcitrant organics particularly those classified as emerging contaminants (e.g. pharmaceuticals and their metabolites, endocrine disruptors, disinfection by-products, personal care products and illicit drugs) could lead to serious ecological impacts [1–3]. Many recalcitrant organics are toxic, biorefractory and difficult to be removed by the conventional treatment methods [4]. As such, advanced treatment techniques with chemical oxidation that offer remarkable treatment efficiency are highly desired.

Sulfate radical-based advanced oxidation processes (SR-AOPs) are increasingly gaining attention as effective solution to the destruction of recalcitrant organics in water. The SR-AOPs utilize highly–reactive sulfate radical ($SO_4^{\bullet-}$) to oxidize organic contaminants to innocuous CO_2 and H_2O. Recent studies have showed that SR-AOPs are effective in removing various types of recalcitrant contaminants such as volatile organic compounds [5,6], endocrine disruptors [7], pharmaceuticals and their metabolites [8,9], cyanotoxins [10,11] and perfluorinated compounds [12] in water. The SR-AOPs are also effective in many other applications including disintegration of activated sludge [13], disinfection [14] and decontamination of pool water [15].

Most commonly, $SO_4^{\bullet-}$ is generated *via* peroxymonosulfate (PMS) or persulfate (PS) activation. Various activation methods have been proposed which include the use of heat [16], chemicals [17,18], base [19], UV [20], transition metals [21–23] and ultrasound [24]. The transition metal activation method is less complex in reactor/system configuration and more economical compared to the energy-based activation methods (e.g. ultrasound, UV and heat etc.). The transition metal activation of PMS and PS can be achieved in the homogeneous and heterogeneous systems. The heterogeneous system is advantageous over the homogeneous system because (i) the solid heterogeneous catalyst can be easily separated from the treated water for reuse, (ii) secondary treatment to remove dissolved metals from the treated water is not required, and (iii) it is more tolerant towards extreme operating conditions [25]. The heterogeneous system is effective over a broader pH range including the common pH for natural water and wastewater (pH 2–9) whereas for the homogeneous system, the dissolved catalyst could precipitate at circumneutral and basic pH decreasing its performance [26,27]. Compared to PS, PMS is relatively easier to be activated with metal oxide catalysts due to the differences in their molecular structures (i.e. PMS is asymmetrical while PS is symmetrical) and bond dissociation energies. The PS activation by heterogeneous catalyst, most commonly Fe^0, consumes the catalyst through the irreversible conversion of Fe^0 to Fe^{3+}. On the other hand, the PMS catalysts have a relatively longer lifespan as they can potentially be regenerated through a redox cycle with PMS (e.g. Co^{2+} to Co^{3+} to Co^{2+}).

For activation of PMS by heterogeneous catalyst, many studies have adopted heterogeneous cobalt oxide catalysts for PMS activation because Co has been identified as the most efficient PMS activator [21,23,28–30]. To date, several review articles [31–33] and book chapter [34] have emerged to provide overviews of SR-AOPs involving the PMS activation by homogeneous and heterogeneous Co catalysts. However, Co leaching from heterogeneous Co catalysts during PMS activation poses a concern as Co is considerably toxic and potentially carcinogenic [35]. Dissolved Co concentration ranging from 0.002 to 0.107 mg L^{-1} has been detected in drinking water [36]. To avoid potential Co leaching, the research direction has shifted towards the use of other catalysts, namely metal (Mn-, Fe- and Cu- based) and nonmetal catalysts. To date, investigation of the nonmetal catalyst consists only of the carbon-based catalysts because they are relatively abundant and have tremendous potential for practical application. Considering that the SR-AOPs have been the subject of tremendous research interest due to their potential environmental applications, Mn-, Fe-, Cu- and carbon-based catalysts are extensively being investigated as PMS activators. To the best of our knowledge, there is no review on the development of heterogeneous catalysts as PMS activator other than those for heterogeneous Co catalysts.

This review aims to provide a timely overview on the development of metal- and nonmetal- based heterogeneous catalysts for the destruction of recalcitrant organics in water with particular focus on PMS activation. The heterogeneous transition metal-based catalysts can be classified into the single and mixed metal catalysts. The mixed metal catalysts have at least two different metal species in their metal framework. The topics discussed herein include a brief summary of the chemistry of $SO_4^{\bullet-}$, mechanisms of PMS activation, recent progresses in the development of single metal, mixed metal and nonmetal carbon catalysts for PMS activation, hybrid heterogeneous catalyst/PMS system integrated with other advanced

Table 1
Comparison of standard reduction potentials of various common oxidants.

Half equation	Standard reduction potential, E° (V)	Ref.
$F_2 + 2\,e^- \rightarrow 2F^-$	2.87	[170]
$^\bullet OH + e^- \rightarrow OH^-$	2.80	[38]
$SO_4^{\bullet-} + e^- \rightarrow SO_4^{2-}$	2.60	[37]
$SO_5^{\bullet-} + e^- \rightarrow SO_5^{2-}$	1.10	[76]
$HSO_5^- + 2H^+ + 2e^- \leftrightarrow HSO_4^- + 2H_2O$	1.82	[68]
$HSO_5^- + H^+ + 2e^- \leftrightarrow SO_4^{2-} + H_2O$	1.75	[68]
$SO_5^{2-} + H_2O + 2e^- \leftrightarrow SO_4^{2-} + OH^-$	1.22	[68]
$S_2O_8^{2-} + 2e^- \leftrightarrow 2SO_4^{2-}$	2.01	[170]
$S_2O_8^{2-} + 2H^+ + 2e^- \leftrightarrow 2HSO_4^-$	2.12	[170]
$H_2O_2 + 2H^+ + 2e^- \leftrightarrow 2H_2O$	1.78	[170]
$O_3 + 2H^+ + 2e^- \leftrightarrow O_2 + H_2O$	2.08	[170]
$O_3 + 2\,H_2O + 2e^- \leftrightarrow O_2 + 2OH^-$	1.24	[170]

oxidation technologies, and critical insights into identification of the dominant reactive species produced during SR-AOPs. The challenges and prospects of employing heterogeneous SR-AOPs such as the undesired formation of oxyanions and harmful disinfection byproducts, treatment of sulfate and residual PMS, practical applications for treating recalcitrant organics and future research direction are also discussed.

2. The chemistry of sulfate radical

Table 1 shows a comparison of the standard reduction potentials of $SO_4^{\bullet-}$ with various oxidants. In general, $SO_4^{\bullet-}$ is a powerful oxidant with a standard redox potential of +2.60 V *vs.* NHE (normal hydrogen electrode), comparable to the standard redox potential of the $^\bullet OH$ (+2.80 V *vs.* NHE) but slightly below that of F_2 (+3.03 V *vs.* NHE) [37,38]. Compared to $^\bullet OH$ ($t_{1/2}$ = < 1 μs), the freely-diffusible $SO_4^{\bullet-}$ has a longer lifetime ($t_{1/2}$ = 30–40 μs) allowing excellent mass transfer and contact between $SO_4^{\bullet-}$ with the target pollutant in the heterogeneous catalysis system [39,40]. The reactivity of $SO_4^{\bullet-}$ is pH independent while that of $^\bullet OH$ is pH dependent (removal efficiency of $^\bullet OH$–based reaction decreases with increasing pH). At circumneutral pH (most prevailing in aquatic system), $SO_4^{\bullet-}$ could be more reactive than $^\bullet OH$ since the redox potential of $SO_4^{\bullet-}$ has been reported to be higher than that of $^\bullet OH$ (E° = 2.60–3.10 V and 1.90–2.70 V, respectively) [41]. The reaction between $SO_4^{\bullet-}$ with the organic molecule is very fast, typically near diffusion controlled rate with second–order rate constants between 10^5 to 10^9 M^{-1} s^{-1} [42,43] while the typical reaction rates for $^\bullet OH$ are between 10^6 to 10^{11} M^{-1} s^{-1} [44]. The $SO_4^{\bullet-}$-induced degradation could lead to a better mineralization rate than $^\bullet OH$ [45]. Owning to the higher selectivity of $SO_4^{\bullet-}$ compared to $^\bullet OH$, $SO_4^{\bullet-}$ can be employed to attack directly at specific functional groups (that may give rise to the molecular ecotoxicity characteristics of the pollutant) *via* electron transfer reaction. On the contrary, higher amount of $^\bullet OH$ is required to attack a specific functional group because $^\bullet OH$ reacts non-selectively through a series of reactions involving electron transfer, electrophilic/radical addition and hydrogen abstraction [43,46]. As $SO_4^{\bullet-}$ is electrophilic, it prefers to react with electron-donating groups such as amino (–NH_2), hydroxyl (–OH), alkoxy (–OR), π electrons present on aromatic molecules, and other organic compounds that contain unsaturated bonds. The reaction of $SO_4^{\bullet-}$ with electron-withdrawing groups such as nitro (–NO_2) and carbonyl (C=O) substitutes is generally slower.

Hydroxyl radical can be generated from the pH dependent redox reaction between H_2O/OH^- and $SO_4^{\bullet-}$ as follows [47–50]:

$$SO_4^{\bullet-} + H_2O \rightarrow SO_4^{2-} + {}^\bullet OH + H^+,\ k_{SO_4^{\bullet-}+H_2O} < 1.0 \times 10^3 M^{-1}s^{-1} \quad (2.1)$$

$$SO_4^{\bullet-} + OH^- \rightarrow SO_4^{2-} + {}^\bullet OH,\ k_{SO_4^{\bullet-}+OH^-} = 6.5 \times 10^7 M^{-1}s^{-1} \quad (2.2)$$

At pH < 9, $SO_4^{\bullet-}$ is the dominant reactive radical while at pH > 9, $^\bullet OH$ becomes the dominant reactive radical [51]. The $SO_4^{\bullet-}$ is less influenced by the dissolved organic matter (DOM) compared to $^\bullet OH$ (with the second–order rate constant, $k_{SO_4^{\bullet-}+DOM} = 6.8 \times 10^3\,mgC^{-1}s^{-1}$ and $k_{^\bullet OH+DOM} = 1.4 \times 10^4\,mgC^{-1}s^{-1}$ for the reaction of DOM with $SO_4^{\bullet-}$ and $^\bullet OH$, respectively) and thus $SO_4^{\bullet-}$ can selectively attacks the target pollutant in the presence of DOM [52]. However, $SO_4^{\bullet-}$ is more influenced by anionic species (particularly halides) in water than $^\bullet OH$ [53]. For instance, $SO_4^{\bullet-}$ reacts with common water anions such as Cl^- [54,55], Br^- [56–58], CO_3^{2-}/HCO_3^- [42,59–61] and HPO_4^- [62] to form weaker radicals.

$$SO_4^{\bullet-} + Cl^- \rightarrow Cl^\bullet + SO_4^{2-},\ k_{SO_4^{\bullet-}+Cl^-} = 3.0 \times 10^8 M^{-1}s^{-1} \quad (2.3)$$

$$SO_4^{\bullet-} + Br^- \rightarrow Br^\bullet + SO_4^{2-},\ k_{SO_4^{\bullet-}+Br^-} = 2.5 \times 10^9 M^{-1}s^{-1} \quad (2.4)$$

$$SO_4^{\bullet-} + HCO_3^- \rightarrow HCO_3^\bullet + SO_4^{2-},\ k_{SO_4^{\bullet-}+HCO_3^-} = 2.8 - 9.1 \times 10^6 M^{-1}s^{-1} \quad (2.5)$$

$$SO_4^{\bullet-} + CO_3^{2-} \rightarrow CO_3^\bullet + SO_4^{2-},\ k_{SO_4^{\bullet-}+CO_3^{2-}} = 6.1 - 410 \times 10^6 M^{-1}s^{-1} \quad (2.6)$$

$$SO_4^{\bullet-} + HPO_4^{2-} \rightarrow HPO_4^\bullet + SO_4^{2-},\ k_{SO_4^{\bullet-}+HPO_4^{2-}} = 1.2 \times 10^6 M^{-1}s^{-1} \quad (2.7)$$

Under certain conditions, the $SO_4^{\bullet-}$ can oxidize Cl^- and Br^- to produce oxyanions and halogenated disinfection byproducts (HDBPs) [54,55,57,58]. Sulfate radical can be scavenged by another $SO_4^{\bullet-}$ or transition metal (e.g. Fe^{2+} and Co^{2+}) [22,61,63,64].

$$SO_4^{\bullet-} + SO_4^{\bullet-} \rightarrow S_2O_8^{2-},\ k_{SO_4^{\bullet-}+SO_4^{\bullet-}} = 3.7 \times 10^8 M^{-1}s^{-1} \quad (2.8)$$

$$M^{n+} + SO_4^{\bullet-} \rightarrow M^{(n+1)+} + SO_4^{2-} \quad (2.9)$$

The self-scavenging effect (Eq. (2.8)) is not significant provided that the concentration of $SO_4^{\bullet-}$ is low attributed to the rapid consumption of $SO_4^{\bullet-}$ during oxidation reactions [65].

3. Activation of peroxymonosulfate by heterogeneous catalysts

Peroxymonosulfate (HSO_5^-, pKa = 9.4) is commercially available in the form of a triple salt $2KHSO_5{\cdot}KHSO_4{\cdot}K_2SO_4$ with the trade name Oxone® and Caroat®. It is an acidic oxidant with standard reduction potentials for the aqueous half-reactions as follow [66–68]:

$$HSO_5^- + H^+ + 2e^- \leftrightarrow SO_4^{2-} + H_2O,\ E^\circ = 1.75\,V\,vs.NHE \quad (3.1)$$

$$SO_5^{2-} + H_2O + 2e^- \leftrightarrow SO_4^{2-} + OH^-,\ E^\circ = 1.22\,V\,vs.NHE \quad (3.2)$$

Peroxymonosulfate is widely used as a versatile oxidant for various organic syntheses [69]. Although PMS can oxidize organic contaminant, it is kinetically not favorable compared to the radical-based oxidation. The molecular structure of PMS is similar to that of H_2O_2 except that one of the H atoms is replaced with a $-SO_3$ group. The distance of the peroxide bond (—O—O—) in PMS (1.460 Å) is comparable to that of solid state H_2O_2 (1.453 Å) but shorter than that of $S_2O_8^{2-}$ (1.497 Å) [70]. It is estimated that the (—O—O—) bond energy

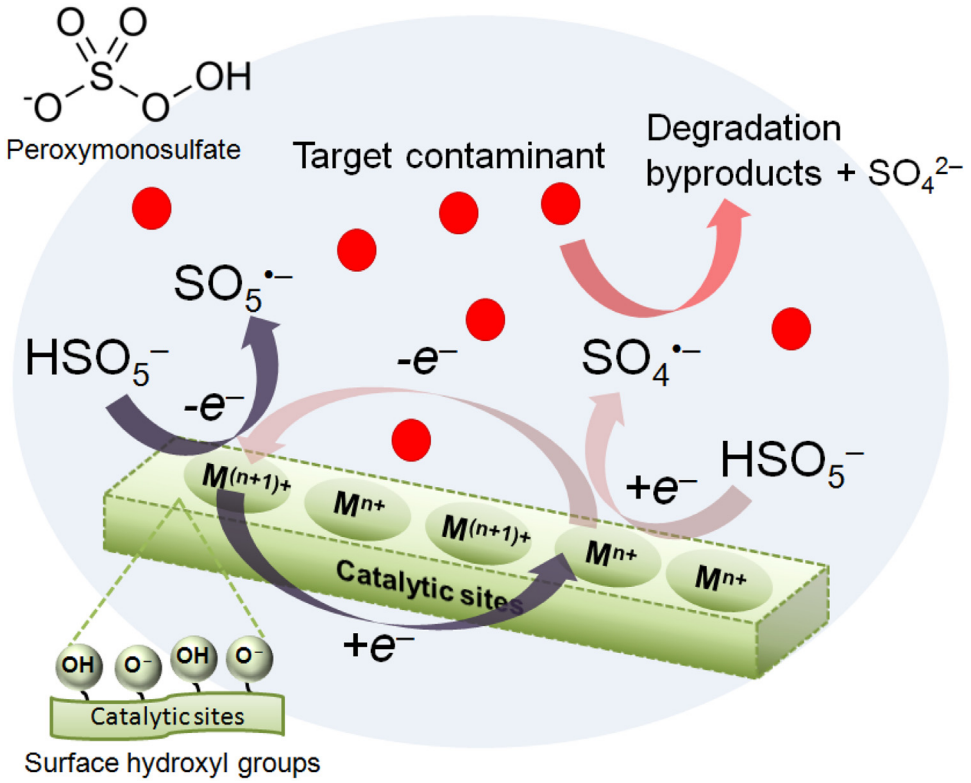

Fig. 1. The redox reaction involving peroxymonosulfate and heterogeneous transition metal catalyst.

of PMS is between the bond energies of H_2O_2 (213 kJ mol^{-1} [71]) and PS (140 kJ mol^{-1} [72]). The PMS concentration can be quantified by an iodometric method coupled with titration or spectrophotometric technique [48,73–75].

The prerequisite for the generation of $SO_4^{\bullet-}$ from PMS *via* heterogeneous catalysis is to have the PMS to be in close proximity to the redox active surface of the catalyst. At close proximity, various surface PMS-catalyst interactions take place. Generally, PMS is activated to produce both $SO_4^{\bullet-}$ and $^{\bullet}OH$ when its peroxide bond (—O—O—) is homolytically cleaved by accepting one electron from the transition metal (M) (Eqs. (3.3) and (3.4), respectively) [21]:

$$M^{n+} + HSO_5^- \rightarrow M^{(n+1)+} + SO_4^{\bullet-} + OH^- \quad (3.3)$$

$$M^{n+} + HSO_5^- \rightarrow M^{(n+1)+} + SO_4^{2-} + {}^{\bullet}OH \quad (3.4)$$

As the $SO_4^{\bullet-}$ has a short lifetime, the target pollutant must be within the diffusion limit of the $SO_4^{\bullet-}$ for the oxidation reaction to occur effectively. Meanwhile, the oxidized transition metal can be reduced back to its original oxidation state *via* a one-electron reduction process by PMS (Eq. (3.5)) producing peroxymonosulfate radical ($SO_5^{\bullet-}$, + 1.1 V *vs.* NHE) which is a relatively weaker transient species but serves to regenerate the catalyst [76].

$$M^{(n+1)+} + HSO_5^- \rightarrow M^{n+} + SO_5^{\bullet-} + H^+ \quad (3.5)$$

$$2HSO_5^- \rightarrow SO_5^{\bullet-} + SO_4^{\bullet-} + H_2O \text{(net reaction of Eqs. (3.3) and (3.5))} \quad (3.6)$$

$$2HSO_5^- \rightarrow SO_5^{\bullet-} + HSO_4^- + {}^{\bullet}OH \text{(net reaction of Eqs. (3.4) and (3.5))} \quad (3.7)$$

Peroxymonosulfate radical is more reactive than the molecular oxygen and can also reduce certain transition metals [77]. The oxidized transition metal ions can also be regenerated by directly oxidizing organics *via* disproportionation reactions. The working mechanism of the electron transfer reaction is illustrated in Fig. 1.

The surface hydroxyl group (M–OH) on the catalyst surface plays a functional role in facilitating the activation of PMS [78–80]. The presence of surface hydroxyl group, either on the catalyst surface or support, has been reported to enhance PMS activation [78,81]. It has been reported that the protonated form of the surface hydroxyl group ($M–OH_2^+$) is less effective in activating PMS [82]. At constant temperature, several common factors affecting the performance of the catalyst are pH, catalyst loading and PMS dosage which can be described by the following kinetics [82]:

$$C_t = C_o e^{\frac{k_i}{k_{PMS}} \frac{[Cat-OH]_o}{(K_{eq}[H^+]+1)} C_{PMSO}(e^{-k_{PMS}t}-1)} \quad (3.7)$$

where C_t and C_o are the pollutant concentrations at time t and $t = 0$, respectively, K_{eq} is the equilibrium constant for the catalyst, k_i is the intrinsic rate constant, k_{PMS} is the first-order rate constant for PMS decomposition, $[Cat–OH]_o$ is the catalyst loading and C_{PMSo} is the initial PMS dosage.

It should be noted that the standard reduction potential is not the only governing factor involved in predicting the catalytic activity of the metal catalyst. Also, the reactivity and behavior of the heterogeneous catalysts cannot be predicted exclusively based on the ionic size and charge of the transition metal [21]. For instance, Co-based catalysts are efficient PMS activator and the high standard reduction potential of Co^{3+}/Co^{2+} (E° = +1.92 V *vs.* NHE) enables efficient self-recycling of Co^{2+} for the catalytic reaction to proceed until all the PMS has been consumed. Similarly, despite having a relatively low standard reduction potential to participate in the redox reaction with PMS, Cu-based catalysts (Cu^{2+}/Cu^+, E° = +0.15 V *vs.* NHE) have also been reported to be able to activate PMS. In

general, the mechanisms of PMS activation by various heterogeneous transition metal catalysts are still not fully understood.

4. Heterogeneous transition metal catalysts

4.1. Single metal catalysts

Table 2 summarizes the synthesis methods and performances of various single metal catalysts as PMS activator. In general, the single metal catalysts can be grouped into Co-, Cu-, Fe-, and Mn-based catalysts. Although Ag [11] and Ru catalysts [83] can activate PMS, they are not extensively investigated as catalysts for PMS activation due to their relatively high cost and potential toxicity.

4.1.1. Co-based catalysts

Several reported studies employed cobalt oxides to activate PMS and observed undesirable Co leaching during catalysis especially under acidic condition [23,29,30]. Up to 0.73 and 0.03 mg L^{-1} of Co were detected in the treated water after catalytic PMS activation reaction at acidic and neutral pHs, respectively [23]. In order to reduce the Co leaching problem, Co_3O_4 has been decorated on various supports including inert 1/2/3-D materials [84,85], metal oxides [86], industrial wastes [87–89], magnetic particles [90], molecular sieves [48,91] and adsorbents [92,93]. The supported Co_3O_4 catalysts generally have better catalytic activity than Co_3O_4, improved Co_3O_4 dispersion, reduced Co leaching, better separation/recovery of the catalysts from the treated water, and added functionality (such as antibacterial and photocatalytic). However, this did not eliminate the Co leaching problem. As Co_3O_4 and supported Co_3O_4 catalysts have been extensively investigated, several reviews on the development of Co_3O_4-based catalysts for PMS activation are available [31,33]. Thus, for a more comprehensive overview on the development of the heterogeneous Co_3O_4-based catalysts, we refer readers to these reviews.

4.1.2. Cu-based catalysts

Comparing the two most stable Cu oxide catalysts (CuO and Cu_2O), the catalytic activity of CuO is ~1.5–2.0 times higher than that of Cu_2O [94,95]. However, a considerably high CuO loading (up to 1.5 g L^{-1} of CuO and 1.5 mM of Oxone® for treating 50 mg L^{-1} of phenol) is required for effective performance [96]. The CuO catalyst is also not as redox stable and efficient compared to the mixed metal catalyst such as $CuFe_2O_4$ (Cu leaching of 46 ± 3 and 1.5 ± 0.1 μg L^{-1} for CuO and $CuFe_2O_4$ after catalytic PMS activation under the same condition) [97]. Further improvement of the CuO catalytic activity can be achieved by incorporating the CuO onto a support with high surface area, high stability and good adsorption affinity for the pollutant such as ZSM5 [98,99] to decrease the CuO aggregation and improve its specific surface area for catalytic reaction [100]. Besides activating PMS, CuO can also activate PS to degrade selected organic pollutants without producing $SO_4^{\bullet-}$ [101].

4.1.3. Fe-based catalysts

Iron-based materials are widely employed for catalysis because they are cost-effective, eco-friendly and efficient materials [102]. Common PMS activators based on Fe are zero valent iron (ZVI), Fe_2O_3 and Fe_3O_4. The mechanism of PMS activation by ZVI can be delineated as follows [103,104]:

$$\equiv Fe^0 + HSO_5^- + 2H^+ \rightarrow \equiv Fe^{2+} + HSO_4^- + H_2O (E^\circ = +2.26\,V\,vs.\,NHE) \quad (4.1.3.1)$$

$$\equiv Fe^{2+} + HSO_5^- \rightarrow \equiv Fe^{3+} + SO_4^{\bullet-} + OH^- \quad (4.1.3.2)$$

$$\equiv Fe^{3+} + HSO_5^- \rightarrow \equiv Fe^{2+} + SO_5^{\bullet-} + H^+ \quad (4.1.3.3)$$

Besides $SO_4^{\bullet-}$, $^\bullet OH$ can also be selectively produced from the reaction between PMS and ZVI as follows [105]:

$$\equiv Fe^0 + HSO_5^- \rightarrow Fe^{3+} + SO_4^{2-} + {}^\bullet OH \quad (4.1.3.4)$$

As both $SO_4^{\bullet-}$ and $^\bullet OH$ are produced from PMS activation *via* irreversible ZVI oxidation, the catalyst needs to be periodically added into the reaction system. In order to decrease the treatment cost, optimization of the ZVI loading, PMS dosage and pH is critical. This also reduces the corrosion effect and undesirable reactions of $SO_4^{\bullet-}$ and Fe^0 with either Fe^{2+} and/or Fe^{3+} [22,106–109] as follow:

$$\equiv Fe^0 + 2H^+ \rightarrow Fe^{2+} + H_2 \quad (4.1.3.5)$$

$$\equiv Fe^0 + 2SO_4^{\bullet-} \rightarrow Fe^{2+} + SO_4^{2-} \quad (4.1.3.6)$$

$$\equiv Fe^{3+} + \equiv Fe^0 \rightarrow 2Fe^{2+} \quad (4.1.3.7)$$

$$\equiv Fe^{2+} + SO_4^{\bullet-} \rightarrow Fe^{3+} + SO_4^{2-} \quad (4.1.3.8)$$

Zero valent iron tends to have a serious particle aggregation and high deposition rate due to their strong interparticle attraction and intrinsic magnetic interaction [110,111]. Carbon encapsulation of ZVI can solve these problems while improving the hydrophilicity/hydrophobicity and adsorption affinity of the catalyst for pollutants [105,112]. For instance, carbon encapsulation of ZVI with glucose increases the hydrophilicity of the catalysts due to the presence of surface C—OH and —C=O groups [113]. It has been reported that the introduction of melamine during the encapsulation of ZVI can induce the formation of Fe_3C with better stability and magnetic property for efficient separation from the treated water [105]. However, the conversion of Fe^0 to Fe_2O_3 during catalytic reaction can potentially deactivate the catalyst over repeated used. This also implies that Fe_2O_3 is less active than Fe^0 for PMS activation. In another study, the deposition of Co on Fe^0 to form bimetallic Co–Fe^0 is reported to have a relatively better catalytic activity than that of the monometallic catalyst [114]. The bimetallic system can potentially provide new intrinsic catalytic property which leads to a higher reaction stoichiometric efficiency and better PMS utilization efficiency over the monometallic system [115].

The Fe_2O_3 particles consisting of mainly Fe^{3+} species have been employed for rhodamine B removal *via* PMS activation but the catalysis process requires a relatively high Fe_2O_3 loading (specific surface area = 34 m^2 g^{-1}, up to 1.8 g L^{-1} for 50 mg L^{-1} of rhodamine B) for effective application [116]. The surface Fe^{3+} must be reduced to Fe^{2+} (by electron transfer reaction with PMS) before it is able to generate $SO_4^{\bullet-}$ from PMS. The unfavorable standard reduction potential for Fe^{3+}/Fe^{2+} (−0.77 V *vs.* NHE) compared to that of Co^{3+}/Co^{2+} (+1.92 V *vs.* NHE) suggests that Fe^{3+} cannot be reduced effectively by PMS. Although Fe^{3+} reduction by PMS can still proceed (assisted by many factors such as improved electron transfer due to the complexation of PMS on the surface Fe^{3+}), Fe^{3+} cannot generate $SO_4^{\bullet-}$ directly from PMS without being initially reduced implying that it has a relatively poorer catalytic activity than Fe^{2+}. The slower generation of $SO_4^{\bullet-}$ by Fe^{3+} enables $SO_4^{\bullet-}$ to be utilized more effectively for pollutant oxidation while minimizing the Fe^{2+} scavenging effect (Eq. (4.1.3.8)) [22].

The catalytic activity of Fe_2O_3 can be further enhanced by increasing the Fe_2O_3 surface area and encapsulating Fe_2O_3 with an electron transfer mediator. For instance, dipicolinic acid encapsulated Fe_2O_3 with specific surface area = 188 m^2 g^{-1} has been found to performed relatively better (100% bisphenol A removal in 2 h) as a PMS activator than FeOOH (95%), FeO(OH,Cl) (70%) and Fe_2O_3 (65%) [74]. The dipicolinic acid coating contains electron-rich nitrogen and oxygen groups which can serve as an electron shutter to mediate the electron transfer between Fe^{3+} and PMS. The complexation of surface Fe^{3+} could induce changes in the redox potential of Fe^{3+}/Fe^{2+} which could have positive effect on PMS activation

Table 2
Synthesis methods and performances of various single metal catalysts as PMS activator.

Ref	Catalysts	Synthesis method	Target pollutant	Performance
Co-based catalysts				
Anipsitakis et al. [23]	Co_3O_4	Commercial	2,4-dichlorophenol	• Catalytic activity of Co_3O_4 > CoO • >99% of 20 mg L^{-1} 2,4-dichlorophenol removed in 15 min with 0.157 g L^{-1} catalyst (as Co) pH neutral, and 2.67 mM Oxone® (as PMS) • Co leaching <0.07 mg L^{-1} and >0.59 mg L^{-1} at neutral and acidic pH, respectively, for Co_3O_4
	CoO			
Chen et al. [29]	Co_3O_4	Precipitation method	Acid orange 7	• > 99% of 0.2 mM acid orange 7 removed in 30 min with 0.50 g L^{-1} catalyst, pH neutral, and 2.0 mM PMS
Guo et al. [30]	Co_3O_4	Commercial	Amoxicillin	• > 95% of 0.12 mM amoxicillin removed in 60 min with 0.060 g L^{-1} catalyst, pH 6.0, T = 60 °C, and 10 mM Oxone®
Cu-based catalysts				
Ji et al. [96]	CuO	CTAB-assisted hydrothermal method	Phenol	• 100% of 50 mg L^{-1} phenol removed in 60 min with 1.50 g L^{-1} catalyst, pH 4.0, and 1.50 mM Oxone® • Cu leaching was 0.78 mg L^{-1}
Ji et al. [100]	Cu/ZSM5	Wet impregnation method	Rhodamine B	• Catalytic activity of Cu/ZSM5 > CuO • For at least 4 cycles, 95% of 50 mg L^{-1} rhodamine B removed in 1 h with 1.0 g L^{-1} Cu/ZSM5, pH 7.0, and 0.60 g L^{-1} PMS • Cu leaching between 0.684–0.139 mg L^{-1} at pH 3.0–11.0
Fe-based catalysts				
Al-Shamsi et al. [114]	Co–Fe^0	Reduction of Fe^{3+} with $NaBH_4$ + deposition of Co on the as-prepared Fe^0.	Trichloroethylene	• Catalytic activity of Co–Fe^0 > Pd–Fe^0=Mn–Fe═Cd–Fe^0 > Ni–Fe^0 > Cr–Fe^0 > Zn–Fe^0 > Cu–Fe^0 > Ag–Fe^0 • > 95% of trichloroethylene removed in 5 h with trichloroethylene:PMS:catalyst molar ratio of 1:10:10
Chen et al. [124]	$Fe_3O_4/Cu_{1.5}Ni_{0.5}Cr$-LDH	Two-step microwave-hydrothermal method	Acid orange 7	• 100% of 25 mg L^{-1} acid orange 7 removed with 100 mg L^{-1} catalyst, and AO7/PMS molar ratio of 1:10 • Both Fe^{2+} and Cu^{+} are the active species generating $SO_4^{\bullet -}$ • Activation energy for AO7 degradation is 34.31 kJ mol^{-1}
Ghanbari et al. [104]	Fe^0 and Cu°	Commercially-purchased	Real textile wastewater	• > 99% and >80% of decolourization in 150 min with 3.0 g L^{-1} Fe^0 and 4.0 g L^{-1} Cu°, respectively, at pH 4.0, and 20 mM PMS • First-order kinetics
Gong et al. [119]	Fe@ACFs	Wet impregnation method	Reactive red M-3BE	• > 99% of 50 μM Reactive red M-3BE removed in 15 min with 2.0 g L^{-1} catalyst, pH = 3.0, T = 50 °C, and 0.50 mM PMS • NaCl > 0.1 M increase the decolourization while NaCl < 0.1 M inhibit the decolourization • First-order kinetics with activation energy of 32.89 kJ mol^{-1} • Fe leaching was <0.50 mg L^{-1}
Ji et al. [116]	Fe_2O_3	Hydrothermal-calcination method	Rhodamine B	• 100% of 50 mg L^{-1} rhodamine B removed in 1 h with 1.50 g L^{-1} catalyst, pH 6.2, and 1.0 mM PMS • First-order kinetics with activation energy of 69.225 kJ mol^{-1} • Fe leaching was <0.14 mg L^{-1}
Oh et al. [74]	DPA-Fe_2O_3	Low temperature co-precipitation method	Bisphenol A	• Catalytic activity of DPA-Fe_2O_3 ~ Co_3O_4 > commercial goethite > commercial akaganeite > commercial hematite • > 90% of 15 mg L^{-1} bisphenol A removed in 120 min with 0.50 g L^{-1} catalyst, pH 7.0, and 2.0 g L^{-1} Oxone®
Sun et al. [112]	nano-Fe^0@CS	hydrothermal-carbonization method	Phenol	• Catalytic activity of nano-Fe^0@CS is better than ZVI particles, iron ions, iron oxides and cobalt oxide • 100% of 20 mg L^{-1} phenol removed in 10 min with 0.50 g L^{-1} catalyst, T = 30 °C, and 2.0 g L^{-1} Oxone®
Tan et al. [122]	Fe_3O_4	Commercially-purchased	Acetaminophen	• 75% of 10 mg L^{-1} acetaminophen removed in 120 min with 0.80 g L^{-1} catalyst, pH 4.5, and 0.20 mM PMS • Pseudo first-order kinetics • Fe leaching was <4.0 μg L^{-1}
Wang et al. [105]	Fe^0/Fe_3C@CS	Hydrothermal method followed by self reduction under N_2 atmosphere	Phenol	• 100% of 20 mg L^{-1} phenol removed in 10 min with 1.0 g L^{-1} catalyst, pH 7.0, and 2 g L^{-1} Oxone® • First-order kinetics

Table 2
(*Continue*)

Ref	Catalysts	Synthesis method	Target pollutant	Performance
Wei et al. [123]	$Fe_{3-x}M_xO_4$ (M = Cr, Mn, Co, Ni)	Precipitation-oxidation method	Acid orange II	• Incorporation of Co, Mn and Ni improved the catalytic activity of Fe_3O_4 in the order of Mn < Ni < Co while Cr substitution showed inert effect • 81% of 0.10 mM acid orange II removed in 40 min with 1.0 g L^{-1} $Fe_{2.10}Co_{0.90}O_4$, pH 7.0, and 0.20 mmol L^{-1} Oxone® • Pseudo first-order kinetics
Zhang et al. [150]	Fe_3O_4/MnO_2 (ball–in–ball hollow spheres)	*in situ* growth process + etching method	Methylene blue	• Catalytic activity of Fe_3O_4/MnO_2 (ball–in–ball hollow spheres) > MnO_2 (hollow spheres) > Fe_3O_4 (hollow spheres) > MnO_2 (hollow spheres) > MnO_2 (solid) > Fe_3O_4 (hollow spheres) > Fe_3O_4 (solid) • 00% of 30 mg L^{-1} methylene blue removed in 30 min with 300 mg L^{-1} catalyst, pH = 7.94, and 20 mM PMS • Mn and Fe leaching for Fe_3O_4/MnO_2 were 0.22–0.45% and 0.51–0.87%, respectively
Mn-based catalysts				
Liu et al. [143]	Fe_3O_4/MnO_2	Hydrothermal method	4-chlorophenol	• >95% of 50 mg L^{-1} 4-chlorophenol removed in 30 min with 0.20 g L^{-1} catalyst, pH 7.5, T = 25 °C, and 0.50 g L^{-1} PMS. • First-order kinetics.
Luo et al. [144]	OMS-2	Reflux method	Acid orange 7	• Catalytic activity of OMS-2 > MnO_2 • >95% of 20 mg L^{-1} acid orange 7 removed in 10 min with 0.25 g L^{-1} catalyst, pH 2.65, T=25 °C, and 0.25 g L^{-1} PMS • Mn leaching was <0.10 mg L^{-1}
Saputra et al. [132]	nanowires α-MnO_2 nanosphere α-MnO_2 nanorod α-MnO_2	Hydrothermal method Reduction of $KMnO_4$ by maleic acid and calcination (300 °C) Reduction of $KMnO_4$ by maleic acid and calcination (500 °C)	Phenol	• Catalytic activity of nanowires α-MnO_2 > nanorod α-MnO_2 > spherical α-MnO_2. • 100% of 30 mg L^{-1} phenol removed in 90 min with 0.40 g L^{-1} catalyst, and 2.0 g L^{-1} Oxone®. • First-order kinetics.
Saputra et al. [128]	α-, β-, γ-MnO_2	Modified hydrothermal method based on the redox reaction of Mn^{2+} with persulfate	Phenol	• Catalytic activity of α-MnO_2 nanowires > γ-MnO_2 > β-MnO_2 • 100% of 25 mg L^{-1} phenol removed in 60 min using 0.40 g L^{-1} of catalyst, and 2.0 g L^{-1} of Oxone® • First-order kinetics with activation energy of 21.9 kJ mol^{-1}
Saputra et al. [129]	MnO_2 Mn_2O_3 Mn_3O_4 MnO	Commercially-obtained Calcination of MnO_2 Calcination of MnO_2 Two step hydrothermal and calcination method	Phenol	• Catalytic activity of Mn_2O_3 > MnO > Mn_3O_4 > MnO_2 • 100% of 25 mg L^{-1} phenol removed in 60 min with 0.40 g L^{-1} catalyst, and 2.0 g L^{-1} PMS • Pseudo first-order kinetics with activation energy of 11.4 kJ mol^{-1} • Reusability required thermal treatment at 500 °C for 1 h
Saputra et al. [131]	cubic-Mn_2O_3 octahydra-Mn_2O_3 truncated-Mn_2O_3	Two-step hydrothermal and calcination method Solvothermal method Solvothermal method	Phenol	• Catalytic activity of Mn_2O_3-cubic > Mn_2O_3-octahydra > Mn_2O_3-truncated • 100% of 25 mg L^{-1} phenol removed in 60 min with 0.40 g L^{-1} catalyst, and 2.0 g L^{-1} PMS • First-order kinetics with activation energy of 61.2 kJ mol^{-1}

Table 2
(*Continue*)

Ref	Catalysts	Synthesis method	Target pollutant	Performance
Saputra et al. [130]	Mn_3O_4	Solvothermal method	Phenol	• Catalytic activity of $Mn_3O_4 \sim Co_3O_4 > Fe_3O_4$ • 00% of 25 mg L^{-1} phenol and 68% TOC removed in 60 min with 0.40 g L^{-1} catalyst, and 2.0 g L^{-1} Oxone® • Pseudo first-order kinetics with activation energy of 38.5 and 66.2 kJ mol^{-1} for Mn_3O_4 and Co_3O_4, respectively
	Fe_3O_4	Solvothermal method		
	Co_3O_4	Hydrothermal method		
Tang et al. [138]	Mn_3O_4	Co-precipitation-calcination method	Acid red G	• 100% of 50 mg L^{-1} acid red G removed in 90 min with 0.50 g L^{-1} catalyst, pH 7.0, T = 25 °C, and 1.0 g L^{-1} Oxone® • Pseudo first-order kinetics with activation energy of 65.33 kJ mol^{-1}
Wang et al. [137]	corolla-like $MnO_2/ZnFe_2O_4$	Modified hydrothermal method	Phenol	• Catalytic activity of urchin-shaped $MnO_2/ZnFe_2O_4$ > corolla-like $MnO_2/ZnFe_2O_4$ > $ZnFe_2O_4$ • 100% of 20 mg L^{-1} phenol removed in 180 min with 0.20 g L^{-1} catalyst, T=25 °C, and 2.0 g L^{-1} Oxone® • First-order kinetics activation energy for urchin-shaped $MnO_2/ZnFe_2O_4$ and corolla-like $MnO_2/ZnFe_2O_4$ were 49.4 and 41.7 kJ mol^{-1}, respectively
	urchin-shaped $MnO_2/ZnFe_2O_4$			
Wang et al. [135]	Mn/Fe_3O_4/carbon (N_2)	Hydrothermal method followed by calcination in N_2	Phenol	• Catalytic activity Mn/Fe_3O_4/carbon (N_2) > Mn/Fe_3O_4/carbon (air) • 100% of 20 mg L^{-1} phenol removed in 180 min with 0.20 g L^{-1} catalyst, T = 25 °C, and 2.0 g L^{-1} Oxone® • Pseudo first-order kinetics with activation energy of 59.5 and 63.2 kJ mol^{-1} for Mn/Fe_3O_4/carbon (air) and Mn/Fe_3O_4/carbon (N_2), respectively
	Mn/Fe_3O_4/carbon (air)	Hydrothermal method followed by calcination in air		
Wang et al. [134]	corolla-like δ-MnO_2	Modified hydrothermal method with reduction of $KMnO_4$	Phenol	• Catalytic activity of corolla-like δ-MnO_2 > urchin-shaped δ-MnO_2 • 100% of 20 mg L^{-1} phenol removed in 30 min with 0.20 g L^{-1} catalyst, T=25 °C, and 2.0 g L^{-1} Oxone® • First-order kinetics activation energy for corolla-like δ-MnO_2 was 25.3 kJ mol^{-1} • Mn leaching was ~3 mg L^{-1}
	urchin-shaped δ-MnO_2			
Wei et al. [148]	OMS-2/Fe_3O_4	Solvent free method	Acid orange 7	• 97% of 20 mg L^{-1} acid orange 7 removed in 15 min with 0.40 g L^{-1} catalyst, pH 3.75, and 0.40 g L^{-1} PMS • Mn leaching was <0.05 mg L^{-1}
Xu et al. [139]	MnO_x/HCAS	Hydrothermal method	Acid Red 73	• >98% of 50 mg L^{-1} acid red 73 removed in 30 min with 1.0 g L^{-1} catalyst, pH 7.0, T=25 °C, and 1.0 g L^{-1} Oxone® • Cl^- (1–150 mg L^{-1}) improve decolourization while HCO_3^- (>1 mg L^{-1}) inhibit decolourization • First-order kinetics activation energy of 21.87 kJ mol^{-1}
Yang et al. [149]	Fe_3O_4/GO Mn_3O_4/rGO	co-precipitation method reduction of $Mn(C_2H_3O_2)_2.3H_2O$ and GO with hydrazine	Methylene blue	• Catalytic activity of Fe_3O_4/Mn_3O_4/rGO > Mn_3O_4/rGO > Fe_3O_4/GO • >95% of 50 mg L^{-1} methylene blue removed in 30 min with 0.10 g L^{-1} catalyst, pH 7.0, T = 25 °C, and 0.3 g L^{-1} PMS • Pseudo second-order kinetics with activation energy of 25.4 kJ mol^{-1}
	Fe_3O_4/Mn_3O_4/rGO	reduction of $Mn(C_2H_3O_2)_2.3H_2O$ and Fe_3O_4/GO with hydrazine		
Yao et al. [136]	Mn_3O_4/rGO	Reduction of $Mn(C_2H_3O2)_2.4H_2O$-loaded graphene oxide by hydrazine.	Orange II	• Catalytic activity of Mn_3O_4/rGO > Mn_3O_4 > rGO • 100% of 30 mg L^{-1} Orange II removed in 120 min with 0.05 g L^{-1} catalyst, pH 7.0, and 1.50 g L^{-1} Oxone® • Pseudo second–order kinetics with activation energy of 49.5 kJ mol^{-1}
Zhang et al. [140]	Mn_3O_4/rGO	Hydrothermal method	Orange II	• Catalytic activity of Mn_3O_4/rGO > Mn_3O_4 > rGO • 100% of 30 mg L^{-1} Orange II removed in 90 min with 0.050 g L^{-1} catalyst, pH neutral, and 1.50 g L^{-1} Oxone® • Mn leaching was 20 μg L^{-1} (0.04%)
Other catalysts				
Muhammad et al. [83]	RuO_2/AC	General impregnation method	Phenol	• Catalytic activity of RuO_2/AC > RuO_2/ZSM–5 • 100% of 50 mg L^{-1} phenol removed in 60 min using 0.40 g L^{-1} catalyst and 1.0 g L^{-1} Oxone® • First-order kinetics with activation energy of 61.4 and 42.2 kJ mol^{-1} for RuO_2/AC and RuO_2/ZSM-5, respectively
	RuO_2/ZSM-5			

[22,117]. Other electron shutter (e.g. quinolinic acid, α-picolinic acid and fusaric acid [118]) can potentially be selected as the organic coating material to enhance the catalytic activity of Fe_2O_3.

Another strategy to increase the catalytic activity of Fe^{3+} is by immobilization of the Fe^{3+} ion on activated carbon fibers (ACFs) [119]. The Fe^{3+} forms considerably strong electrostatic bond with ACFs and <0.5 mg L^{-1} of Fe leached out after 10 cycles of reuse. The hydrophilic groups present on the ACFs is capable of reducing Fe^{3+} to Fe^{2+}, which can then generate $SO_4^{\bullet-}$ from PMS [120]. It has been reported that the addition of a reducing agent such as hydroxylamine during catalytic PMS activation by dissolved Fe^{3+} can improve the performance of the system by promoting the reduction of Fe^{3+} to Fe^{2+} [121]. Although this may seems unsuitable for the heterogeneous system due to the inherent effect on the stability of the catalyst as hydroxylamine promotes the dissolution of Fe^{3+} from Fe-based catalyst, it can potentially be employed for controlled dissolution-reduction of Fe^{3+} for PMS activation.

Another common form of iron oxide, namely magnetic Fe_3O_4, can adsorb water molecule and activate PMS *via* the following mechanism [122]:

$$\equiv Fe^{2+} + HSO_5^- \rightarrow \equiv Fe^{3+} + SO_4^{2-} + {}^{\bullet}OH \quad (4.1.3.9)$$

$$\equiv Fe^{2+} - {}^{-}OH + HSO_5^- \rightarrow \equiv Fe^{2+} - (HO)OSO_3^- + OH^- \quad (4.1.3.10)$$

$$\equiv Fe^{2+} - (HO)OSO_3^- \rightarrow \equiv Fe^{3+} - {}^{-}OH + SO_4^{\bullet-} \quad (4.1.3.11)$$

The slower Fe^{2+} regeneration in the Fe_3O_4 after generating $^{\bullet}OH$ and $SO_4^{\bullet-}$ from PMS results in the increase in Fe^{3+}:Fe^{2+} ratio in Fe_3O_4 [122]. The catalytic activity of Fe_3O_4 can be enhanced by doping with other transition metals such as Co (achieving >10 times improvement over that of Fe_3O_4), Mn, Ni and Cr with the order of decreasing dopant-induced reactivity as follows: Co > Mn > Ni > Cr > Fe [123]. The degree of improvement in catalytic activity after Co doping is directly proportional to the percentage of Co present in the Co-doped Fe_3O_4. It is also reported that immobilizing Fe_3O_4 on CuNiCr–LDH support can increase the catalytic activity of Fe_3O_4 but the potential Cr leaching from the support may significantly hinder its application as a catalyst in SR-AOPs [124].

A possible disadvantage of iron-based catalysts such as ZVI, Fe_2O_3 and FeOOH is that they can be deactivated by SO_4^{2-} *via* the replacement of two surface hydroxyl groups with SO_4^{2-} forming a binuclear bridge complex consisting of Fe–O–S(O_2)–O–Fe which deactivates the Fe sites [125–127].

$$\equiv Fe^0 + SO_4^{2-} + 2H_2O \rightarrow \equiv FeSO_4 + 2OH^- + H_2 \quad (4.1.3.12)$$

$$2\equiv FeOOH + 2SO_4^{2-} + 2H_2O \rightarrow 2\equiv FeSO_4 + 4OH^- + H_2 + O_2 \quad (4.1.3.13)$$

4.1.4. Mn-based catalysts

Wang and co-workers [128–137] investigated the performance of various single-metal Mn oxide catalysts as PMS activators. They include Mn oxides with different crystallographic dimensions (α-, β-, and γ-MnO_2), Mn oxides at different oxidation states and supported Mn oxides. In general, the catalytic activity of Mn oxides depends on many factors, namely (i) the presence of oxygen liability which allows a better oxidative transformation between various Mn oxidation states, (ii) density of exposed reactive facets such as MnO_6 edges with double tunneled structure, (iii) presence of mixed valence Mn, (iv) redox potential of different Mn oxidation states, (v) specific surface area, and (vi) degree of crystallinity [128,129,131,132,134,138,139]. The degree of crystallinity exerts a greater influence on the catalytic activity of Mn oxide than the specific surface area. It is reported that crystalline MnO_2 (146 m^2 g^{-1}) performed ~8 times better (0.359 min^{-1} *vs.* 0.0457 min^{-1}) than the amorphous MnO_2 (179 m^2 g^{-1}) [132].

The ability of Mn to form many stable oxides makes it versatile for use in a wide range of applications. The mechanisms of PMS activation by heterogeneous Mn oxides (with different oxidation states) can be delineated by the following reactions [129]:

$$2MnO_2 + 2HSO_5^- \rightarrow Mn_2O_3 + 2SO_5^{\bullet-} + 2OH^- \quad (4.1.4.1)$$

$$2Mn_3O_4 + 2HSO_5^- \rightarrow 3Mn_2O_3 + 2SO_4^{\bullet-} + 2H^+ \quad (4.1.4.2)$$

$$Mn_2O_3 + 2HSO_5^- \rightarrow 2MnO_2 + 2SO_4^{\bullet-} + 2H^+ \quad (4.1.4.3)$$

$$2MnO + 2HSO_5^- \rightarrow Mn_2O_3 + 2SO_4^{\bullet-} + 2H^+ \quad (4.1.4.4)$$

$$3Mn_2O_3 + HSO_5^- \rightarrow 2Mn_3O_4 + SO_5^{\bullet-} + OH^- \quad (4.1.4.5)$$

Under the same experimental condition (0.4 g L^{-1} of catalyst loading, 2 g L^{-1} of PMS, 120 min), the catalytic activities of Mn oxides with different oxidation states are in the following order: α-Mn_2O_3 (100%) > MnO (90%) > γ-Mn_3O_4 (65%) > γ-MnO_2 (60%) [129]; evidencing that the Mn(IV) species has the poorest redox activity with PMS. It is interesting to note that Mn_3O_4 has a comparable catalytic activity with Co_3O_4 [130]. However, Mn_3O_4 suffers from poor chemical and thermal stabilities but its stability can be ameliorated by depositing Mn_3O_4 on reduced-graphene oxide (rGO) [136,140]. The Mn oxides can also act as a support to improve the catalytic activity of various metal oxides such as Co_3O_4 and CuO [137,141–143].

In several studies, the Mn octahedral molecular sieve (OMS-2) was selected as a catalyst for PMS activation because it has favorable properties such as a large specific surface area, high density of lattice oxygen favorable for catalysis and presence of mixed-valence Mn (2+, 3+ and 4+) [144–146]. As OMS-2 generally contains high density of acidic sites [147] and PMS activation favors basic surface [78], surface modification of OMS-2 is usually required for use as an efficient PMS activator. Ferromagnetism can be introduced to OMS-2 by encapsulating Fe_3O_4 with OMS-2 to produce a core shell structure [148]. However, this could lead to the catalytic activity reduction of OMS-2 [144,148]. The technique of introducing ferromagnetism to the catalyst using Fe_3O_4 has also been adopted to prepare Fe_3O_4/Mn_3O_4/rGO [149] and Fe_3O_4/MnO_2 [150] but in this case, improvement in the catalytic activity of the catalyst was observed.

Because Mn has many stable oxidation states, it is relatively difficult to retain the chemical phases of Mn oxides after PMS activation reactions. It was previously found that phenol removal *via* PMS activation catalyzed by α-Mn_2O_3 decreased from 100% (first cycle) to 30% (second cycle) due to the change in chemical phase and deposition of degradation intermediates on the surface of the α-Mn_2O_3 catalyst [129]. A post treatment of the catalyst (e.g. calcination, simple washing, chemical treatment etc. depending on the nature of the catalyst) is usually required to restore its performance [151].

4.2. Mixed metal catalysts

Table 3 presents an overview of the performances of various mixed metal catalysts. The mixed metal catalysts have improved stability (reduced leaching), polyfunctionality (e.g. photoactive, magnetically separable etc.), high redox activity and better catalytic activity compared to single metal catalysts. This is due to the improvement in the specific surface area, synergistic redox coupling of different metals, increase in the density of basic sites on the surface of the catalyst, and presence of mixed-valence transition metals [152]. The mixed metal catalysts can be grouped into Co

Table 3
Synthesis methods and performances of various mixed metal catalysts as PMS activator.

References	Catalysts	Synthesis method	Target pollutant	Performance
Co–based catalysts				
Andrew Lin et al. [85]	ZIF–67/GO	Carbonization of Co–based MOF (ZIF–67) and GO	Acid Yellow 17	• Catalytic activity of ZIF–67/GO > ZIF–67 > rGO • >75% of 100 mg L^{-1} acid yellow 17 removed in 120 min with 0.50 g L^{-1} catalyst, pH 3.8, and 90 mg L^{-1} PMS • First–order kinetics with activation energy of 12 kJ mol^{-1}
Du et al. [158]	$CoFe_2O_4$/titanate nanotubes	Hydrothermal method to prepare titanate nanotube follow by impregnation–calcination method	Rhodamine B	• Catalytic activity of $CoFe_2O_4$/titanate nanotubes > $CoFe_2O_4$ • 100% of 100 mg L^{-1} Rhodamine B removed in 60 min with 0.20 g L^{-1} catalyst, T = 20 °C, and 4.0 g L^{-1} Oxone® • Pseudo first–order kinetics with activation energy of 70.56 kJ mol^{-1} • Co leaching was ~928 μg L^{-1}
Hu et al. [154]	$CoFe_2O_4$/SBA–15	Wet impregnation method	Rhodamine B	• >95% of 5 mg L^{-1} Rhodamine B removed in 120 min with 0.10 g L^{-1} catalyst, and PMS:rhodamine B molar ratio of 20:1 • First–order kinetics. • Co leaching was ~60 μg L^{-1}
Li et al. [160]	CoAlMn	Hydrothermal + calcination method	Bisphenol A	• >99% of 10 mg L^{-1} bisphenol A removed in 100 min with 0.020 g L^{-1} catalyst, pH 3.6, T = 25 °C, and 0.15 g L^{-1} Oxone® • First–order kinetics activation energy of 76.83 kJ mol^{-1} • Co leaching was 0.19 (0.19%) and < 0.01 μg L^{-1} for acidic and neutral pH, respectively. Mn leaching was 0.014 (0.67%) and < 0.005 μg L^{-1} for acidic and neutral pH, respectively
Li et al. [161]	$Fe_{0.8}Co_{2.2}O_4$	Heating $Fe_yCo_{1-y}[Co(CN)_6]_{0.67}\bullet nH_2O$	Bisphenol A	• Catalytic activity of $Fe_{0.8}Co_{2.2}O_4$ > Co_3O_4 > Fe_3O_4 • >95% of 20 mg L^{-1} bisphenol A removed in 60 min with 0.10 g L^{-1} catalyst, pH 6, T = 298 K, and 0.2 g L^{-1} PMS • Co leaching was 0.36 mg L^{-1} • Fe leaching was 0.11 mg L^{-1}
Qin et al. [157]	$Fe_2O_3/Co_3O_4/CoFe_2O_4$	Template synthesis	Phenol	• >99% of 50 mg L^{-1} phenol removed in 120 min with 0.20 g L^{-1} catalyst, and 4 g L^{-1} PMS
Ren et al. [81]	XFe_2O_4 (X = Co, Cu, Mn, Zn)	Sol–gel method	di–n–butyl phthalate	• Catalytic activity of $CoFe_2O_4$ > $CuFe_2O_4$ > $MnFe_2O_4$ > $ZnFe_2O_4$ • ~60% and ~80% of 2 μmol L^{-1} di–n–butyl phthalate removed with 0.10 g L^{-1} $CuFe_2O_4$ and $CoFe_2O_4$, respectively, in the presence of 20 μmol L^{-1} PMS and pH 7.0

Table 3 (*Continued*)

References	Catalysts	Synthesis method	Target pollutant	Performance
Su et al. [153]	$Co_{0.75}Fe_{2.25}O_4$	Hydrothermal method	Rhodamine B	• >99% of 0.014 mM Rhodamine B removed in 40 min with 0.050 g L^{-1} catalyst, pH 6, and 1 mM Oxone® • Pseudo first–order kinetics with activation energy of 49.01 kJ mol^{-1}
Xu et al. [155]	$CoFe_2O_4$/ graphene	Modified Hummers method + precipitation method	Dimethyl phthalate	• Catalytic activity of $CoFe_2O_4$/graphene > $CoFe_2O_4$ > graphene • >99% of 0.05 mM dimethyl phthalate removed in 10 min with 0.50 g L^{-1} catalyst, pH 4, and 2 mM PMS
Yang et al. [80]	$Fe_2O_3/Co_3O_4/CoFe_2O_4$	Thermal oxidation of Fe and Co salts	2,4–dichlorophenol	• Catalytic activity of $Fe_2O_3/Co_3O_4/CoFe_2O_4$ > Co_3O_4 > Fe_2O_3+Co_3O_4 (Fe:Co = 1:1) > Fe_2O_3 • ~80% of 50 mg L^{-1} 2,4–dichlorophenol removed in 120 min with 0.1 g L^{-1} catalyst, pH 7, and 2,4–dichlorophenol:Oxone® molar ratio of 1:3 • Co leaching was 20–50 μg/L at neutral pH
Yao et al. [156]	$CoFe_2O_4$/rGO	Hummers method + precipitation method	Phenol	• Catalytic activity of $CoFe_2O_4$/rGO > $CoFe_2O_4$ > rGO • >99% of 20 mg L^{-1} phenol removed in 40 min with 67 mg L^{-1} catalyst, and 2 g L^{-1} PMS • Pseudo first–order kinetics with activation energy of 15.8 kJ mol^{-1}
Yao et al. [159]	$CoMn_2O_4$	Hydrothermal method	Rhodamine B	• Catalytic activity of $CoMn_2O_4$ > Co_2MnO_4 > $Co_{0.5}Mn_{2.5}O_4$ > Co_3O_4 > Co_3O_4 +Mn_2O_3 > Mn_2O_3 • >95% of 0.03 g dm^{-3} rhodamine B removed in 10 min with 0.020 g dm^{-3} catalyst, pH 6.29, T = 25 °C, and 0.2 g dm^{-3} PMS • Co and Mn leaching were <0.1 mg dm^{-3}
Cu–based catalysts				
Ding et al. [162]	$CuFe_2O_4$	Sol–gel method	Tetrabromobisphenol A	• $CuFe_2O_4$ performed better than CuO and Fe_2O_3, respectivel • 99% of 10 mg L^{-1} tetrabromobisphenol A removed in 30 min with 0.20 g L^{-1} catalyst, pH 6.3–7.1, and 0.2 mmol L^{-1} PMS • Pseudo–first order kinetics • Cu leaching was ~0.094 mg L^{-1}
Feng et al. [167]	$CuFeO_2$	Hydrothermal method	Sulfadiazine	• Catalytic activity of $CuFeO_2$ ~ $CuFe_2O_4$ > Cu_2O ~ Fe_2O_3 • >80% of 8.0 μM sulfadiazine removed in 12 min with 0.10 g L^{-1} catalyst, pH = 6.8, and 33.0 μM PMS • Pseudo-first order kinetics. • Cu leaching for $CuFeO_2$ was ~21 μg L^{-1}

Table 3 (*Continued*)

References	Catalysts	Synthesis method	Target pollutant	Performance
Guan et al. [163]	$CuFe_2O_4$	Sol–gel method	Atrazine	• >98% of 2 μM atrazine removed in 15 min with 0.1 g L^{-1} catalyst, and 1 mM PMS • Detrimental effect at HCO_3^- concentration ≥ 4 mM while enhancement at HCO_3^- concentration of 2 mM • Detrimental effect of NOM (0–3.2 mg L^{-1} NOM corresponding to 98–23% removal)
Oh et al. [173]	$CuO/Cu_{1.2}Bi_{1.6}O_{0.36}$	Hydrothermal method	Benzotriazole	• $CuO/Cu_{1.2}Bi_{1.6}O_{0.36}$ performed better than $CuBi_2O_4$ and CuO • ~100% of 2.5 mg L^{-1} benzotriazole removed in 10 min with 0.50 g L^{-1} catalyst, pH 7, and 0.2 g L^{-1} PMS • Cl^- (100–500 mg L^{-1}) significantly affects the degradation of benzotriazole • Pseudo first–order kinetics • Cu leaching was 57 μg L^{-1}
Oh et al. [164]	$CuFe_2O_4$/AC	Two step low temperature co–precipitation and calcination method	Methylene blue	• ~100% of 20 mg L^{-1} methylene blue removed in 2 h with 0.20 g L^{-1} catalyst, pH 5, and 2.0 g L^{-1} Oxone® • No significant effect by Cl^- (100 mg L^{-1}) and NO_3^- (10 mg L^{-1}) but negative effect on rate of degradation by humic acid (5 mg L^{-1}) • Pseudo first–order kinetics • Cu leaching was 0.68 mg L^{-1} (~0.85%)
Oh et al. [82]	$CuFe_2O_4$–Fe_2O_3	low temperature co–precipitation method	Bisphenol A	• Catalytic activity of $CuFe_2O_4$–Fe_2O_3 > $CuFe_2O_4$ > $CoFe_2O_4$ > $CuBi_2O_4$ > $CuAl_2O_4$ > Fe_2O_3 > $MnFe_2O_4$ • 100% of 5 mg L−1 bisphenol A removed in 10 min with 0.20 g L−1 catalyst, pH = 7, and 0.36 g L−1 PMS • Cu leaching was <0.9 mg L−1 (< 0.1%) • Humic acid and Cl− decrease the catalytic activity of $CuFe_2O_4$–Fe_2O_3
	Fe_2O_3 $CuBi_2O_4$ $CoFe_2O_4$ $MnFe_2O_4$ $CuFe_2O_4$ $CuAl_2O_4$	Solvothermal method Sol–gel method		
Xu et al. [165]	$CuFe_2O_4$	Sol–gel method	Bisphenol A	• Catalytic activity of $CuFe_2O_4$ > Fe_2O_3 > CuO • >95% of 50 mg L^{-1} bisphenol A removed in 60 min with 0.40 g L^{-1} catalyst, pH = 6.72, and 0.5 g L^{-1} PM • Cu leaching in $CuFe_2O_4$ was 1.27 (0.795%) and 0.7 mg L^{-1}, for first and second cycle, respectively
Zhang et al. [97]	$CuFe_2O_4$	Sol–gel method	Iopromide	• $CuFe_2O_4$ performed better than $MnFe_2O_4$, Fe_2O_3, CuO and homogeneous Cu^{2+}, respectively • 80% of 10 μM iopromide removed in 30 min with 100 mg L^{-1} catalyst, pH 6, and 20 μM PMS • Pseudo first–order kinetics • Cu leaching in $CuFe_2O_4$ and CuO were 1.5 ± 0.1 and 46 ± 3 μg L^{-1}, respectively

Table 3 (*Continued*)

References	Catalysts	Synthesis method	Target pollutant	Performance
Other mixed metal catalyst				
Wang et al. [177]	$NiFe_2O_4$	Thermal decomposition of mixed inorganic salts	Benzoic acid	• Catalytic activity of $CoFe_2O_4$ > $NiFe_2O_4$ > $MnFe_2O_4$ > NiO > Fe_3O_4 > Fe_2O_3 • >80% of 10 μM benzoic acid removed in 60 min with 0.10 g L^{-1} $NiFe_2O_4$, T=25 °C, pH = 7.0 and 1.0 mM PMS • Ni leaching was <0.128 mg L^{-1}
Yao et al. [178]	$MnFe_2O_4$	Co–precipitation method	Methyl violet, methyl orange, methylene blue, orange II rhodamine B	• Catalytic activity of $MnFe_2O_4$/rGO > $MnFe_2O_4$ • >90% of 20 mg L^{-1} Orange II removed in 120 min with 0.050 g L^{-1} catalyst, T=25 °C, and 0.5 g L^{-1} PMS • Order of effects on anions (0.1 M) on decolourization of Orange II: Cl^- > HCO_3^- > CH_3COO^- > NO_3^- • Pseudo first–order kinetics with activation energy of 25.7 kJ mol^{-1} • Mn and Fe leaching for $MnFe_2O_4$ were 0.0043 mM and 0.0013 mM, respectively, while for $MnFe_2O_4$/rGO were 0.0045 mM and 0.0020 mM, respectively
	$MnFe_2O_4$/rGO	Co–precipitation during reduction of GO		

mixed metal catalysts, Cu mixed metal catalysts, and other mixed metal catalysts. A schematic illustration of the advantages of mixed metal catalysts over the single metal catalysts is presented in Fig. 2a.

4.2.1. Co mixed-metal catalysts

The performance of various Co mixed metal catalysts as PMS activators including $CoFe_2O_4$ [79–81,153–158], $CoMn_2O_4$ [159], CoMnAl [160], magnetic Co-based metal organic framework [85], and $Fe_{0.8}Co_{2.2}O_4$ [161] have been investigated by many researchers. Compared to CoO and Co_3O_4, Co mixed metal catalysts exhibit better catalytic activity, improved stability (lower Co leaching), and ferromagnetism (in some catalysts) for the ease of separation of the catalyst from the treated water.

Magnetic $CoFe_2O_4$ is the most widely investigated Co mixed metal catalyst. Magnetic $CoFe_2O_4$ has a better resistance to Co leaching due to its strong Co–Fe interactions [80]. Magnetic $CoFe_2O_4$ activates PMS *via* the following mechanism:

$$\equiv Co^{2+} + HSO_5^- \rightarrow \equiv Co^{3+} + SO_4^{\bullet -} + OH^- \quad (4.2.1.1)$$

$$\equiv Co^{3+} + HSO_5^- \rightarrow \equiv Co^{2+} + SO_5^{\bullet -} + OH^+ \quad (4.2.1.2)$$

$$\equiv Fe^{3+} + HSO_5^- \rightarrow \equiv Fe^{2+} + SO_5^{\bullet -} + H^+ \quad (4.2.1.3)$$

$$\equiv Fe^{2+} + HSO_5^- \rightarrow \equiv Fe^{3+} + SO_4^{\bullet -} + OH^- \quad (4.2.1.4)$$

$$\equiv Fe^{2+} + \equiv Co^{3+} \rightarrow \equiv Fe^{3+} + \equiv Co^{2+} (E^\circ = 1.04\,V\,vs.NHE) \quad (4.2.1.5)$$

Although Fe^{3+} (the predominant Fe species in $CoFe_2O_4$) can activate PMS, it seems unlikely to have a major contribution to PMS activation due to its relatively poor catalytic activity compared to Co^{2+}. This suggests that the thermodynamically-favorable electron transfer from Fe^{2+} (produced mainly from the one electron reduction of Fe^{3+}) to Co^{3+} has a minimum effect on the performance enhancement (Eq. (4.2.1.5)). The promotional effect is more likely to be due to the higher content of the surface hydroxyl groups and high catalytic activity of Co^{2+} in the mixed metal catalysts [80]. The excellent catalytic activities of XFe_2O_4 type catalysts (X = Co, Cu, Mn and Zn) are due to the balance between $X^{n+}/X^{(n+1)+}$, O^{2-}/O_2 and PMS catalysis [81]. The catalytic activity of $CoFe_2O_4$ can be improved by ~2–4 times by depositing $CoFe_2O_4$ on a support (i.e. SBA-15, titanate nanotubes, rGO and MgO) for the treatment of various organic pollutants (e.g. plasticizer, acid orange 7, rhodamine B, phenol, etc.) *via* PMS activation [79,154–156,158].

The catalytic activities of various spinel-type Co–Mn catalysts prepared at various Co:Mn ratios for dye degradation *via* PMS activation are in the following order: $CoMn_2O_4$ (99% in 80 min) ~ Co_2MnO_4 (98% in 80 min) > $Co_{0.5}Mn_{2.5}O_4$ (70% in 80 min)[159]. This implies that (i) Co^{2+} is the main redox species because increasing Mn does not improve the catalytic activity, and (ii) Co^{3+} has lower catalytic activity than Co^{2+} in the Co–Mn coupling. Because Mn has many stable oxidation states, it is difficult for the mixed-valence Mn species in $CoMn_2O_4$ to be retained at their initial oxidation states after use.

4.2.2. Cu mixed-metal catalysts

Several studies [81,82,95,97,162–165] reported the performances of spinel $CuFe_2O_4$ and supported $CuFe_2O_4$ catalysts prepared *via* sol–gel and co-precipitation techniques as PMS activators. The $CuFe_2O_4$ is catalytically more stable than $CuFeO_2$, which has also been used to generate $SO_4^{\bullet -}$ from PMS in a recent study [166,167]. Depending on the catalysts, the selection of a suitable synthesis technique is important for preparing an efficient catalyst. For instance, the solvothermally-prepared $CuFe_2O_4$, $CoFe_2O_4$, and $MnFe_2O_4$ (with organic solvent and surfactant) exhibit reduced catalytic activity and organics leaching compared to the catalyst prepared without the use of any organic precursors [82].

The schematic illustration of the mechanisms of PMS activation by $CuFe_2O_4$ is presented in Fig. 2b. The $CuFe_2O_4$ catalyst is ferromagnetic and has two synergistically-coupled redox active transition metals (Fe^{3+} and Cu^{2+}) which can activate PMS *via* the following mechanism:

$$\equiv Cu^{2+} + HSO_5^- \rightarrow \equiv Cu^{+} + SO_5^{\bullet -} + H^+ \quad (4.2.2.1)$$

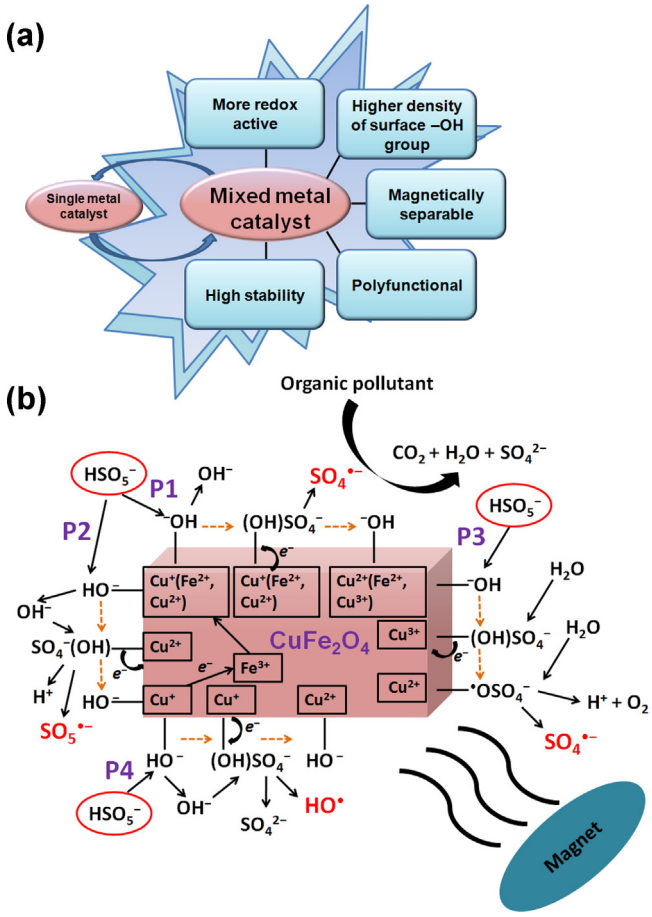

Fig. 2. Schematic illustrations of (a) the advantages of mixed metal catalysts over the single metal catalysts, and (b) the mechanisms of PMS activation by magnetic $CuFe_2O_4$ catalyst. P1–P4 indicates various mechanisms of PMS activation.

$$\equiv Cu^{+} + HSO_5^{-} \rightarrow \equiv Cu^{2+} + SO_4^{\bullet -} + OH^{-} \quad (4.2.2.2)$$

$$\equiv Cu^{+} + \equiv Fe^{3+} \rightarrow \equiv Cu^{2+} + \equiv Fe^{2+} (E^{\circ} = +0.60\,V \textit{vs.} NHE) \quad (4.2.2.3)$$

$$\equiv Fe^{3+} + HSO_5^{-} \rightarrow \equiv Fe^{2+} + SO_5^{\bullet -} + H^{+} \quad (4.2.2.4)$$

$$\equiv Fe^{2+} + HSO_5^{-} \rightarrow \equiv Fe^{3+} + SO_4^{\bullet -} + OH^{-} \quad (4.2.2.5)$$

The X-ray photoelectron spectroscopy provide evidences of the changes in the Cu valence state from Cu^{2+} to a mixture of Cu^{2+}/Cu^{+} in $CuFe_2O_4$ before and after reaction [163]. The synergistic effect could be clearly observed between Cu^{2+} and Fe^{3+}. Because Cu^{+} generated (Eq. (4.2.2.1)) could undergo disproportionation readily (e.g. with molecular oxygen), the electron transfer from Cu^{+} to Fe^{3+} (Eq. (4.2.2.3)) produces Fe^{2+} which is thermodynamically more stable to disproportionation and hence, increases the $SO_4^{\bullet -}$ generation from PMS [168].

$$4\equiv Cu^{+} + O_2 + 4H^{+} \rightarrow 4\equiv Cu^{2+} + 2H_2O (E^{\circ} = +1.08\,V \textit{vs.} NHE) \quad (4.2.2.6)$$

$$4\equiv Fe^{2+} + O_2 + 4H^{+} \rightarrow 4\equiv Fe^{3+} + 2H_2O (E^{\circ} = +0.46\,V \textit{vs.} NHE) \quad (4.2.2.7)$$

It is interesting to note that the one-electron transfer from PMS to Cu^{2+} to form $SO_5^{\bullet -}$ is unfavorable under standard conditions, with Cu^{2+}/Cu^{+} ($E^{\circ} = +0.17$ V *vs.* NHE), $SO_5^{\bullet -}/HSO_5^{-}$ ($E^{\circ} = +1.1$ V *vs.* NHE) and $SO_5^{\bullet -}/SO_5^{2-}$ ($E^{\circ} = +0.81$ V *vs.* NHE) [163]. In order for the redox reaction to occur, PMS forms a surface complex on the surface of the catalyst possibly by replacing the surface hydroxyl groups (Fig. 2b, P1 and P2). The enhancement of the interfacial electron transfer rate from the formation of PMS–metal oxide complex [169] coupled with the relatively low concentration of $SO_5^{\bullet -}$ in the reaction vicinity results in a relatively lower values of the actual reduction potential of $SO_5^{\bullet -}/HSO_5^{-}$ and $SO_5^{\bullet -}/SO_5^{2-}$ in the practical aqueous system, thus making it thermodynamically feasible for the reaction (Eq. (4.2.2.1)) to occur [50,76,163]. Evidences of PMS complex on metal oxide surfaces have been observed *via* IR and Raman spectroscopies [81,163].

It is also likely for PMS to be activated by $CuFe_2O_4$ through the Cu^{2+}–Cu^{3+}–Cu^{2+} (Cu^{3+}/Cu^{2+}, $E^{\circ} = 2.40$ V *vs.* NHE [170]) redox transition as follows (Fig. 2b, P1 and P3) [95,97]:

$$\equiv Cu^{2+} - {}^{-}OH + HSO_5^{-} \rightarrow \equiv Cu^{2+} - (HO)OSO_3^{-} + OH^{-} \quad (4.2.2.8)$$

$$\equiv Cu^{2+} - (HO)OSO_3^{-} \rightarrow \equiv Cu^{3+} - {}^{-}OH + SO_4^{\bullet -} \quad (4.2.2.9)$$

$$\equiv Cu^{3+} - {}^{-}OH + HSO_5^{-} \rightarrow \equiv Cu^{2+} - {}^{\bullet}OOSO_3^{-} + H_2O \quad (4.2.2.10)$$

$$2\equiv Cu^{2+} - {}^{\bullet}OOSO_3^{-} + 2H_2O \rightarrow 2\equiv Cu^{2+} - {}^{-}OH + O_2 + 2SO_4^{\bullet -} + 2H^{+} \quad (4.2.2.11)$$

The Cu^{3+}/Cu^{2+} has a relatively high standard reduction potential (E° of Cu^{3+}/Cu^{2+} in dissolved and solid phases are +1.57 *vs.* NHE and +2.30 V *vs.* NHE, respectively) [171]. The differences in E° values corresponding to the dissolved and solid Cu^{2+} phases also explains the relatively lower performance of dissolved Cu^{2+} ion compared to that of the heterogeneous Cu^{2+} catalysts.

Compared to the other types of mixed metal oxides, the catalytic activity of $CuFe_2O_4$ is ~23 and ~1.3 times lower than that of $CuCo_2O_4$ [95] and $CoFe_2O_4$ [81], respectively. Judging from the mixed metal species (which exists in $CoFe_2O_4$ as Co^{2+} and $CuCo_2O_4$ as mixed valence Co^{2+} and Co^{3+}), the major PMS activation reaction is expected to come from Co^{2+} species [172]. Clearly, these results imply that Co is an essential transition metal for developing the mixed metal catalyst for efficient PMS activation.

Various $CuBi_2O_4$ composite catalysts consisting of either Co-, Fe- or Cu-oxide deposited on the $CuBi_2O_4$ surface have been employed as catalysts for PMS activation [94,173]. The $CuBi_2O_4$ composite with CuO shows remarkable polyfunctional catalytic activity for benzotriazole removal *via* PMS and PS activations due to the presence of high density of surface hydroxyl groups [174] which could bring the pollutant to close proximity with the catalyst surface *via* hydrogen bonding and maximize the utilization of the generated $SO_4^{\bullet -}$. The catalytic activity of $CuBi_2O_4$ composite decorated with Co-oxide ($Co/CuBi_2O_4$) is ~12 times higher than that of Co_3O_4 at the same reaction condition for sulfanilamide removal. Our investigation indicates that $Co/CuBi_2O_4$ can be used to generate $SO_4^{\bullet -}$ for rapid degradation of a myriad of pollutants (Fig. 3) [94].

In several studies, it is reported that the Cu^{+} can react directly with PMS to produce •OH (Fig. 2b, P4) [96,175,176].

$$\equiv Cu^{+} + HSO_5^{-} \rightarrow \equiv Cu^{2+} + SO_4^{2-} + {}^{\bullet}OH \quad (4.2.2.12)$$

However, our investigation with Cu catalysts prepared in our previous studies ($CuBi_2O_4$ composites [173] and $CuFe_2O_4$–Fe_2O_3 [82], FESEM micrographs presented in Fig. 4a–c) using nitrobenzene (NB) as the •OH scavenger shows minimal contribution of •OH at pH 7.0, suggesting that Eq. (4.2.2.12) may not be a major PMS activation mechanism (Fig. 4d).

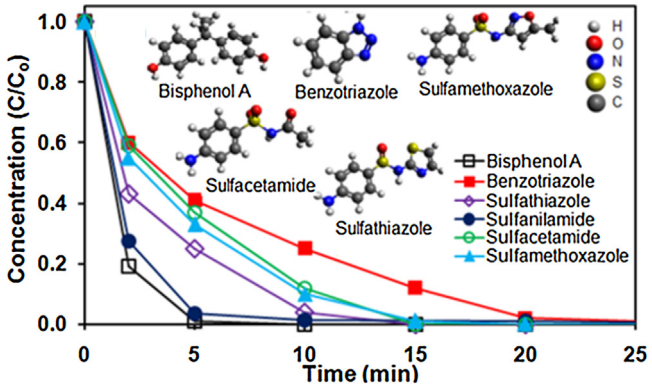

Fig. 3. The degradation of various pollutants *via* PMS activation with $Co/CuBi_2O_4$. Initial conditions: pH 7.0, $Co/CuBi_2O_4$ loading = 0.2 g L^{-1}, PMS dosage = 0.15 g L^{-1}, pollutant concentration = 2.5 mg L^{-1}. Reproduced from [94] with permission from the Royal Society of Chemistry.

4.2.3. Other mixed metal catalysts

The performance of other mixed metal catalysts such as $NiFe_2O_4$ [177] and $MnFe_2O_4$ [178] have also been investigated as catalysts for PMS activation. In a comparative study, $NiFe_2O_4$ (Ni^{2+} as the main active species for redox reaction) has been reported to performed ~1.3 times better than $MnFe_2O_4$ for benzoic acid removal *via* PMS activation [177]. The magnetic spinel-based $MnFe_2O_4$ generally shows only about 10% improvement in Orange II removal when immobilized on rGO [178]. While these catalysts may have potential for further improvement, at the current state, they are usually not as efficient as $CuFe_2O_4$ and $CoFe_2O_4$ [81,82,177]. Thus, future investigations of mixed metal catalyst as PMS activator should consider benchmarking the performance of new catalyst with either $CuFe_2O_4$ or $CoFe_2O_4$.

5. Nonmetal carbon catalysts

Nonmetal carbon-based catalysts such as activated carbon (AC), graphene oxide (GO), reduced graphene oxide (rGO), and carbon nanotubes (CNTs) provide a potential solution to the metal leaching problem. Table 4 summarizes the performance of various nonmetal carbon catalysts for pollutant removal *via* PMS activation. Activated carbon is one of the most widely-used carbon-based catalyst for various catalytic redox reactions involving H_2O_2, PMS, O_3, and PS [179–186]. Because AC is relatively cheap and widely used in the water and wastewater treatment, it is regarded as the most promising choice of nonmetal catalyst for practical application as PMS activator. The attractive features of AC include high surface area and abundant catalytic moieties such as quinone, ketone, carbonyl, and carboxyl groups. Besides, AC has been used as an adsorptive support for metal catalysts to induce synergistic adsorption and degradation of pollutants by $SO_4^{\bullet-}$ [83,92,164]. The performance of different types of ACs as PMS activator depends on the density of surface moieties with delocalized π-electrons and specific surface area of the AC [179]. In general, the mechanism of PMS activation by AC is mediated by the delocalized π-electrons which is similar to the AC activation of H_2O_2 as follows [187]:

$$C{-}\pi + HSO_5^- \rightarrow C{-}\pi^+ + OH^- + SO_4^{\bullet-} \quad (5.1)$$

$$C{-}\pi^+ + HSO_5^- \rightarrow C{-}\pi + H^+ + SO_5^{\bullet-} \quad (5.2)$$

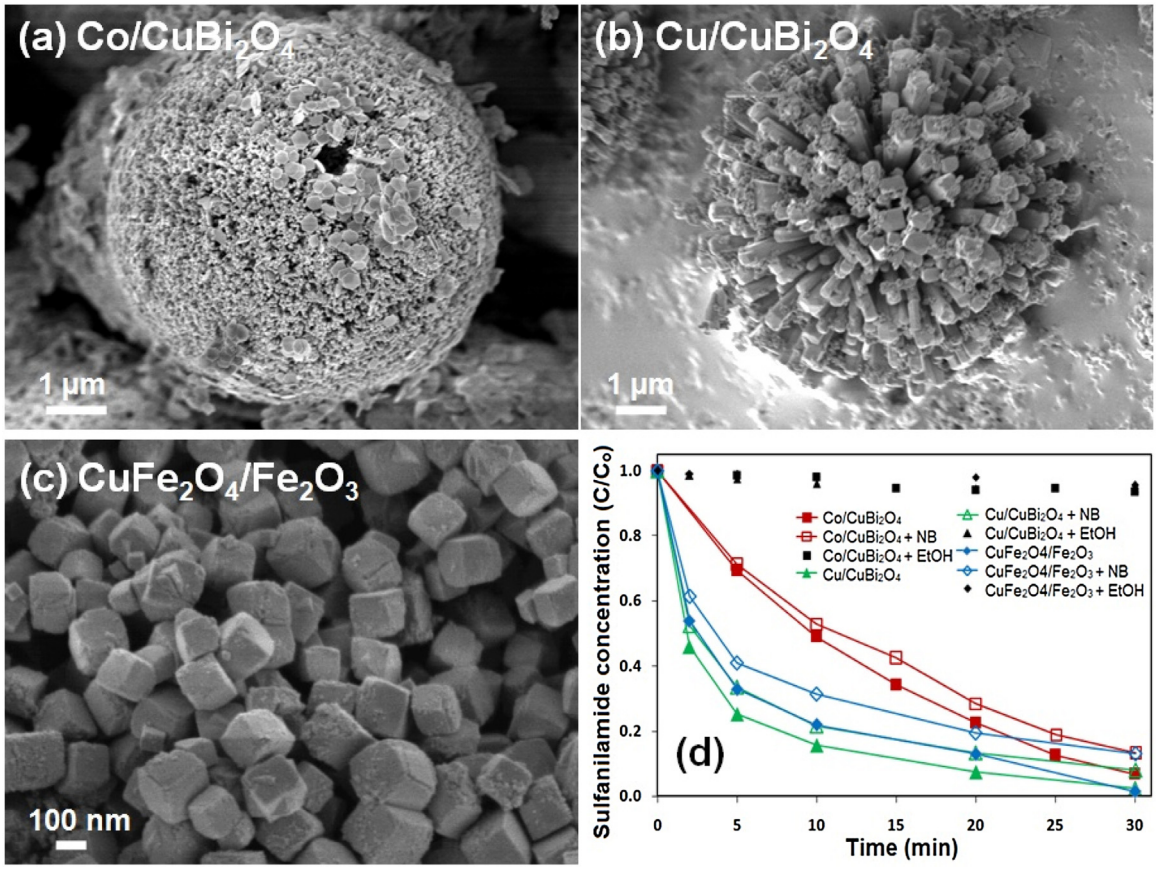

Fig. 4. (a)–(c) show FESEM micrgraphs of $Co/CuBi_2O_4$, $Cu/CuBi_2O_4$ and $CuFe_2O_4/Fe_2O_3$, respectively, and (d) shows the degradation of sulfanilamide (2.5 mg L^{-1}) in the presence/absence of 0.15 mM nitrobenzene (NB) and 1 mM ethanol (EtOH) at pH 7.0. Nitrobenzene acts as •OH scavenger while EtOH acts as both •OH and $SO_4^{\bullet-}$ scavenger. For (d), conditions: [$Co/CuBi_2O_4$] = 0.10 g L^{-1} with 0.075 g L^{-1} Oxone®, [$Cu/CuBi_2O_4$] = 0.40 g L^{-1} with 0.30 g L^{-1} Oxone®, [$CuFe_2O_4/Fe_2O_3$] = 0.10 g L^{-1} with 0.30 g L^{-1} Oxone®.

Table 4
Performances of various types of nonmetal carbon catalysts as PMS activator.

Catalysts	Synthesis method	Target pollutant	Performance	References
Activated carbon				
Activated carbon	Commercially–purchased	Phenol	• Catalytic activity of powdered activated carbon > granular activated carbon • 100% of 25 mg L^{-1} phenol removed in 15 min using 0.20 g L^{-1} PAC, T = 30 °C, and 6.5 mM PMS • First–order kinetics with PAC activation energy of 17.6 kJ mol^{-1}	Saputra et al. [179]
Activated carbon	Commercial activated carbon fiber	Acid orange 7	• Catalytic activity of ACF > GAC • 100% of 100 mg L^{-1} Acid orange 7 was removed in 60 min using 0.30 g L^{-1} GAC, and 20:1 PMS/AO7 molar ratio • Pseudo–first order kinetics	Yang et al. [190]
Activated carbon	Commercial granular activated carbon	Acid orange 7	• GAC/PMS performed better than GAC or PMS alone • 100% of 20 mg L^{-1} acid orange 7 was removed in 60 min using 1.0 g L^{-1} GAC, and 100:1 PMS/acid orange 7 molar ratio • First–order kinetics with activation energy of 25.13 kJ mol^{-1} • The GAC loses its adsorption capacity after one cycle but retain its catalytic activity	Zhang et al. [180]
Activated carbon modified with ammonia	Carbonization, activation and modification of AC with ammonia	Reactive Black 5	• Ammonia modification of AC > unmodified AC • 70% of 0.25 mM Reactive Black 5 was removed in 180 min using 0.040 g L^{-1} AC, pH 5.0, and 25:1 PMS/RB5 molar ratio • First–order kinetics	Yang et al. [188]
Graphene and rGO				
rGO	Hummer's method+ thermal reduction and activation	Methylene Blue	• Reduced graphene oxide activated with 60 min of CO_2 at 800 °C performed the best *vs.* 25, 75 and 0 min • 100% of 10 mg L^{-1} methylene blue was removed in 1 h using 60 mg L^{-1} catalyst, and 0.25 g L^{-1} Oxone®	Peng et al. [197]

Table 4
(*Continue*)

Catalysts	Synthesis method	Target pollutant	Performance	References
rGO	Modified Hummers' method + hydrothermal method followed by chemical activation	Phenol, 2,4–dichlorophenol, methylene blue	• Structure defective graphite preformed better than Co_3O_4 • 95.6% of 2.125×10^{-4} mol L^{-1} phenol was removed in 90 min using 0.50 g L^{-1} of graphene and 3.188×10^{-3} mol L^{-1} of Oxone® • Second–order kinetics with activation energy of 84.0 kJ mol^{-1}	Sun et al. [198]
rGO	Hummer's method + thermal reduction under N_2 atmosphere followed by activation (Physically and chemically activated)	Methylene blue	• Catalytic activity of rGO activated with CO_2 > rGO–$ZnCl_2$/ CO_2 ~ rGO > rGO–$ZnCl_2$ • 100% of 10 mg L^{-1} methylene blue was removed in 250 min using 50 mg L^{-1} catalyst, and 0.50 g L^{-1} PMS. • First–order kinetics	Liu et al. [214]
N–doped rGO	Hummers' method + ammonium nitrate as N precursor followed by thermal reduction	Phenol	• Catalytic activity of N–doped rGO > B, N–codoped rGO > P, N–codoped rGO > B–doped rGO > rGO > P–doped rGO • >90% of 20 mg L^{-1} phenol removed in 90 min with 0.20 g L^{-1} catalyst, T = 25 °C, and 2.0 g L^{-1} PMS • First–order kinetics with activation energy of 19.7 kJ mol^{-1}	Duan et al. [202]
N–doped rGO	Low temperature simultaneous reduction and N doping	Phenol	• N–rGO prepared at 400 °C performed better than rGO and N–rGO prepared at 300–375 °C • 100% of 20 mg L^{-1} phenol removed in 15 min with 0.20 g L^{-1} N–rGO prepared at 400 °C, T = 25 °C and 2.0 g L^{-1} PMS • First–order kinetics with activation energy of 31.6 kJ mol^{-1}	Indrawirawan et al. [196]
N–doped graphene	Calcination of solid mixture (prepared by drying glucose, $FeCl_3.6H_2O$ and urea at 80 °C) under nitrogen flow	Phenol	• Catalytic activity of N–doped graphene > graphene • 100% of 20 mg L^{-1} phenol removed in 90 min with 0.20 g L^{-1} catalyst, T = 25 °C, and 2.0 g L^{-1} PMS • First–order kinetics with activation energy of 96.65 kJ mol^{-1}	Wang et al. [204]

Table 4
(*Continue*)

Catalysts	Synthesis method	Target pollutant	Performance	References
S, N–codoped rGO	Modified Hummers' method + oxidation with concentrated H_2SO_4/$KMnO_4$ + H_2O_2 reaction + mixing with ammonium nitrate and diphenyl disulfide + annealing at 623 K	Phenol	• Catalytic activity of S, N–codoped rGO > N–doped rGO > S–doped rGO > rGO • >99% of 20 mg L^{-1} phenol removed in 90 min with 0.20 g L^{-1} catalyst, T = 25 °C, and 6.5 mM PMS • First–order kinetics with activation energy of 49.6 kJ mol^{-1}	Duan et al. [201]
N, B–codoped rGO	Hummers' method using GO and ammonium nitrate mixture followed by thermal reduction	Phenol	• Catalytic activity of N, B–codoped rGO (with 0.10% B_2O_3 and 5.61% at. N) ~ α–MnO_2 > N–doped rGO ~ Co_3O_4 > rGO(hydrothermal) > rGO • 100% of 20 mg L^{-1} phenol removed in 20 min with 0.20 g L^{-1} catalyst, pH 6.5, and 2.0 g L^{-1} Oxone®	Sun et al. [199]
Carbon nanotubes				
Pristine and N–doped CNTs	Mixing CNT with ammonium nitrate followed by calcination	Phenol	• Catalytic activity of acid treated N–doped carbon nanotubes (at 350 °C)> N–doped carbon nanotubes (at 350 °C) > acid treated CNT ~ CNT • 100% of 30 mg L^{-1} phenol removed in 20 min with 0.20 g L^{-1} catalyst, T = 25 °C and 2.0 g L^{-1} PMS • For CNT, first–order kinetics with activation energy of 33.3 kJ mol^{-1}	Sun et al. [192]
N–doped CNTs	Annealing CNT and melamine under N_2 atmosphere	Phenol	• Catalytic activity of N–doped carbon nanotubes (at 700 °C) > N–doped carbon nanotubes (at 350 °C) > carbon nanotubes (at 700 °C) > Co_3O_4 ~ α–MnO2 > CNT • 100% of 20 mg L^{-1} phenol removed in 20 min with 0.10 g L^{-1} catalyst, T = 30 °C, and 6.5 mM PMS • First–order kinetics with activation energy of 36.0 kJ mol^{-1}	Duan et al. [194]
N–doped single–walled CNTs	Annealing CNT and melamine under N_2 atmosphere	Phenol	• Catalytic activity of N–doped carbon nanotubes > carbon nanotubes • >99% of 20 mg L^{-1} phenol removed in 60 min with 0.10 g L^{-1} catalyst, T = 25 °C, and 6.5 mM PMS	Duan et al. [200]

Table 4
(*Continue*)

Catalysts	Synthesis method	Target pollutant	Performance	References
N, S–codoped CNT–COOH	Thermal decomposition method	Benzophenone–4	• Catalytic activity of N, S–codoped CNT–COOH > N–doped CNT–COOH > N, S–codoped CNT–OH> N, S–codoped CNT > CNT–COOH > CNT–OH > CNT • 100% of 10 mg L^{-1} benzophenone–4 removed in 30 min with 0.10 g L^{-1} catalyst, T = 25 °C, pH = 7.0 and 1.0 g L^{-1} PMS • Pseudo first–order kinetics	Liu et al. [222]
Others				
0D fullerene	Commercially–purchased	Phenol	• Catalytic activity of 3D hexagonally–ordered mesoporous carbon > 1D single–walled CNTs > cubically–ordered mesoporous carbon > 2D graphene nanoplate > 0D fullerene • 100% of 20 mg L^{-1} phenol removed in 40 min with 0.20 g L^{-1} catalyst, T = 25 °C and 2.0 g L^{-1} PMS • First–order kinetics	Indrawirawan et al. [195]
1D single–walled CNTs				
2D graphene nanoplate				
3D hexagonally–ordered mesoporous carbon				
Cubically–ordered mesoporous carbon				
Multi–walled CNTs	Commercially – purchased	Phenol, methylene blue, catechol, sulfachloropyridazine	• Catalytic activity of rGO> Nanodiamonds > Cubically–ordered mesoporous carbon> Multi–walled CNTs > GO > Diamond nanopowders • 100% of 20 mg L^{-1} phenol removed in 10 min with 0.10 g L^{-1} catalyst, T = 25 °C and 6.5 mM • 100% of 20 mg L^{-1} phenol (or 20 mg L^{-1} catechol or 20 mg L^{-1} sulfachloropyridazine or 10 mg L^{-1} methylene blue) removed in 10 min with 0.050 g L^{-1} catalyst, T = 25 °C and 6.5 mM	Duan et al. [203]
Cubically–ordered mesoporous carbon				
Diamond nanopowders				
Nanodiamonds	Annealing diamond nanopowders at 900 °C under N_2 atmosphere			
GO	Modified Hummers method			
rGO	Annealing GO at 900 °C under N_2 atmosphere			

The mechanism is explicitly-derived from the black-box approach. As there are many surface moieties with delocalized π-electrons, quantitative assessment of the performance of each surface moiety could be useful for the selection of a suitable and stable and stable AC for PMS activation. In a recent study, it is reported that modification of the AC surface with ammonia can increase the pyrrolic group which has a promotional effect on electron transfer for PMS activation [188]. However, AC might not be a durable catalyst as its adsorption capacity decreases with repeated use and the catalytic moieties such as carboxyl, carbonyl, quinones, lactones and phenols are susceptible to aggressive oxidation by both PMS and generated radicals [180,189]. The undesirable oxidation of the AC surface moieties decreases the effective utilization of the generated radicals and increases the surface acidity of AC due to the conversion of the surface moieties to carboxylic groups [164,190]. Post-treatment processes (e.g. heat treatment and/or chemical reactivation) are usually required to partially restore the adsorption capacity and catalytic activity of AC for reuse. Another class of carbonaceous material, which is the CNTs, has also been investigated as catalyst for various oxidation processes involving PS and PMS but CNTs are relatively more expensive and without modification, have limited advantage over AC [191,192].

Wang, Sun and co-workers [192–204] investigated the performance of various carbon-based catalysts including graphene and their derivatives, and carbon with different structural dimensions for PMS activation. Generally, PMS activation favors a basic surface and due to the high surface acidity of GO/rGO, chemical modification is usually required [78,205]. The chemically-modified graphene catalysts are regarded as good candidates for catalysis because they have (i) high theoretical specific surface area of $2600\,m^2\,g^{-1}$ (which is at least 2 times higher than that of the average specific surface areas of CNT and AC) for adsorption and catalysis, (ii) good electrical conductivity, and (iii) excellent electron mobility for redox reaction due to the high density sp^2 electrons [206–209]. It is reported that surface defective rGO ($I_D/I_G > 1.4$, defective to graphite) with smooth surface and zigzag edges contains high densities of redox active moieties with mobile π-electrons for PMS activation suggesting that increasing the defect density could have promotional effect on PMS activation (Fig. 5a) [198,210,211]. The surface ketonic group on rGO (in Fig. 5a) can undergo electron transfer reactions with PMS to produce $SO_4^{\bullet-}$ and $SO_5^{\bullet-}$. The effective catalytic active sites for rGO are the oxygen functional groups such as the nucleophilic ketonic and quinoidic groups which are electron rich and can mediate redox reactions [212,213]. The heterogeneous PMS activation by the oxygen functional groups of rGO was proposed as follows [197]:

$$C{=}C{=}O + HSO_5^- \rightarrow SO_4^{\bullet-} + C{=}C{-}O^+ + OH^- \quad (5.3)$$

$$C{=}C{-}O^+ + HSO_5^- \rightarrow C{=}C{=}O + SO_5^{\bullet-} + H^+ \quad (5.4)$$

The rGO activated with physical activation method (with CO_2) could performed significantly better (~2 times in rate) than the chemically – (with $ZnCl_2$) and physiochemically – activated (with CO_2 and $ZnCl_2$) rGO [214]. The better catalytic activity of physically activated rGO is because CO_2 promotes the formation of higher density of the oxygen functional groups and greater porosity (higher specific surface area and more defective edges) due to effective gasification compared to the activation by $ZnCl_2$ which leads to only dehydration and coking [215].

Comparing different pristine nanocarbon materials, it is reported that the 3D hexagonally-ordered mesoporous carbon was superior over other nanocarbon materials with different structural dimensions (i.e. 0D fullerence, 1D single-walled carbon nanotube, 2D graphene nanoplate, and cubically-ordered mesoporous carbon) owing to its high surface area and edge defects with high density of electronic states, a key factor to electron transfer reactions [195,216]. The ketonic moiety (C=O) is highly responsible for the high performance of 3D hexagonally-ordered mesoporous carbon as evidence by the 25% reduction in phenol removal rate with the reduction of ketonic moiety from 3.72 at.% to 0.05 at.% [195]. In another comparison of the carbon-based catalysts [203], it is reported that heat treatment of GO and nanodiamonds under N_2 atmosphere can improve their catalytic activities due to the increase in the density of defective edges, removal of excess oxygen functional groups and increase in the mobility of electrons for redox reactions.

The catalytic activity of carbon-based catalysts can be further enhanced by heteroatom doping (e.g. N, P, S or B) [193,194,196,199–202,204]. Doping carbon-based catalysts with heteroatom can (i) increase the defective edges, (ii) improve π-electron mobility through conjugation, (iii) alter the electron density in the local carbon atom, (iv) introduce new electrocatalytic active sites and functionalities (e.g. sites for selective adsorption), (v) increase surface hydrophilicity, and (vi) accelerate the catalytic electron transfer reaction with PMS [199,217–222]. It has been reported that the S, N-codoped rGO performed ~3 times better as PMS activator than the undoped rGO [201] while N-doped single-walled CNT has ~2 times higher catalytic activity than the undoped single-walled CNT [200]. After doping rGO with B and N heteroatoms, the B, N-codoped rGO is ~2 times more efficient as PMS activator than Co_3O_4 [199]. Similarly, simultaneous functionalization of CNTs with oxygenic functional groups (—COOH and —OH) and doping with N and S heteroatoms increases the pyridinic and pyrrolic N atoms, and thiophenic S atoms which improves the catalytic activity of CNTs by ~28.9 times [222]. However, excessive heteroatom doping is not recommended as it could be detrimental to the performance due to many factors such as blockage of zig–zag defects by B_2O_3 (for B doping) which is similar to that reported for multi-walled CNTs [223]. Future investigations of doped carbon-based catalysts could be further extended by doping with other electron donors (such a K and Rb) and acceptors (such as Br_2 and I_2) for performance enhancement [224,225].

While the carbon-based catalysts are potentially more sustainable alternatives to metal-based catalysts, the current shortcomings of carbon-based catalysts are (i) the low durability for long term use due to cannibalistic oxidation, and (ii) the high cost of certain carbon-based catalysts (e.g. CNTs and graphene etc.) compared to metal-based catalysts. Several reported studies show that the performance of carbon-based catalysts decreased significantly after first use (e.g. from 100% to 31% removal in 45 min for N-doped rGO [193] and 100% to 20% removal for N, B-codoped rGO [199]). The cannibalistic reaction after a single use also implies that the generated radicals are not fully utilized for pollutant degradation. As such, improving the durability of the carbon-based catalysts is anticipated to have a positive effect on the overall pollutant removal rate. The mechanisms of PMS activation involving carbon-based catalysts are also not fully understood. Besides radical-based mechanism involving $^{\bullet}OH$ and $SO_4^{\bullet-}$ generation, it has been reported that a nonradical pathway emerged along with the formation of both $^{\bullet}OH$ and $SO_4^{\bullet-}$ using N-doped single-walled CNT as the PMS activator (Fig. 5b) [194]. As indicated in Fig. 5b, PMS and phenol are first adsorbed on the electron rich sp^2 sites. This is then follow by the activation of PMS (either by radical or nonradical pathway) and subsequent degradation of phenol on the N-doped single-walled CNT surface. It is thought that the asymmetric PMS structure coupled with its relatively weak oxidation and adsorption on CNTs may be the contributing factor for the emergence of nonradical pathway [200]. The occurrence of radical and nonradical pathways depends on the type of carbon structure [203]. The sp^2 conjugation and ketonic groups promote the dissociation of PMS to generate $^{\bullet}OH$ and $SO_4^{\bullet-}$ for pollutant degradation. On the other hand, the presence of carbon networks with defective

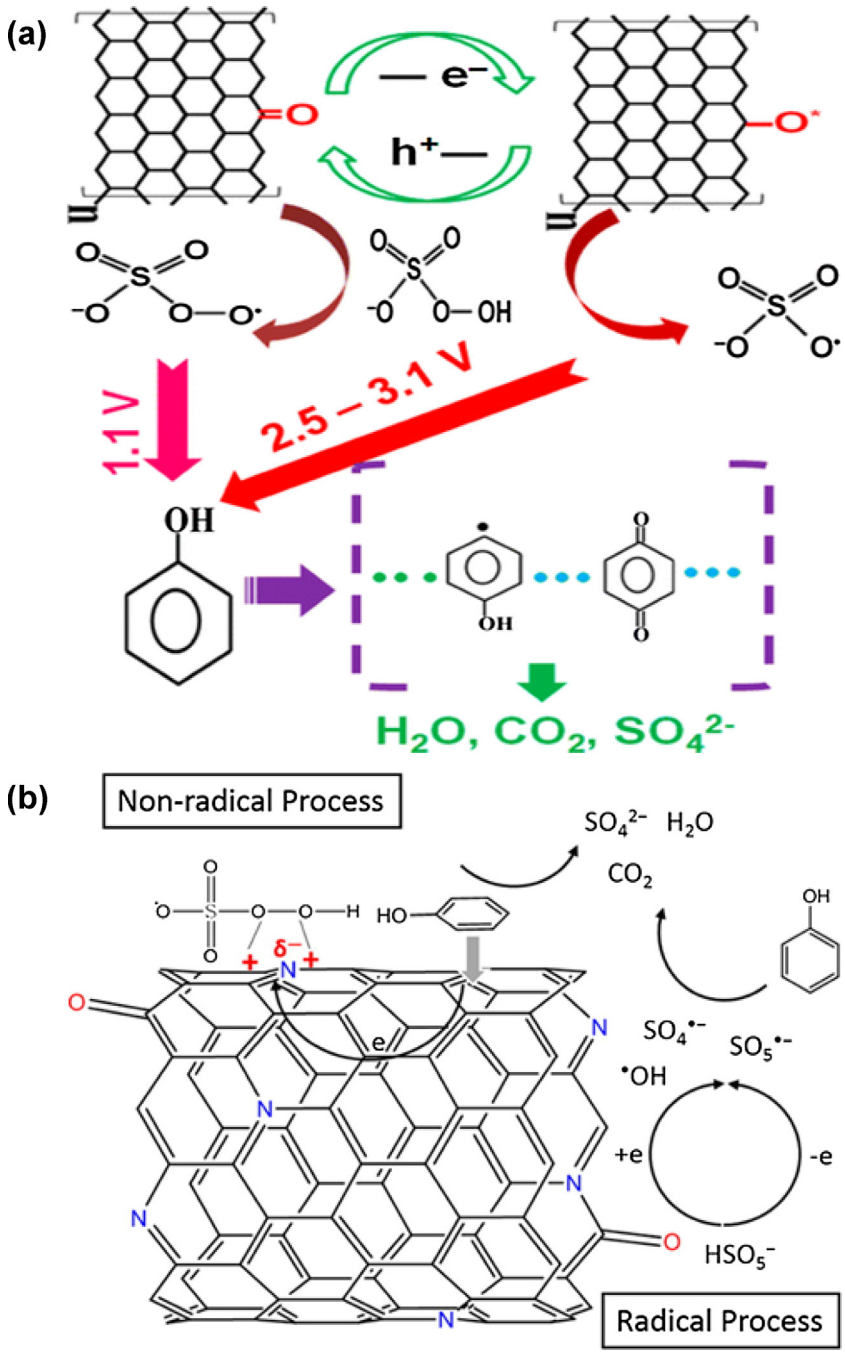

Fig. 5. (a) The mechanism of PMS activation by rGO for the degradation of phenol, and (b) The nonradical and radical mechanism of PMS activation by N-doped CNTs. Reprinted with permission from [198] and [194] for (a) and (b), respectively. Copyright 2016 American Chemical Society.

edges promotes nonradical pathway which have the advantages of being more selective in targeting organic contaminants, resistant to pH variation, and less influenced by the presence of water matrix species. In another study, singlet oxygen ($^1O_2$) has been detected as the dominant reactive radical during PMS activation by quinones [18]. Future investigation can be conducted to detect the generated radicals and ascertain the role of different surface functional groups in facilitating the nonradical pathway. This could allow the exploitation of the nonradical pathway which could be a potential solution to the cannibalistic oxidation. This also provides an attractive research opportunity for engineering heterogeneous carbon-based catalysts *via* chemical functionalization with specific functional groups such as quinones that could activate PMS.

6. Coupling heterogeneous catalyst/PMS system with other advanced oxidation processes

As summarized in Table 5 , several advanced oxidation processes such as ozonation, ultrasonic irradiation, UV–vis irradiation, and microwave irradiation have been integrated with the heterogeneous catalyst/PMS to form a hybrid AOP system. While the introduction of additional AOPs increase the complexity of the reaction system (e.g. difficulties to design, install, operate, optimize etc.), the hybrid systems have several potential advantages, namely (i) provide synergistic enhancement of the rate of organic contaminant degradation, and (ii) increase the PMS utilization efficiency (and minimize PMS dosage used) for organic contaminant degradation. However, prior to introducing additional AOPs, three

Table 5
Coupling heterogeneous catalyst/PMS system with other advanced oxidation processes.

Coupling heterogeneous catalyst/PMS with other processes	Catalyst	Model pollutant	Synthesis method	Conditions	Ref	Comments
UV–vis irradiation	Activated carbon (UV)	2,4,6–trichlorophenol	Commercial	>65% removal in 90 min, [2,4,6–trichlorophenol] = 50 mg L^{-1}, [Activated carbon] = 0.75 g L^{-1}, [PMS] = 8 mM, 6 W UV–C lamp ($\lambda_{max} \geq 253.7$ nm).	[319]	• PMS reacts with the photogenerated e^- or $O_2^{\bullet-}$ and to produce $SO_4^{\bullet-}$, and h^+ to produce $SO_5^{\bullet-}$ • PMS acts as an electron acceptor to effectively trap the photogenerated e^-, decreases e^-–h^+ pair recombinant while enhancing the quantum yield • PMS can also be activated directly by UV irradiation to produce $SO_4^{\bullet-}$ and $^{\bullet}OH$ • The UV–vis irradiation can enhance the regeneration of the active transition metal catalyst (Co^{3+} to Co^{2+}) by electron transfer from photogenerated e^- [232]
	$BiFeO_3$ (Vis)	Rhodamine B	Hydrothermal method	>60% removal in 40 min, [Rhodamine B] = 5 mg L^{-1}, [$BiFeO_3$] = 1.0 g L^{-1}, [PMS] = 5 mM, T = 25 °C, 500 W Xe lamp ($\lambda \geq 420$ nm).	[240]	
	OMS–2 (Vis)	Acid orange 7	Reflux method	>95% removal in 15 min, [Acid orange 7] = 40 mg L^{-1}, [OMS–2] = 0.20 g L^{-1}, [PMS] = 0.1 g L^{-1}, T = 25 °C, 300 W Xe lamp.	[146]	
	$CoFe_2O_4$/ZnO (Vis)	Direct blue 71	Co–precipitation method	>83% removal in 30 min, [Direct blue 71] = 0.040 mM, [$CoFe_2O_4$/ZnO] = 1.60 g L^{-1}, [PMS] = 0.20 mM, 150 W tungsten halogen lamp ($\lambda \geq 400$ nm).	[238]	
	$CoFe_2O_4$/TiO_2 (Vis)	Reactive Red 120	Co–precipitation method	>63% removal in 60 min, [Reactive Red 120] = 1×10^{-5} M, [$CoFe_2O_4$/TiO_2] = 4.0 g L^{-1}, 150 W tungsten halogen lamp ($\lambda \geq 400$ nm).	[231]	

Table 5
(*Continue*)

Coupling heterogeneous catalyst/PMS with other processes	Catalyst	Model pollutant	Synthesis method	Conditions	Ref	Comments
	Co–TiO_2 (UV–vis)	Rhodamine B	Sol gel method	100% removal in 50 min, [Rhodamine B] = 0.10 mM, [Oxone®] = 0.40 mM, [Co–TiO_2] = 1.0 g L^{-1}, pH = 6.9, 450 W high–pressure mercury lamp (center wavelength = 365 nm).	[232]	
	Co–$Bi_4Ti_3O_{12}$, Co–$ZnTiO_3$, Co–$FeTiO_3$ (UV–vis)	Phenol	Wet impregnation method	100% removal in 120 min, [Phenol] = 25 mg L^{-1}, [PMS] = 2.0 g L^{-1}, [Co–$Bi_4Ti_3O_{12}$ or Co–$ZnTiO_3$] = 0.50 g L^{-1}, 575 W metal halide lamp ($\lambda \geq 380$ nm).	[234]	
	TiO_2 (Vis)	Acid orange 7	Commercial P25	100% removal in 100 min, [Acid orange 7] = 0.10 mM, [PMS] = 2 mM, [TiO_2] = 1.0 g L^{-1}, 1000 W Xe lamp ($\lambda \geq 420$ nm).	[226]	
	TiO_2 (Vis)	Reactive Red 180	Commercial P25	> 80% removal in 90 min, [Reactive Red 180] = 5×10^{-5} M, [PMS] = 0.20 mM, [TiO_2] = 0.57 g L^{-1}, three 250 W tungsten–halogen lamp (λ = 395–2000 nm).	[228]	
	TiO_2 (UV)	Benzotriazole	Commercial P25	> 80% removal in 90 min, [Benzotriazole] = 0.30 mM, [PMS] = 5 mM, [TiO_2] = 1.0 g L^{-1}, four parallel 6 W UVC lamps.	[229]	
	Co–TiO_2 (UV)	2,4–dichlorophenol	Wet impregnation method	100% removal in 120 min, [2,4–dichlorophenol] = 50 mg L^{-1}, [PMS] = 0.92 mM, [Co–TiO_2] = 0.10 g L^{-1}, pH = 7.0, four 15 W low–pressure mercury UV lamps (λ = 300–400 nm).	[86]	
	Co–TiO_2 (Vis)	Rhodamine B	Sol gel method	100% removal in 50 min, [Rhodamine B] = 50 mg L^{-1}, [PMS] = 0.4 mmol, [Co–TiO_2] = 1.0 g L^{-1}, pH = 7.0, 1000 W Xe arc lamp ($\lambda \geq 420$ nm).	[230]	
	Co–TiO_2 (Vis)	Atrazine	Wet impregnation method	100% removal in 20 min, [Atrazine] = 0.10 mM, [PMS] = 0.10 mM, [Co–TiO_2] = 20 mg, pH = 5–6, Luzchem LZC–420 (lamp centered at 419 nm).	[26]	
	Co–TiO_2 (Vis)	Phenol	Sol gel method	100% removal in 80 min, [Phenol]/[PMS] = 10/1, [Co–TiO_2] = 1.0 g L^{-1}, pH = 7.0, 1000 W Xe arc lamp ($\lambda \geq 420$ nm).	[233]	

Table 5
(*Continue*)

Coupling heterogeneous catalyst/PMS with other processes	Catalyst	Model pollutant	Synthesis method	Conditions	Ref	Comments
	C–doped TiO_2 (Vis)	Reactive red 180	Sol gel method	>95% removal in 30 min, [Reactive red 180] = 5×10^{-5} M, [PMS] = 1 mM, [C–doped TiO_2] = 1.428 g L^{-1}, 250 W tungsten–halogen lamp (λ = 395–2000 nm).	[227]	
	Ag/Co_3O_4 (Vis)	Methyl blue	Hydrothermal method	>80% removal in 20 min, [Methyl blue] = 15 mg L^{-1}, [PMS] = 0.32 mM, [Ag/Co_3O_4] = 50 mg L^{-1}, 9 W fluorescent lamp.	[236]	
	Co_3O_4 (UV)	Phenol	Hydrothermal method	100% removal in 90 min, [Phenol] = 20 mg L^{-1}, [Oxone®] = 6.5 mM, [Co_3O_4] = 0.20 g L^{-1}, T = 25 °C, 575 W metal halide lamp.	[235]	
	γ–C_3N_4 (Vis)	Acid orange 7	Thermal decomposition of melamine	>80% removal in 30 min, [Acid orange 7] = 20 mg L^{-1}, [PMS] = 0.40 g L^{-1}, [γ–C_3N_4] = 0.40 g L^{-1}, T = 25 °C, 500 W Xe arc lamp.	[241]	
	$ZnFe_2O_4$ (Vis)	Orange II	Soft chemical process	>99% removal in 80 min, [Orange II] = 20 mg L^{-1}, [PMS] = 0.50 g L^{-1}, [$ZnFe_2O_4$] = 0.10 g L^{-1}, ambient T, visible light irradiation ($\lambda \geq$ 420 nm).	[242]	
	$ZnFe_2O_4$-rGO(Vis)	Orange II, methyl orange, methyl violet, rhodamine B, methylene blue	*in situ* chemical deposition and reduction	>80% removed in 180 min, [dye] = 20 mg L^{-1}, [PMS] = 0.50 g L^{-1}, [$ZnFe_2O_4$] = 0.10 g L^{-1}, T = 25 °C, 500 W Xe arc lamp, ($\lambda \geq$ 420 nm).	[243]	
	ZnO/MCM-22 (UV-Vis)	Phenol	Wet impregnation method	>50% removal in 150 min, [Phenol] = 25 mg L^{-1}, [PMS] = 2.0 g L^{-1}, [ZnO/MCM-22] = 0.50 g L^{-1}, T = 30 °C, 575 W metal halide lamp ($\lambda \geq$ 380 nm).	[239]	
	TiO_2/rGO, ZnO/rGO, Ta_2O_5/rGO (Vis)	Methylene blue	Deposition of metal on rGO.	>95% removed in 90 min. [Methylene blue] = 10 mg L^{-1}, [PMS] = 2.0 g L^{-1}, [catalyst] = 0.10 g L^{-1}, T = 25 °C, visible light lamp (λ = 400–1000 nm).	[237]	
	α–sulfur (Vis)	Rhodamine B	Disproportionation of $Na_2S_2O_3$ in acidic condition with Triton X–100	>99% removal in 60 min, [Rhodamine B] = 10 mg L^{-1}, [PMS] = 0.30 g L^{-1}, [α–sulfur] = 0.50 g L^{-1}, T = 40 °C, 150 W visible light lamp.	[244]	

Table 5
(*Continue*)

Coupling heterogeneous catalyst/PMS with other processes	Catalyst	Model pollutant	Synthesis method	Conditions	Ref	Comments
Ozonation	γ–MnO_2/rGO	4–nitrophenol	Hydrothermal method	100% removal in 50 min, [4–nitrophenol] = 50 mg L^{-1}, [γ–MnO_2/rGO] = 0.10 g L^{-1}, [PMS] = 0.5 g L^{-1}, ozone flow rate: 100 mL min^{-1}, [ozone] = 30 mg L^{-1}, T = 25 °C.	[245]	• PMS can accelerate the decomposition of ozone to form $SO_4^{\bullet-}$ and •OH [59,246] • Synergistic effect at optimum PMS and oxone dosages for organic pollutant degradation
Ultrasonic irradiation	Fe-Co/SBA-15	Orange II	*in-situ* auto combustion method	>99% removal in 120 min, [Orange II] = 0.30 mM, [Fe–Co/SBA–15] = 1.0 g L^{-1}, [PMS] = 3.2 mM, T = 20 °C, Ultrasound: 20 kHz, 950 W, P = 104.8 W L^{-1}.	[24]	• The optimum ultrasound irradiation increases the surface cleaning of the catalyst and has accelerated cavitation effect • PMS can also be activated directly by the acoustic cavitation phenomenon induced by the ultrasonic irradiation to produce $SO_4^{\bullet-}$ and •OH • The collapse of cavitation bubbles can produce •OH from the pyrolysis of water for pollutant degradation
	Co_3O_4	Amoxicillin	Commercial	>85% COD removal in 60 min, [Amoxicillin] = 0.12 mM, [Co_3O_4] = 0.060 g, [PMS] = 10 mM, T = 40 °C, pH = 6, Ultrasound: 20 kHz, 300 W.	[30]	
Microwave irradiation	$MnFe_2O_4$	4-nitrophenol	Co-precipitation	>95% removal in 120 s, [4-nitrophenol] = 20 mg L^{-1}, [PMS] = 2.0 mM, [$MnFe_2O_4$] = 2.0 g L^{-1}, microwave output = 500 W, pH = 7.0.	[247]	• Microwave irradiation increases the temperature of the water matrix for reaction • Microwave irradiation creates hotspots on the surface of the catalyst which enhances the PMS activation reaction

important issues have to be considered, namely (i) the impact of integrating additional AOPs on stability of the catalyst to prevent premature dissolution of metal ions, (ii) the ability to scale-up the hybrid system, and (iii) the additional treatment cost incurred due to the complex installation, operation and maintenance.

The hybrid system consisting of UV–vis irradiation and heterogeneous catalyst/PMS is the most widely investigated system. Various catalysts such as TiO_2 [226–229], supported TiO_2 [26,86,230–233], Co–$ZnTiO_3$ [234], Co_3O_4 [235], Ag/Co_3O_4 [236], supported ZnO [237–239], $BiFeO_3$ [240], γ-C_3N_4 [241], $ZnFe_2O_4$ [242,243], α-sulfur [244] and OMS-2 [146] have been developed to activate PMS in the presence of UV–vis irradiation. In general, PMS can be activated *via* three possible activation mechanisms in the heterogeneous catalyst/PMS/UV–vis system, namely (i) direct activation by UV irradiation, (ii) redox-based activation (Section 3, depending on the type of transition metal present), and (iii) heterogeneous photocatalytic activation. In a typical photocatalytic PMS activation process, the electron acceptors such as dissolved O_2 and PMS can scavenge the photogenerated e^- to produce $O_2^{\bullet-}$ and $SO_4^{\bullet-}$, respectively, while reducing the undesired e^-/h^+ recombination. The h^+ may react with H_2O and PMS to produce •OH and $SO_5^{\bullet-}$, respectively. In some cases, the photogenerated e^- can also enhance the regeneration of the active transition metal (i.e. Co^{3+} to Co^{2+}) by transferring the photogenerated e^- to the transition metal [232]. While the synergistic effect seems to have a promising potential for future application, the development of the catalyst for the hybrid heterogeneous catalyst/PMS/UV–vis system is still in its infancy and further development of novel catalyst is warranted. As the main working mechanisms are expected to be mechanisms (ii) and (iii), it is important for the catalyst to have a bi-functional role as a photocatalyst and PMS activator to fully exploit the synergistic effect.

The hybrid system consisting of heterogeneous catalyst/PMS/ozone has been previously investigated with γ-MnO_2/rGO as the catalyst [245]. The addition of ozone can increase the generation of reactive radicals in the reaction system as ozone can also activate PMS to generate both $SO_4^{\bullet-}$ and •OH [59,246]. An optimum condition is required to prevent the self-scavenging reactions of the various reactive oxygen species. However, except for catalyzing ozone decomposition, the contribution of heterogeneous catalyst in this hybrid system is not clearly understood.

Other hybrid systems coupling either ultrasonic (US) [24,30] or microwave (MW) [247] irradiation with heterogeneous catalyst/PMS processes have also been reported to have a positive effect on the rate of pollutant removal due to the increase in the dynamics of the reaction matrix. For instance, besides accelerating surface cleaning of the catalyst for redox reaction to occur, the US irradiation creates acoustic cavitation bubbles in water which, upon collapse, generate $SO_4^{\bullet-}$ and •OH are generated from PMS and pyrolysis of water [248]. The MW irradiation increases the water temperature and creates hotspots on the catalyst surface for accelerated PMS activation and redox reactions. However, when the dynamics of the reaction system increases, it is important to consider the stability of the catalyst to avoid premature dissolution of metal ions. Because the mechanism of PMS activation can vary in different systems, design of a novel catalyst with the desired properties is beneficial to fully exploit the advantage of these hybrid systems.

7. Identification of reactive radicals

In SR-AOP system, •OH and $SO_4^{\bullet-}$ co-exist and participate in oxidation reactions. Due to the differences in their reactivities with target pollutants, it is important to identify the principal reactive radical in a SR-AOP system because it has a direct implication on the associated pollutant degradation pathways, intermediates formed, degradation efficiencies and rates. Generally, the two common strategies to discriminate between the contributions of •OH and $SO_4^{\bullet-}$ in the SR-AOP system are (i) direct use of chemical probes or spin trapping agents to react with the short-lived radicals and subsequent detection of the reaction byproducts and/or radical-adduct using various analytical tools, and (ii) indirect competitive kinetic approach using selective chemical probes.

7.1. Use of chemical probes or spin trapping agents

The short-lived $SO_4^{\bullet-}$ can be distinguished qualitatively/semi-quantitatively from other radicals by reacting $SO_4^{\bullet-}$ with a chemical probes or spin trapping agent to form a reaction byproducts or $SO_4^{\bullet-}$–adduct, which can then be detected using analytical tools. To date, the most prevalently–used direct technique for $SO_4^{\bullet-}$ detection in heterogeneous catalysts/PMS (or PS) system involves spin trapping $SO_4^{\bullet-}$ with 5,5-dimethyl-1-pyrroline N-oxide (DMPO) follow by subsequent detection of the $SO_4^{\bullet-}$–adduct with electron spin resonance (ESR) spectroscopy. The main challenges of using DMPO are the poor stability of $SO_4^{\bullet-}$–DMPO and low concentration of the generated $SO_4^{\bullet-}$ making it unsuitable for quantitative analysis. The $SO_4^{\bullet-}$–adduct formed from the nucleophilic addition reaction of $SO_4^{\bullet-}$ with DMPO or other common spin trapping agents (e.g. 5-diethoxyphosphoryl-5-methyl-1-pyrroline-N-oxide and 3,3,4,4-tetramethyl-1-pyrroline N-oxide) react undesirably with H_2O/OH^- *via* nucleophilic substitution reaction to yield their corresponding •OH–adducts at a considerably fast reaction rate (e.g. $t_{1/2}$ of $SO_4^{\bullet-}$–DMPO = 95 s in water) [249–253].

$$SO_4^{\bullet-} + DMPO \rightarrow SO_4^{\bullet-}\text{–}DMPO \rightarrow {}^{\bullet}OH\text{–}DMPO \quad (7.1.1)$$

Fang et al. [254] employed DMPO as the spin trapping agent for semi-quantitative detection of $O_2^{\bullet-}$ and $SO_4^{\bullet-}$ using ESR but observed declined in the $SO_4^{\bullet-}$–DMPO and $O_2^{\bullet-}$–DMPO intensities with reaction time which could also be attributed to the poor stability of the radical adducts in water. Although it has been reported that the stability of $SO_4^{\bullet-}$–DMPO can be increased by conducting the study using a different solvent systems such as the aprotic dimethyl sulfoxide (DMSO) solvent ($t_{1/2}$ of $SO_4^{\bullet-}$–DMPO = 2 h in DMPO), the finding might not reflect the actual process occurring in the aqueous SR-AOP systems [255]. Other investigated spin trapping agents such as N(1)-substituted pyrimidines interact with $SO_4^{\bullet-}$ to form $SO_4^{\bullet-}$–adduct but the radical adduct can decay undesirably *via* two pathways, namely direct S_N2 reactions and S_N1 reactions (*via* base radical-cation intermediates) to form neutral radicals [256]. Maleic acid and fumarate have also been reported to react with $SO_4^{\bullet-}$ to form $SO_4^{\bullet-}$–adduct in water [257–259]. There is no $SO_4^{\bullet-}$–adduct formed when either benzylidene-*tert*-butylamine N-oxide or 1-oxido-4-pyridylmethylene-*tert*-butylamine N-oxide was used as the spin trapping agent for $SO_4^{\bullet-}$ [249].

To the best of our knowledge, there are limited studies on the use of non-ESR detection technique for $SO_4^{\bullet-}$ quantification. Indeed, besides ESR, there are other •OH quantification techniques which may be also appropriate for $SO_4^{\bullet-}$ quantification. For instance, quantitative •OH determination has been conducted by measuring the concentration of the byproducts formed (which is proportional to the concentration of OH) from the reaction between •OH with chemical probes such as 1,5-diphenylcarbohydrazide [260], benzoic acid [261], dimethyl sulfoxide [262], *p*-chlorobenzoic acid [263–265], terephthalate [266], *p*-nitrosodimethylaniline [267], coumarin and its derivatives [268,269], and salicylic acid [270,271] using high performance liquid chromatography, spectrophotometer, photoluminescence spectrometer and fluorescence spectrometer in various aqueous systems. Similarly, $SO_4^{\bullet-}$ can be quantified by detecting the oxidation byproducts formed from the reaction of $SO_4^{\bullet-}$ with a chemical probe. In general, any organic chemical probe can be employed provided that (i) it can react with $SO_4^{\bullet-}$ to produce a stable, quantifiable byproduct, (ii) it is stable to oxidation by PMS, and (iii) it does not affect the catalyst activity (e.g. deposit/adsorb onto and deactivate the catalyst, participate in the reaction with the target pollutant etc.). Because of the selectivity of $SO_4^{\bullet-}$, the byproducts formed from $SO_4^{\bullet-}$ oxidation are expected to be more specific and less diverse compared to those produced from the oxidation by •OH. However, the reaction needs to be carried out either in the presence of OH scavengers or under acidic condition whereby the OH contribution is not prevalent.

7.2. Competitive kinetic approach

7.2.1. Determination of principal reactive radicals

In the reaction systems dominated by •OH and $SO_4^{\bullet-}$, methanol (MeOH) and ethanol (EtOH) are commonly used as chemical scavengers to suppress the contributions of both •OH and $SO_4^{\bullet-}$ due to their reactivities with $SO_4^{\bullet-}$ ($k_{SO_4^{\bullet-}+MeOH} = 3.2 \times 10^6 M^{-1}s^{-1}$ for MeOH and $k_{SO_4^{\bullet-}+EtOH} = 1.6 \times 10^7 M^{-1}s^{-1}$ for EtOH) and •OH ($k_{\bullet OH+MeOH} = 9.7 \times 10^8\ M^{-1}\ s^{-1}$ for MeOH and $k_{\bullet OH+MeOH} = 1.9 \times 10^9\ M^{-1}\ s^{-1}$ for EtOH) [44,50]. Apparently, EtOH is a better choice compared to MeOH because MeOH has a lower reactivity with $SO_4^{\bullet-}$ and its α-hydrogen can react with $SO_4^{\bullet-}$ to produce •CHOH which could decompose PMS [20,272,273]. Other chemical scavengers used that have good reactivities with •OH and $SO_4^{\bullet-}$ are phenol [274], *m*-toluic acid [275], anisole[276], atrazine [59] and isopropanol [277]. Generally, as long as the chemical scavenger is stable, does not affect the catalysts and has considerably good reactivities with •OH and $SO_4^{\bullet-}$ compared to other oxidants in the system, it can be employed to scavenge both •OH and $SO_4^{\bullet-}$.

The relative contributions of •OH and $SO_4^{\bullet-}$ in SR-AOP systems can be quantified using an indirect kinetic approach with the aid of selective chemical scavengers. Given the high reactivities of •OH and $SO_4^{\bullet-}$ with many organics, the choices of chemical scavengers for selective quenching of either •OH or $SO_4^{\bullet-}$ is limited. For the determination of the contribution of $SO_4^{\bullet-}$, the correct strategy is to eliminate •OH contribution using a chemical scavenger selective to •OH. In general, the chemical scavenger selective to •OH should have the following properties: (i) a large difference in reactivities of the chemical scavenger with •OH or $SO_4^{\bullet-}$ (at least 3-order of magnitude in variation), (ii) no significant reaction with other coexisting oxidants (PS or PMS), and (iii) not affecting the catalyst activity (e.g. deposition/adsorption onto catalyst surface which deactivates the catalyst, participate in reaction with target pollutant, etc.). Besides selecting appropriate radical scavengers, the concentration of scavenger should be also carefully selected based on the reactivities of the target pollutant with •OH and $SO_4^{\bullet-}$. Generally, the pollutant-to-chemical scavenger (selective to •OH) molar ratio of 1:20 is required to avoid interference of the chemical scavenger with the reaction system (e.g. undesired quenching of $SO_4^{\bullet-}$).

Many investigators employed *tert*-butyl alcohol (TBA) as a selective •OH scavenger to discriminate between the contributions of •OH and $SO_4^{\bullet-}$ in the overall pollutant degradation in SR-AOP systems [6,96,102,278–281]. TBA has a poor reactivity with $SO_4^{\bullet-}$ ($k_{SO_4^{\bullet-}+TBA} = 4.0 \times 10^5 M^{-1}s^{-1}$) but considerably good

reactivity with •OH ($k_{•OH+TBA} = 6.0 \times 10^8 M^{-1}s^{-1}$) [44,50]. This is because TBA is more susceptible to the hydrogen abstraction by •OH while $SO_4^{•-}$ reacts preferentially through the electron transfer reaction [282]. The selectivity of $SO_4^{•-}$ for electron transfer reaction has been observed using TBA as •OH scavenger in SR-AOP system [283]. A possible drawback of employing TBA for •OH scavenging in the heterogeneous system is that the hydrophilic TBA could be adsorbed onto the surface of the catalyst leading to the decrease of catalytic active sites [163,284]. TBA can also react with PS [274]. Nitrobenzene (NB) is another alternative chemical scavenger which can be applied at a wide range of pH (pH 2–12) for scavenging •OH and has a large variation of reactivities with $SO_4^{•-}$ ($k_{SO_4^{•-}+NB} < 10^6 M^{-1}s^{-1}$) and •OH ($k_{•OH+NB} = 3.9 \times 10^9 M^{-1}s^{-1}$) [43,44,274]. Other potential chemical scavengers with a large difference in reactivities with •OH and $SO_4^{•-}$ are aromatic compounds with strong deactivating substituents/electron withdrawers (–NO_2, –CF_3, etc.) such as 4-nitrobenzoic acid ($k_{SO_4^{•-}+4-NB} < 10^6 M^{-1}s^{-1}$) [43,58].

The relative contributions of •OH and $SO_4^{•-}$ can be determined by comparing the difference in the (i) removal efficiencies, and (ii) rate constants of the pollutant removal with and without •OH scavenger addition.

$$\%\ \text{concentration of}\ SO_4^{•-} = \frac{\%\text{removal (or rate constant) with}\ ^{•}OH\ \text{scavenger}}{\%\text{removal (or rate constant) without scavenger}} \times 100\% \quad (7.2.1.1)$$

The calculation from the rate constants is more practical as the calculation based on the removal efficiencies is time–dependent [285].

7.2.2. Estimation of steady-state $SO_4^{•-}$ concentration

The SR-AOP system can be characterized by determining the steady-state $SO_4^{•-}$ concentration, $[SO_4^{•-}]_{ss}$. The $[SO_4^{•-}]_{ss}$ provides an indication of the efficiency of the reaction system in generating $SO_4^{•-}$. This allows quantitative parametric study of various factors influencing generation $SO_4^{•-}$ (pH, PMS/PS dosage, catalyst loading etc.) in SR-AOP systems. Assuming steady-state •OH ($[•OH]_{ss}$) and $SO_4^{•-}$ concentrations under excess PMS condition (e.g. PMS:probe molar ratio of > 20:1), the change in chemical probe concentration as a function of $[•OH]_{ss}$ and $[SO_4^{•-}]_{ss}$ can be described as follows:

$$\frac{dC_p}{dt} = -\left(k_a\left[^{•}OH\right]_{SS}C_p + k_b\left[SO_4^{•-}\right]_{ss}C_p\right) \approx -k_{a+b1}C_p \quad (7.2.2.1)$$

where C_P is the chemical probe concentration, k_a and k_b are the second–order rate constants of reaction between chemical probe with •OH and $SO_4^{•-}$, respectively, and k_{a+b1} is the apparent first–order rate constant. In the presence of selective •OH scavenger such that $[•OH]_{ss}$ is negligible, the expression becomes:

$$\frac{dC_P}{dt} = -k_b\left[SO_4^{•-}\right]_{ss}C_P \approx -k_{a+b2}C_P \quad (7.2.2.2)$$

where k_{a+b2} is the apparent first-order rate constant. The relative contributions of •OH and $SO_4^{•-}$ can be determined by calculating k_{a+b2}/k_{a+b1} while $[SO_4^{•-}]_{ss}$ can be estimated by comparing the k_{a+b2} with k_b at excess PMS condition. The k_b value for various pollutants can be obtained from the literature [43,50] or *via* a competitive kinetic approach. In our previous study, the estimated $[SO_4^{•-}]_{ss}$ for the heterogeneous $CuBi_2O_4$/PMS system at 1.7×10^{-12} M (pH 7.0, 0.5 g L^{-1} $CuBi_2O_4$ and 0.2 g L^{-1} PMS) [173]. For comparison, the reported $[SO_4^{•-}]_{ss}$ for other systems (homogeneous SR–AOP) are presented in Table 6.

8. Challenges and control strategies

8.1. Formation of XO_3^- (X = Cl^- and Br^-) and halogenated disinfection byproducts

8.1.1. Mechanisms of formation

In SR-AOPs, Cl^-/Br^- can potentially be oxidized in the water matrix to form ClO_3^-/BrO_3^- *via* $SO_4^{•-}$–induced oxidation reactions. This is highly–undesirable because ClO_3^- and BrO_3^- are toxic and potentially carcinogenic [286]. In general, $SO_4^{•-}$ reacts with X^- (X = Cl and Br) in water to form X• which can be subsequently oxidized to HOX and XO_3^- through a series of reactions as follow (Fig. 6a) [15,56–58,287–289]:

$$SO_4^{•-} + X^- \rightarrow X^{•} + SO_4^{2-} \quad (8.1.1.1)$$

$$X^- + X^{•} \rightarrow X_2^{•-} \quad (8.1.1.2)$$

$$X_2^{•-} + X^{•} \rightarrow X_2 + X^- \quad (8.1.1.3)$$

$$X_2^{•-} + X_2^{•-} \rightarrow X_2 + 2X^- \quad (8.1.1.4)$$

$$X^{•} + X^{•} \rightarrow X_2 \quad (8.1.1.5)$$

$$X_2 + H_2O \leftrightarrow HOX + H^+ + X^- \quad (8.1.1.6)$$

$$HOX + SO_4^{•-} \rightarrow XO_3^- \quad (8.1.1.7)$$

Peroxymonosulfate can react very slowly with X^- to form X_2 and HOX, which are also XO_3^- precursors [57,287,290,291] (8.1.1.8).

$$HSO_5^- + X^- \rightarrow HOX + SO_4^{2-} \quad (8.1.1.8)$$

$$HSO_5^- + 2X^- \rightarrow X_2 + SO_4^{2-} + H_2O \quad (8.1.1.9)$$

In the presence of DOM, the halide species/radicals (e.g. $X_2^{•-}$, X•, HOX etc.) can react with DOM to produce HDBPs [292,293]. When both halides are present in the water matrix, brominated DBPs are formed preferentially over chlorinated DBPs because (i) Br^- has a higher reactivity than Cl^-, and (ii) Br^- can replace Cl^- in chlorinated DBPs *via* SN2 reaction. If excessive $SO_4^{•-}$ is generated, the HDBPs will be further degraded to release X^- which ultimately ends up as XO_3^- [57].

8.1.2. Potential control strategies

Fig. 6b shows several potential strategies to mitigate XO_3^- in heterogeneous catalyst/PMS system, namely (i) employment of a secondary treatment unit after $SO_4^{•-}$ oxidation, (ii) kinetic control of the formation rate of XO_3^-, and (iii) use of novel heterogeneous catalysts. The secondary treatment unit such as activated carbon adsorption and biological activated carbon [294,295] after $SO_4^{•-}$ oxidation can be implemented to remove XO_3^- and HDBPs. However, it is not desirable primarily because it could lead to the increase in treatment cost [296].

Kinetic control with pH adjustment and chemical addition before $SO_4^{•-}$ oxidation can be employed to reduce the formation rate of XO_3^-. It has been reported that Cl• is readily transformed to ClO_3^- at pH < 5 but react preferably with water to form •OH at pH > 5 [55]. Similarly, contrary to the trend of BrO_3^- formation at different pHs in the ozonation process [297], BrO_3^- formation rate during $SO_4^{•-}$ oxidation decreases ~90% with the increase of pH from 7 to 9 due to the relatively slower conversion of Br• to HOBr/BrO^- at higher pH [56]. This indicates that the XO_3^- formation rate can be decreased by increasing the reaction pH. Increasing the reaction pH is also advantageous to the heterogeneous catalyst/PMS system because the stability of the heterogeneous catalyst and treatment efficiency generally increase with increasing pH [82].

Chemical addition of bicarbonate/carbonate anion can be used to quench Cl• which is a primary precursor for the formation of ClO_3^-. While HCO_3^-/CO_3^{2-} can react with $SO_4^{•-}$ (~10^6 M^{-1} s^{-1}),

Table 6
Comparison of the steady state $SO_4^{\bullet-}$ concentration, $[SO_4^{\bullet-}]_{ss}$, for various systems.

System	Chemical probes	Findings	Reference
$CuBi_2O_4$/PMS	Benzene	$[SO_4^{\bullet-}]_{ss} = 1.7 \times 10^{-12}$ M at pH 7.0, 0.2 g L^{-1} PMS, 2.5 mg L^{-1} benzene, and 0.5 g L^{-1} catalyst	Oh et al. [173]
UV_{254}/PMS	Benzoic acid, nitrobenzene	Relative quasi–stationary concentration of $SO_4^{\bullet-}$ (RQSC) = $[SO_4^{\bullet-}]_{ss}/(\varphi I_0/V)$ where $I_0 = 1.5 \times 10^{-6}$ E s^{-1}, and ϕ is the apparent quantum yield RQSC = $\sim 10^{-6}$ s at pH 6–12, 9.90 μM benzoic acid, 100 μM PMS	Guan et al. [20]
UV_{254}/PS UV_{254}/PMS	Atrazine	UV_{254}/PS, $[^{\bullet}OH]_{ss}+[SO_4^{\bullet-}]_{ss} = \sim 10^{-12}$–$10^{-13}$ M, pH = 5.88 UV_{254}/PMS, $[^{\bullet}OH]_{ss}+[SO_4^{\bullet-}]_{ss} = \sim 10^{-13}$, pH = 3.65 $I_0 = 1.291 \times 10^{-7}$ E L^{-1} s^{-1}, 0.1–0.5 mM oxidant, 2–6 μM atrazine $[SO_4^{\bullet-}]_{ss}$ is influenced negatively by increasing atrazine concentration and positively by oxidant concentration	Luo et al. [320]
UV_{254}/PS	Acetic acid	pH 2–5, $[SO_4^{\bullet-}]_{ss} = \sim 10^{-9}$ M pH 7–9, $[SO_4^{\bullet-}]_{ss} = \sim 10^{-10}$ M 500 μM acetic acid, 1800 μM PS and incident UV irradiation intensity, $I_0 = 9.9 \times 10^{-6}$ E s^{-1})	Criquet and Leitner [321]
UV_{254}/PS	Nitrobenzene, *p*–nitrobenzoic acid, *m*–toluic acid	$[SO_4^{\bullet-}]_{ss} = 3.10 \times 10^{-13}$ M and $[^{\bullet}OH]_{ss} = 1.84 \times 10^{-14}$ M at 0.1 mW cm^{-2} UV irradiation, 5 mM phosphate buffer (pH = 7.4), 1 mM PS, 50 μM initial organic compound	He et al. [275]
Thermal activation of PS	Methylene blue	pH 3, $[SO_4^{\bullet-}]_{ss} = \sim 10^{-6}$ M pH 7, $[SO_4^{\bullet-}]_{ss} = \sim 10^{-11}$ M and $[^{\bullet}OH]_{ss} = \sim 10^{-10}$ M pH 11, $[^{\bullet}OH]_{ss} = \sim 10^{-6}$ M T = 60–80 °C, $[MB]_0 = 10^{-6}$ M	Liang and Huang [51]
Photo-iron(II) sulfite	Acid orange 7, benzotriazole	$[SO_4^{\bullet-}]_{ss} = 5.3 \times 10^{-14}$ M with illumination and $[SO_4^{\bullet-}]_{ss} = 1.0 \times 10^{-14}$ M without illumination. $[Fe^{2+}]_0 = 0.1$ mM, $[Na_2SO_3]_0 = 1.0$ mM, $[AO7]_0 = 0.029$ mM, $[DO]_0 = 0.28$ mM, pH = 6.1, 255 mW cm^{-2} UV–vis irradiation	Zhou et al. [322]

it is generally at least 100 times slower than its reaction with $Cl^{\bullet}$ ($\sim 10^8$ M^{-1} s^{-1}) [298].

$$HCO_3^- + Cl^{\bullet} \rightarrow HCl + CO_3^{\bullet}, k_{Cl^{\bullet}+HCO_3^-} = 2.2 \times 10^8 M^{-1} s^{-1} \quad (8.1.2.1)$$

$$HCO_3^- + Cl^{\bullet} \rightarrow HCl + CO_3^{\bullet}, k_{Cl^{\bullet}+HCO_3^-} = 2.2 \times 10^8 M^{-1} s^{-1} \quad (8.1.2.2)$$

The strategy similar to BrO_3^- control in ozonation process with ammonia addition and chlorine/ammonia process can be adopted for BrO_3^- control in SR-AOPs [299,300]. In this method, chemical addition of ammonia masks Br^- as NH_2Br which prevents it from being readily available to react with $SO_4^{\bullet-}$. Controlled DOM addition prior to $SO_4^{\bullet-}$ oxidation can also be implemented to eliminate XO_3^- precursors but this also leads to the formation of HDBPs [301]. The DOM contains many aromatic moieties that can react with $SO_4^{\bullet-}$ to form $O_2^{\bullet-}$ which could be used to reduce HOX [58]. The chemical addition method for XO_3^- control is more suitable for the heterogeneous system because homogeneous catalysts could precipitate when external chemicals (such as ammonia) are introduced.

The use of heterogeneous catalyst for $SO_4^{\bullet-}$ generation from PMS (or PS) provides a unique solution to mitigate XO_3^- and HDBPs because the catalyst can be engineered to have attractive features that can be used to reduce/remove XO_3^- and HDBPs. It has been reported that the heterogeneous catalyst incorporating adsorptive activated carbon can reduce the inhibitory effect induced by anions on pollutant degradation [164,302]. As adsorption can bring the pollutant to close proximity with the catalytic reaction sites, the generated $SO_4^{\bullet-}$ can be utilized more effectively for pollutant degradation and the undesired reactions between $SO_4^{\bullet-}$ and X^- are minimized. The heterogeneous catalyst can also be modified to have adsorption affinities for XO_3^- and HDBPs (e.g. decorating the catalyst on LDH, activated carbon, ion exchange etc.) to remove XO_3^- and HDBPs directly if they are formed [303]. It is known that certain organic moieties can react with $X^{\bullet}$ to form halogenated compounds such as for the case of DOM [15,288,301].

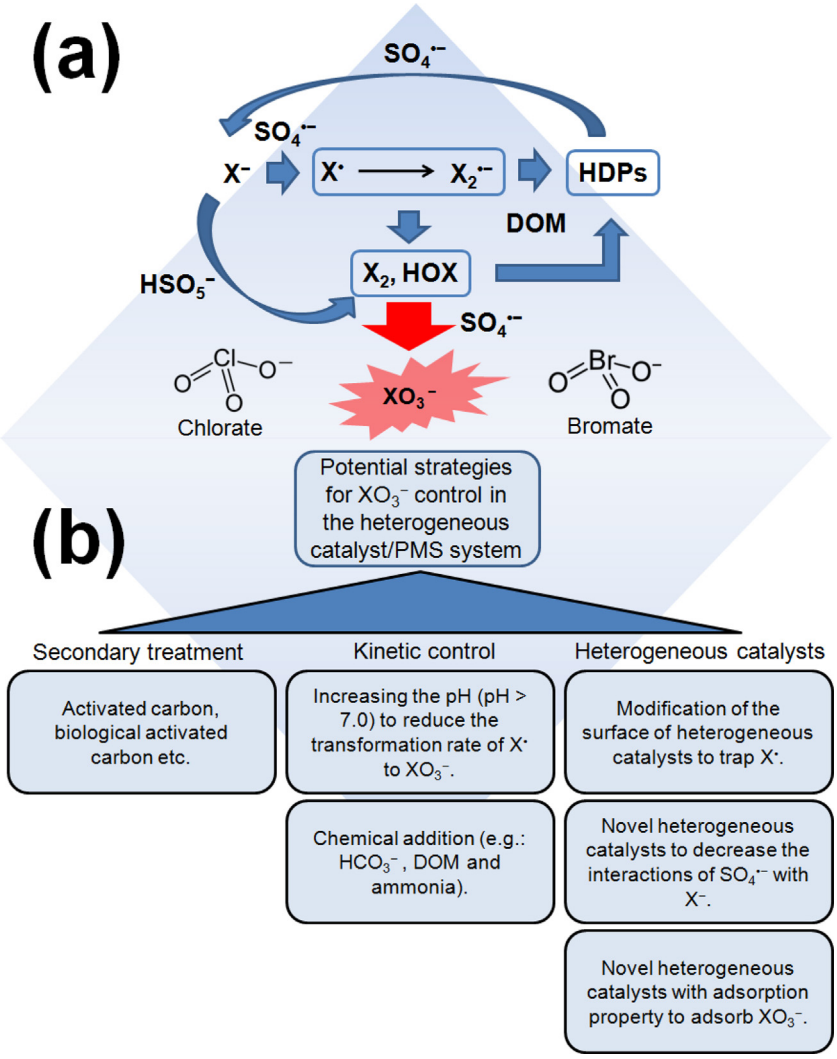

Fig. 6. (a) General transformation of X^- (X = Cl^- and Br^-) to XO_3^- and (b) potential strategies for XO_3^- control in the heterogeneous catalyst/PMS system.

In this regards, it is anticipated that by introducing these organic moieties in the heterogeneous catalyst (e.g. *via* chemical functionalization of rGO, CNT, etc.), $X^\bullet$ can be trapped on the surface of the catalyst and hence effectively inhibits the formation of XO_3^-.

8.2. Sulfate and residual PMS

Sulfate anion is generated as a principal byproduct from the catalytic oxidation reaction between $SO_4^{\bullet-}$ and organic pollutants. The US EPA secondary maximum contaminant level for SO_4^{2-} in drinking water is 250 mg L^{-1} [304] corresponding to ~400 mg L^{-1} (0.65 mM) of Oxone® dosage. Depending on the application, the Oxone® dosage is more than sufficient to oxidize any target pollutants (at μg L^{-1} level) without exceeding the 250 mg L^{-1} of SO_4^{2-} limit in drinking water. However, in cases where SO_4^{2-} in water needs to be removed, ion exchange [305] method is the most applicable technique mainly because it is simple and effective. The SO_4^{2-} concentration in the SR-AOP system is typically low and it will not exhaust the ion exchange capacity at a considerable rate. Other techniques such as crystallization/precipitation technology [306], and biological desulfurization of SO_4^{2-} [307,308] can also be employed. However, crystallization/precipitation technology is more effective for treatment at a higher range of SO_4^{2-} concentration while biological desulfurization coverts SO_4^{2-} to H_2S which is a toxic and volatile gas. It is interesting to note that it is more desirable to remove the residual PMS in water due to its potential hazard and relatively high oxidation potential. While excess PMS can be transformed to SO_4^{2-} by continuous redox reaction with catalyst until all the PMS has been consumed, it has inherent negative effect on the stability of the heterogeneous catalyst. A possible way to remove residual PMS in water is by chemical oxidation of PMS with SO_3^{2-} to become SO_4^{2-} [74].

$$HSO_5^- + SO_3^{2-} \rightarrow H^+ + 2SO_4^{2-} \quad (8.2.1)$$

An additional advantage of using SO_3^{2-} for residual PMS removal is that it can also be photoactivated with UV_{254} to generate hydrated electron for advanced reduction of BrO_3^- [309].

9. Application of heterogeneous catalyst system

To date, studies on the PMS and PS activation by heterogeneous catalysts are limited to the bench-scale batch system. For practical application, future studies can be extended to develop practical design for the heterogeneous catalytic reactor systems based on batch or continuous flow (e.g. completely mixed or plug flow) reactor configuration with catalyst recovery. There are three main ways to retain and recover the catalyst from the treated water, namely (i) sedimentation, (ii) magnetic separation, and (iii) membrane separation. Gravitational sedimentation of the catalyst is the most cost effective option but it is difficult to

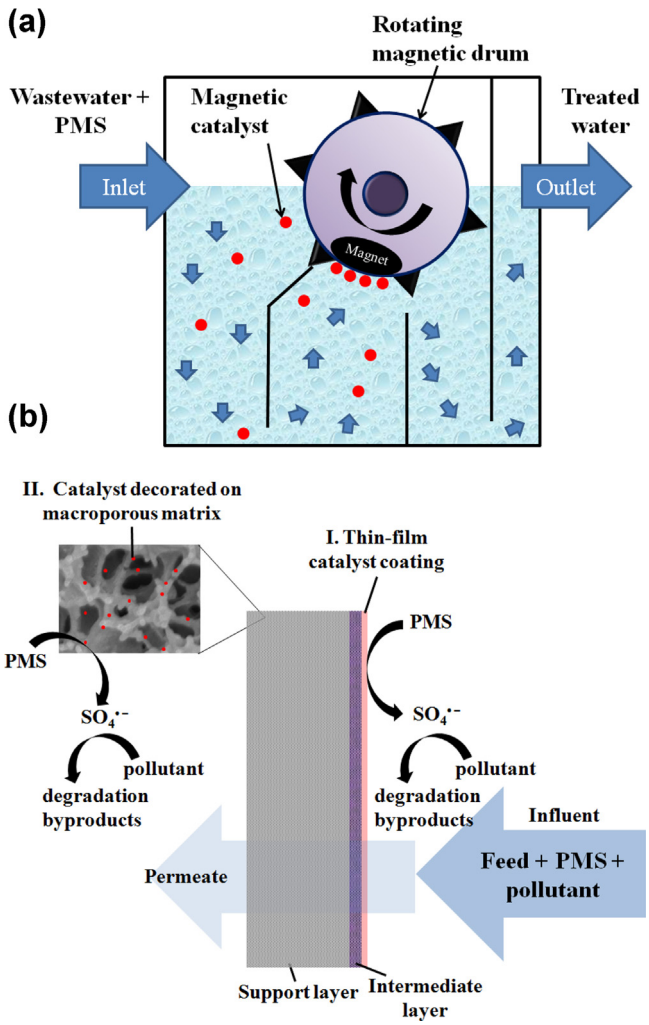

Fig. 7. (a) The possible reactor configuration for heterogeneous magnetic catalyst/PMS system, and (b) two schemes to incorporate catalyst nanoparticles in the ceramic membrane module.

implement because, in general, nanocatalysts have low settling velocity. However, if the catalyst exhibits weak ferromagnetism, its sedimentation can be enhanced through external magnetic field. For (ii), magnetic catalysts, such as $CuFe_2O_4$ and $CoFe_2O_4$, have been extensively reported as effective PMS activators (Section 4.2). These catalysts can be separated from the treated water by incorporating magnetic separator as shown in Fig. 7a. Further enhancement of the performance of the magnetic catalyst can be achieved by immobilization the catalyst on adsorbent to promote synergistic adsorption and $SO_4^{\bullet-}$ oxidation. When magnetic separation is not feasible, a membrane module can be incorporated in the hybrid membrane-catalytic reactor similar to the membrane reactors we proposed in our previous study [310,311]. Ceramic membrane is preferred over polymeric membrane because of its better chemical and mechanical stabilities [312].

Alternatively, the heterogeneous catalyst can be immobilized on the membrane support (typically microfiltration or ultrafiltration type ceramic membrane) to produce an intrinsically catalytic membrane with PMS/PS activation and membrane separation dual functionality for a continuous flow-through operation. Several reported catalytic membranes decorated with metal oxide catalysts (MnO_2–Co_3O_4 [313], iron oxide [314] and Mn oxide [315,316]) have the potential to be employed as catalytic membranes with PMS activation functionality. We have also developed several catalytic ceramic membranes with almost defect–free coating using sol–gel technique [317,318]. Depending on the type of application and quality of the feed water, there are two practical schemes to incorporate catalyst nanoparticles in the ceramic membrane module (Fig. 7b), namely (i) thin-film coating on the membrane feed side, and (ii) decorating catalyst nanoparticles on the macroporous matrix of the membrane support through impregnation technique. In general, immobilizing the catalyst on the feed side (as top layer) of the ceramic membrane imparts self-cleaning or antifouling property (*via* foulant oxidation by $SO_4^{\bullet-}$ generated on the membrane surface), and thus the membrane will exhibit improved flux. However, the catalyst can be susceptible to deactivation by the foulant when treating the water with high DOM concentration. Immobilization of the catalyst in the internal pores of the membrane support layer creates microreactor environment whereby the target pollutant and their intermediates are degraded more effectively by $SO_4^{\bullet-}$ due to the longer reaction time and much less interference by DOM (which can be mostly retained by the membrane top layer). It is proposed that future study should aim to (i) develop novel reactor for heterogeneous SR-AOP system based on batch or continuous flow (e.g. completely mixed or plug flow) reactor configuration with catalyst recovery, and (ii) develop a robust dual functional catalytic ceramic membrane incorporating SR-AOPs and membrane filtration process.

10. Conclusions

In summary, we provide a state–of–the–art review on the current development of heterogeneous catalysts for pollutant removal *via* PMS activation. The SR-AOPs have promising potentials to be implemented as an effective treatment of recalcitrant organics pollution in water. Sulfate radical has many advantages such as being more selective and have longer lifetime compared to $^{\bullet}OH$. The metal-based catalysts particularly the mixed metal catalysts have many salient features such as being highly redox active for PMS activation, versatile, ferromagnetic and multifunctional (e.g. photocatalytic, antibacterial, etc.). The new generation of catalysts, namely carbon-based catalysts enable the exploitation of PMS activation without the metal leaching concern. Hybrid system consisting of heterogeneous catalyst/PMS system integrated with another AOP is discussed. We evaluated and proposed several strategies to detect $SO_4^{\bullet-}$, namely (i) use of chemical probe or spin trapping agent coupled with analytical tools, and (ii) competitive kinetic approach using selective chemical scavengers. Several practical issues such as the undesired formation of bromate and chlorate, and sulfate after $SO_4^{\bullet-}$ oxidation and residual PMS need to be addressed prior to application in a larger scale study. It is suggested that future studies can be extended to investigate (i) novel reactor design for the heterogeneous catalytic system based on batch or continuous flow (e.g. completely mixed or plug flow) reactor configuration with catalyst recovery, and (ii) catalytic ceramic membrane incorporating SR-AOPs to provide a suitable platform to fully exploit the advantage of $SO_4^{\bullet-}$ oxidation processes.

Acknowledgements

The authors would like to thank the Interdisciplinary Graduate School (IGS), Nanyang Technological University and Nanyang Environment and Water Research Institute (NEWRI) for the award of a PhD research scholarship. The generous assistances from the research and technical staffs of Environmental Labs and Facilities for Analysis Characterization Testing (FACTS) are deeply appreciated.

References

[1] B. Petrie, R. Barden, B. Kasprzyk-Hordern, Water Res. 72 (2015) 3–27.

[2] S. Sauvé, M. Desrosiers, Chem. Cent. J. 8 (2014) 15.
[3] S.W. Krasner, Philos T. Roy, Soc. A 367 (2009) 4077–4095.
[4] A. Babuponnusami, K. Muthukumar, J. Environ. Chem. Eng. 2 (2014) 557–572.
[5] K.-C. Huang, Z. Zhao, G.E. Hoag, A. Dahmani, P.A. Block, Chemosphere 61 (2005) 551–560.
[6] G.P. Anipsitakis, D.D. Dionysiou, Environ. Sci. Technol. 37 (2003) 4790–4797.
[7] J. Sharma, I.M. Mishra, D.D. Dionysiou, V. Kumar, Chem. Eng. J. 276 (2015) 193–204.
[8] P. Nfodzo, H. Choi, Environ. Eng. Sci. 28 (2011) 605–609.
[9] R. Zhang, P. Sun, T.H. Boyer, L. Zhao, C.-H. Huang, Environ. Sci. Technol. 49 (2015) 3056–3066.
[10] M.G. Antoniou, A.A. de la Cruz, D.D. Dionysiou, Environ. Sci. Technol. 44 (2010) 7238–7244.
[11] M.G. Antoniou, A.A. de la Cruz, D.D. Dionysiou, Appl. Catal. B: Environ. 96 (2010) 290–298.
[12] Y.-C. Lee, S.-L. Lo, J. Kuo, C.-P. Huang, J. Hazard. Mater. 261 (2013) 463–469.
[13] W. Ren, Z. Zhou, Y. Zhu, L.-M. Jiang, H. Wei, T. Niu, P. Fu, Z. Qiu, Int. Biodeterior. Biodegrad. 104 (2015) 384–390.
[14] I. Michael-Kordatou, M. Iacovou, Z. Frontistis, E. Hapeshi, D.D. Dionysiou, D. Fatta-Kassinos, Water Res. 85 (2015) 346–358.
[15] G.P. Anipsitakis, T.P. Tufano, D.D. Dionysiou, Water Res. 42 (2008) 2899–2910.
[16] Y. Ji, C. Dong, D. Kong, J. Lu, Q. Zhou, Chem. Eng. J. 263 (2015) 45–54.
[17] G. Fang, J. Gao, D.D. Dionysiou, C. Liu, D. Zhou, Environ. Sci. Technol. 47 (2013) 4605–4611.
[18] Y. Zhou, J. Jiang, Y. Gao, J. Ma, S.-Y. Pang, J. Li, X.-T. Lu, L.-P. Yuan, Environ. Sci. Technol. 49 (2015) 12941–12950.
[19] O.S. Furman, A.L. Teel, R.J. Watts, Environ. Sci. Technol. 44 (2010) 6423–6428.
[20] Y.-H. Guan, J. Ma, X.-C. Li, J.-Y. Fang, L.-W. Chen, Environ. Sci. Technol. 45 (2011) 9308–9314.
[21] G.P. Anipsitakis, D.D. Dionysiou, Environ. Sci. Technol. 38 (2004) 3705–3712.
[22] A. Rastogi, S.R. Al-Abed, D.D. Dionysiou, Appl. Catal. B: Environ. 85 (2009) 171–179.
[23] G.P. Anipsitakis, E. Stathatos, D.D. Dionysiou, J. Phys. Chem. B 109 (2005) 13052–13055.
[24] C. Cai, H. Zhang, X. Zhong, L. Hou, J. Hazard. Mater. 283 (2015) 70–79.
[25] M.E. Davis, R.J. Davis, Fundamentals of chemical reaction engineering, Courier Corporation, 2012.
[26] K.H. Chan, W. Chu, Water Res. 43 (2009) 2513–2521.
[27] D. Zhou, H. Zhang, L. Chen, J. Chem. Technol. Biotechnol. 90 (2014) 775–779.
[28] J.B. Gerken, J.G. McAlpin, J.Y.C. Chen, M.L. Rigsby, W.H. Casey, R.D. Britt, S.S. Stahl, J. Am. Chem. Soc. 133 (2011) 14431–14442.
[29] X. Chen, J. Chen, X. Qiao, D. Wang, X. Cai, Appl. Catal. B: Environ. 80 (2008) 116–121.
[30] W. Guo, S. Su, C. Yi, Z. Ma, Environ. Prog. Sustain. 32 (2013) 193–197.
[31] P. Hu, M. Long, Appl. Catal. B: Environ. 181 (2016) 103–117.
[32] B.-T. Zhang, Y. Zhang, Y. Teng, M. Fan, Crit. Rev. Environ. Sci. Technol. 45 (2015) 1756–1800.
[33] Q. Han, X. Yang, X. Shao, R. Biu, L. Wang, Prog. Chem. 24 (2012) 144–156.
[34] H. Sun, S. Wang, Catalysis, R. Soc. Chem. 27 (2015) 209–247.
[35] L.O. Simonsen, H. Harbak, P. Bennekou, Sci. Total Environ. 432 (2012) 210–215.
[36] W. Qiu, Y. Zheng, Chem. Eng. J. 145 (2009) 483–488.
[37] L. Eberson, V. Gold, D. Bethell, Adv. Phys. Org. Chem. Academic Press (1982) 79–185.
[38] T.-T. Lim, P.-S. Yap, M. Srinivasan, A.G. Fane, Crit. Rev. Environ. Sci. Technol. 41 (2011) 1173–1230.
[39] R. Matta, S. Tlili, S. Chiron, S. Barbati, Environ. Chem. Lett. 9 (2011) 347–353.
[40] T. Olmez-Hanci, I. Arslan-Alaton, Chem. Eng. J. 224 (2013) 10–16.
[41] J. Spivey, Y. Han, K. Dooley, Catal. R. Soc. Chem. (2015).
[42] A. Tsitonaki, B. Petri, M. Crimi, H. MosbÆK, R.L. Siegrist, P.L. Bjerg, Crit. Rev. Environ. Sci. Technol. 40 (2010) 55–91.
[43] P. Neta, V. Madhavan, H. Zemel, R.W. Fessenden, J. Am. Chem. Soc. 99 (1977) 163–164.
[44] G.V. Buxton, C.L. Greenstock, W.P. Helman, A.B. Ross, J. Phys. Chem. Ref. Data 17 (1988) 513–886.
[45] M. Sánchez-Polo, M.M. Abdel daiem, R. Ocampo-Pérez, J. Rivera-Utrilla, A.J. Mota, Sci. Total Environ. 463–464 (2013) 423–431.
[46] F.P. Tully, A.R. Ravishankara, R.L. Thompson, J.M. Nicovich, R.C. Shah, N.M. Kreutter, P.H. Wine, J. Phys. Chem. 85 (1981) 2262–2269.
[47] M. Mahdi Ahmed, S. Barbati, P. Doumenq, S. Chiron, Chem. Eng. J. 197 (2012) 440–447.
[48] P. Shukla, S. Wang, K. Singh, H.M. Ang, M.O. Tadé, Appl. Catal. B: Environ. 99 (2010) 163–169.
[49] M. Pagano, A. Volpe, G. Mascolo, A. Lopez, V. Locaputo, R. Ciannarella, Chemosphere 86 (2012) 329–334.
[50] P. Neta, R.E. Huie, A.B. Ross, J. Phys. Chem. Ref. Data 17 (1988) 1027–1284.
[51] C.-J. Liang, S.-C. Huang, Change 2 (2012) 2.
[52] H.V. Lutze, S. Bircher, I. Rapp, N. Kerlin, R. Bakkour, M. Geisler, C. von Sonntag, T.C. Schmidt, Environ. Sci. Technol. 49 (2015) 1673–1680.
[53] Y. Yang, J.J. Pignatello, J. Ma, W.A. Mitch, Environ. Sci. Technol. 48 (2014) 2344–2351.
[54] G.P. Anipsitakis, D.D. Dionysiou, M.A. Gonzalez, Environ. Sci. Technol. 40 (2006) 1000–1007.
[55] H.V. Lutze, N. Kerlin, T.C. Schmidt, Water Res. 72 (2015) 349–360.
[56] J.-Y. Fang, C. Shang, Environ. Sci. Technol. 46 (2012) 8976–8983.
[57] K. Liu, J. Lu, Y. Ji, Water Res. 84 (2015) 1–7.
[58] H.V. Lutze, R. Bakkour, N. Kerlin, C. von Sonntag, T.C. Schmidt, Water Res. 53 (2014) 370–377.
[59] Y. Yang, J. Jiang, X. Lu, J. Ma, Y. Liu, Environ. Sci. Technol. 49 (2015) 7330–7339.
[60] R.E. Huie, C.L. Clifton, J. Phys. Chem. 94 (1990) 8561–8567.
[61] L. Dogliotti, E. Hayon, J. Phys. Chem. 71 (1967) 2511–2516.
[62] S. Yang, P. Wang, X. Yang, L. Shan, W. Zhang, X. Shao, R. Niu, J. Hazard. Mater. 179 (2010) 552–558.
[63] R.E. Huie, C.L. Clifton, P. Neta, Int. J. Radiat. Appl. Instrum. C Radiat. Phys. Chem. 38 (1991) 477–481.
[64] J. Kim, J.O. Edwards, Inorg. Chim. Acta 235 (1995) 9–13.
[65] A. Ghauch, A.M. Tuqan, N. Kibbi, Chem. Eng. J. 197 (2012) 483–492.
[66] W.V. Steele, E.H. Appelman, J. Chem. Thermodyn. 14 (1982) 337–344.
[67] S.K. Rani, D. Easwaramoorthy, I.M. Bilal, M. Palanichamy, Appl. Catal. A: Gen. 369 (2009) 1–7.
[68] M. Spiro, Electrochim. Acta 24 (1979) 313–314.
[69] R.J. Kennedy, A.M. Stock, J. Org. Chem. 25 (1960) 1901–1906.
[70] J. Flanagan, W.P. Griffith, A.C. J. Chem. Soc. Skapski, Chem. Commun. (1984) 1574–1575.
[71] W. Reints, D.A. Pratt, H.-G. Korth, P. Mulder, J. Phys. Chem. A 104 (2000) 10713–10720.
[72] I.M. Kolthoff, I.K. Miller, J. Am. Chem. Soc. 73 (1951) 3055–3059.
[73] J. Zou, J. Ma, X. Zhang, P. Xie, Chem. Eng. J. 253 (2014) 34–39.
[74] W.-D. Oh, S.-K. Lua, Z. Dong, T.-T. Lim, J. Mater. Chem. A 2 (2014) 15836–15845.
[75] S. Wacławek, K. Grübel, M. Černík, Spectrochim. Acta A Mol. Biomol. Spectrosc. 149 (2015) 928–933.
[76] T.N. Das, R.E. Huie, P. Neta, J. Phys. Chem. A 103 (1999) 3581–3588.
[77] G. Duca, Homogeneous Catalysis with Metal Complexes: Fundamentals and Applications, Springer Science & Business Media, 2012.
[78] W. Zhang, H.L. Tay, S.S. Lim, Y. Wang, Z. Zhong, R. Xu, Appl. Catal. B: Environ. 95 (2010) 93–99.
[79] M. Stoyanova, I. Slavova, S. Christoskova, V. Ivanova, Appl. Catal. A: Gen. 476 (2014) 121–132.
[80] Q. Yang, H. Choi, S.R. Al-Abed, D.D. Dionysiou, Appl. Catal. B: Environ. 88 (2009) 462–469.
[81] Y. Ren, L. Lin, J. Ma, J. Yang, J. Feng, Z. Fan, Appl. Catal. B: Environ. 165 (2015) 572–578.
[82] W.-D. Oh, Z. Dong, Z.-T. Hu, T.-T. Lim, J. Mater. Chem. A 3 (2015) 22208–22217.
[83] S. Muhammad, P.R. Shukla, M.O. Tadé, S. Wang, J. Hazard. Mater. 215–216 (2012) 183–190.
[84] P. Shi, R. Su, S. Zhu, M. Zhu, D. Li, S. Xu, J. Hazard. Mater. 229–230 (2012) 331–339.
[85] K.-Y. Andrew Lin, F.-K. Hsu, W.-D. Lee, J. Mater. Chem. A 3 (2015) 9480–9490.
[86] Q. Yang, H. Choi, Y. Chen, D.D. Dionysiou, Appl. Catal. B: Environ. 77 (2008) 300–307.
[87] S. Muhammad, E. Saputra, H. Sun, H.-M. Ang, M.O. Tadé, S. Wang, Ind. Eng. Chem. Res. 51 (2012) 15351–15359.
[88] E. Saputra, S. Muhammad, H. Sun, H.M. Ang, M.O. Tadé, S. Wang, Catal. Today 190 (2012) 68–72.
[89] S. Muhammad, E. Saputra, H. Sun, J.d.C. Izidoro, D.A. Fungaro, H.M. Ang, M.O. Tade, S. Wang, RSC Adv. 2 (2012) 5645–5650.
[90] Y. Wang, H. Sun, H.M. Ang, M.O. Tadé, S. Wang, Chem. Eng. J. 245 (2014) 1–9.
[91] P. Shukla, H. Sun, S. Wang, H.M. Ang, M.O. Tadé, Catal. Today 175 (2011) 380–385.
[92] P.R. Shukla, S. Wang, H. Sun, H.M. Ang, M. Tadé, Appl. Catal. B: Environ. 100 (2010) 529–534.
[93] Z. Huang, H. Bao, Y. Yao, J. Lu, W. Lu, W. Chen, J. Chem. Technol. Biotechnol. (2015).
[94] W.-D. Oh, S.K. Lua, Z. Dong, T.-T. Lim, Nanoscale 8 (2016) 2046–2054.
[95] Y. Feng, J. Liu, D. Wu, Z. Zhou, Y. Deng, T. Zhang, K. Shih, Chem. Eng. J. 280 (2015) 514–524.
[96] F. Ji, C. Li, L. Deng, Chem. Eng. J. 178 (2011) 239–243.
[97] T. Zhang, H. Zhu, J.-P. Croué, Environ. Sci. Technol. 47 (2013) 2784–2791.
[98] H. Kušić, N. Koprivanac, I. Selanec, Chemosphere 65 (2006) 65–73.
[99] J. Liu, G. Jiang, Y. Liu, J. Di, Y. Wang, Z. Zhao, Q. Sun, C. Xu, J. Gao, A. Duan, J. Liu, Y. Wei, Y. Zhao, L. Jiang, Sci. Rep. 4 (2014) 7276.
[100] F. Ji, C. Li, Y. Liu, P. Liu, Sep. Purif. Technol. 135 (2014) 1–6.
[101] T. Zhang, Y. Chen, Y. Wang, J. Le Roux, Y. Yang, J.-P. Croué, Environ. Sci. Technol. 48 (2014) 5868–5875.
[102] J. Zhao, Y. Zhang, X. Quan, S. Chen, Sep. Purif. Technol. 71 (2010) 302–307.
[103] A. Volpe, M. Pagano, G. Mascolo, A. Lopez, R. Ciannarella, V. Locaputo, Chemosphere 91 (2013) 1250–1256.
[104] F. Ghanbari, M. Moradi, M. Manshouri, J. Environ. Chem. Eng. 2 (2014) 1846–1851.
[105] Y. Wang, H. Sun, X. Duan, H.M. Ang, M.O. Tadé, S. Wang, Appl. Catal. B: Environ. 172–173 (2015) 73–81.
[106] I. Hussain, Y. Zhang, S. Huang, X. Du, Chem. Eng. J. 203 (2012) 269–276.
[107] S. Rodriguez, L. Vasquez, D. Costa, A. Romero, A. Santos, Chemosphere 101 (2014) 86–92.
[108] S. Ahn, T.D. Peterson, J. Righter, D.M. Miles, P.G. Tratnyek, Environ. Sci. Technol. 47 (2013) 11717–11725.

[109] S.-Y. Oh, H.-W. Kim, J.-M. Park, H.-S. Park, C. Yoon, J. Hazard. Mater. 168 (2009) 346–351.
[110] Y. Li, Y. Zhang, J. Li, X. Zheng, Environ. Pollut. 159 (2011) 3744–3749.
[111] A. Tiraferri, K.L. Chen, R. Sethi, M. Elimelech, J. Colloid Interface Sci. 324 (2008) 71–79.
[112] H. Sun, G. Zhou, S. Liu, H.M. Ang, M.O. Tadé, S. Wang, ACS Appl. Mater. Interfaces 4 (2012) 6235–6241.
[113] X. Sun, Y. Li, Angew. Chem. Int. Ed. 43 (2004) 3827–3831.
[114] M.A. Al-Shamsi, N.R. Thomson, S.P. Forsey, Chem. Eng. J. 232 (2013) 555–563.
[115] G. Ayoub, A. Ghauch, Chem. Eng. J. 256 (2014) 280–292.
[116] F. Ji, C. Li, X. Wei, J. Yu, Chem. Eng. J. 231 (2013) 434–440.
[117] J.L. Pierre, M. Fontecave, Biometals 12 (1999) 195–199.
[118] H. Iwahashi, H. Kawamori, K. Fukushima, Chem. Biol. Interact. 118 (1999) 201–215.
[119] F. Gong, L. Wang, D. Li, F. Zhou, Y. Yao, W. Lu, S. Huang, W. Chen, Chem. Eng. J. 267 (2015) 102–110.
[120] M. Uchida, O. Shinohara, S. Ito, N. Kawasaki, T. Nakamura, S. Tanada, J. Colloid Interface Sci. 224 (2000) 347–350.
[121] J. Zou, J. Ma, L. Chen, X. Li, Y. Guan, P. Xie, C. Pan, Environ. Sci. Technol. 47 (2013) 11685–11691.
[122] C. Tan, N. Gao, Y. Deng, J. Deng, S. Zhou, J. Li, X. Xin, J. Hazard. Mater. 276 (2014) 452–460.
[123] G. Wei, X. Liang, Z. He, Y. Liao, Z. Xie, P. Liu, S. Ji, H. He, D. Li, J. Zhang, J. Mol. Catal. A: Chem. 398 (2015) 86–94.
[124] D. Chen, X. Ma, J. Zhou, X. Chen, G. Qian, J. Hazard. Mater. 279 (2014) 476–484.
[125] M.A. Al-Shamsi, N.R. Thomson, Ind. Eng. Chem. Res. 52 (2013) 13564–13571.
[126] R.L. Parfitt, R.S.C. Smart, J. Chem. Soc. Farad. T. 173 (1977) 796–802.
[127] R.L. Parfitt, R.S.C. Smart, Soil Sci. Soc. Am. J. 42 (1978) 48–50.
[128] E. Saputra, S. Muhammad, H. Sun, H.M. Ang, M.O. Tade, S. Wang, Environ. Sci. Technol. (2013).
[129] E. Saputra, S. Muhammad, H. Sun, H.-M. Ang, M.O. Tadé, S. Wang, Appl. Catal. B: Environ. 142–143 (2013) 729–735.
[130] E. Saputra, S. Muhammad, H. Sun, H.-M. Ang, M.O. Tadé, S. Wang, J. Colloid Interface Sci. 407 (2013) 467–473.
[131] E. Saputra, S. Muhammad, H. Sun, H.-M. Ang, M.O. Tadé, S. Wang, Appl. Catal. B: Environ. 154–155 (2014) 246–251.
[132] E. Saputra, S. Muhammad, H. Sun, A. Patel, P. Shukla, Z.H. Zhu, S. Wang, Catal. Commun. 26 (2012) 144–148.
[133] Y. Wang, S. Indrawirawan, X. Duan, H. Sun, H.M. Ang, M.O. Tadé, S. Wang, Chem. Eng. J. 266 (2015) 12–20.
[134] Y. Wang, H. Sun, H.M. Ang, M.O. Tadé, S. Wang, Appl. Catal. B: Environ. 164 (2015) 159–167.
[135] Y. Wang, H. Sun, H.M. Ang, M.O. Tadé, S. Wang, J. Colloid Interface Sci. 433 (2014) 68–75.
[136] Y. Yao, C. Xu, S. Yu, D. Zhang, S. Wang, Ind. Eng. Chem. Res. 52 (2013) 3637–3645.
[137] Y. Wang, H. Sun, H.M. Ang, M.O. Tadé, S. Wang, ACS Appl. Mater. Interfaces 6 (2014) 19914–19923.
[138] D. Tang, G. Zhang, S. Guo, J. Colloid Interface Sci. 454 (2015) 44–51.
[139] L. Xu, W. Liu, X. Li, S. Rashid, C. Shen, Y. Wen, RSC Adv. 5 (2015) 12248–12256.
[140] L. Zhang, L. Zhao, J. Lian, RSC Adv. 4 (2014) 41838–41847.
[141] H. Liang, H. Sun, A. Patel, P. Shukla, Z.H. Zhu, S. Wang, Appl. Catal. B: Environ. 127 (2012) 330–335.
[142] Z. Yang, Y. Yang, X. Zhu, G. Chen, W. Zhang, Ind. Eng. Chem. Res. 53 (2014) 9608–9615.
[143] J. Liu, Z. Zhao, P. Shao, F. Cui, Chem. Eng. J. 262 (2015) 854–861.
[144] S. Luo, L. Duan, B. Sun, M. Wei, X. Li, A. Xu, Appl. Catal. B: Environ. 164 (2015) 92–99.
[145] Y.-s. Ding, X.-f. Shen, S. Sithambaram, S. Gomez, R. Kumar, V.M.B. Crisostomo, S.L. Suib, M. Aindow, Chem. Mater. 17 (2005) 5382–5389.
[146] L. Duan, B. Sun, M. Wei, S. Luo, F. Pan, A. Xu, X. Li, J. Hazard. Mater. 285 (2015) 356–365.
[147] Z.-R. Tian, W. Tong, J.-Y. Wang, N.-G. Duan, V.V. Krishnan, S.L. Suib, Science 276 (1997) 926–930.
[148] M. Wei, Y. Ruan, S. Luo, X. Li, A. Xu, P. Zhang, New J. Chem. (2015).
[149] B. Yang, Z. Tian, B. Wang, Z. Sun, L. Zhang, Y. Guo, H. Li, S. Yan, RSC Adv. 5 (2015) 20674–20683.
[150] S. Zhang, Q. Fan, H. Gao, Y. Huang, X. Liu, J. Li, X. Xu, X. Wang, J. Mater. Chem. A (2016).
[151] H. Sun, H. Liang, G. Zhou, S. Wang, J. Colloid Interface Sci. 394 (2013) 394–400.
[152] W. Wu, Z.-H. Huang, T.-T. Lim, Appl. Catal. A: Gen. 480 (2014) 58–78.
[153] S. Su, W. Guo, Y. Leng, C. Yi, Z. Ma, J. Hazard. Mater. 244–245 (2013) 736–742.
[154] L. Hu, F. Yang, L. Zou, H. Yuan, X. Hu, Chinese J. Catal. 36 (2015) 1785–1797.
[155] L.J. Xu, W. Chu, L. Gan, Chem. Eng. J. 263 (2015) 435–443.
[156] Y. Yao, Z. Yang, D. Zhang, W. Peng, H. Sun, S. Wang, Ind. Eng. Chem. Res. 51 (2012) 6044–6051.
[157] F.X. Qin, S.Y. Jia, Y. Liu, X. Han, H.T. Ren, W.W. Zhang, J.W. Hou, S.H. Wu, Mater. Lett. (2013).
[158] Y. Du, W. Ma, P. Liu, B. Zou, J. Ma, J. Hazard. Mater. 308 (2016) 58–66.
[159] Y. Yao, Y. Cai, G. Wu, F. Wei, X. Li, H. Chen, S. Wang, J. Hazard. Mater. 296 (2015) 128–137.
[160] W. Li, P.-x. Wu, Y. Zhu, Z.-j. Huang, Y.-h. Lu, Y.-w. Li, Z. Dang, N.-w. Zhu, Chem. Eng. J. 279 (2015) 93–102.
[161] X. Li, Z. Wang, B. Zhang, A.I. Rykov, M.A. Ahmed, J. Wang, Appl. Catal. B: Environ. 181 (2016) 788–799.
[162] Y. Ding, L. Zhu, N. Wang, H. Tang, Appl. Catal. B: Environ. 129 (2013) 153–162.
[163] Y.-H. Guan, J. Ma, Y.-M. Ren, Y.-L. Liu, J.-Y. Xiao, L.-q. Lin, C. Zhang, Water Res. 47 (2013) 5431–5438.
[164] W.-D. Oh, S.-K. Lua, Z. Dong, T.-T. Lim, J. Hazard. Mater. 284 (2015) 1–9.
[165] Y. Xu, J. Ai, H. Zhang, J. Hazard. Mater. 309 (2016) 87–96.
[166] B. Viswanathan, V. Subramanian, J.S. Lee, Materials and Processes for Solar Fuel Production, Springer New York, 2014.
[167] Y. Feng, D. Wu, Y. Deng, T. Zhang, K. Shih, Environ. Sci. Technol. (2016).
[168] D.A. Johnson, Some Thermodynamic Aspects of Inorganic Chemistry, University Press, Cambridge, 1982.
[169] J. Moser, S. Punchihewa, P.P. Infelta, M. Graetzel, Langmuir 7 (1991) 3012–3018.
[170] W.M. Haynes, CRC Handbook of Chemistry and Physics, 94th ed., CRC Press, 2013.
[171] T.V. Popova, N.V. Aksenova, Russ. J. Coord. Chem. 29 (2003) 743–765.
[172] S.K. Bikkarolla, P. Papakonstantinou, J. Power Sour. 281 (2015) 243–251.
[173] W.-D. Oh, S.-K. Lua, Z. Dong, T.-T. Lim, Nanoscale 7 (2015) 8149–8158.
[174] M. Kosmulski, Adv. Colloid Interface Sci. 152 (2009) 14–25.
[175] B.C. Gilbert, J.K. Stell, J. Chem. Soc. Faraday Trans. 86 (1990) 3261–3266.
[176] B.C. Gilbert, J.K. Stell, A.C. Whitwood, C. Halliwell, W.R. Sanderson, J. Chem. Soc. Perk. T. 2 (1991) 629–634.
[177] Z. Wang, Y. Du, Y. Liu, B. Zou, J. Xiao, J. Ma, RSC Adv. 6 (2016) 11040–11048.
[178] Y. Yao, Y. Cai, F. Lu, F. Wei, X. Wang, S. Wang, J. Hazard. Mater. 270 (2014) 61–70.
[179] E. Saputra, S. Muhammad, H. Sun, S. Wang, RSC Adv. 3 (2013) 21905–21910.
[180] J. Zhang, X. Shao, C. Shi, S. Yang, Chem. Eng. J. 232 (2013) 259–265.
[181] S. Yang, X. Yang, X. Shao, R. Niu, L. Wang, J. Hazard. Mater. 186 (2011) 659–666.
[182] H.-H. Huang, M.-C. Lu, J.-N. Chen, C.-T. Lee, Chemosphere 51 (2003) 935–943.
[183] S. Karthikeyan, A. Titus, A. Gnanamani, A.B. Mandal, G. Sekaran, Desalination 281 (2011) 438–445.
[184] E.C. Larsen, J.H. Walton, J. Phys. Chem. 44 (1940) 70–85.
[185] J. Ma, M.-H. Sui, Z.-L. Chen, L.-N. Wang, Ozone: Sci. Eng. 26 (2004) 3–10.
[186] M. Sánchez-Polo, U. von Gunten, J. Rivera-Utrilla, Water Res. 39 (2005) 3189–3198.
[187] C. Moreno-Castilla, M.A. Fontecha-Cámara, M.A. Álvarez-Merino, M.V. López-Ramón, F. Carrasco-Marín, Adsorption 17 (2011) 413–419.
[188] S. Yang, L. Li, T. Xiao, Y. Zhang, D. Zheng, Sep. Purif. Technol. 160 (2016) 81–88.
[189] A. Dąbrowski, P. Podkościelny, Z. Hubicki, M. Barczak, Chemosphere 58 (2005) 1049–1070.
[190] S. Yang, T. Xiao, J. Zhang, Y. Chen, L. Li, Sep. Purif. Technol. 143 (2015) 19–26.
[191] H. Lee, H.-J. Lee, J. Jeong, J. Lee, N.-B. Park, C. Lee, Chem. Eng. J. 266 (2015) 28–33.
[192] H. Sun, C. Kwan, A. Suvorova, H.M. Ang, M.O. Tadé, S. Wang, Appl. Catal. B: Environ. 154–155 (2014) 134–141.
[193] X. Duan, Z. Ao, H. Sun, S. Indrawirawan, Y. Wang, J. Kang, F. Liang, Z.H. Zhu, S. Wang, ACS Appl. Mater. Interfaces 7 (2015) 4169–4178.
[194] X. Duan, H. Sun, Y. Wang, J. Kang, S. Wang, ACS Catal. 5 (2015) 553–559.
[195] S. Indrawirawan, H. Sun, X. Duan, S. Wang, Appl. Catal. B: Environ. 179 (2015) 352–362.
[196] S. Indrawirawan, H. Sun, X. Duan, S. Wang, J. Mater. Chem. A 3 (2015) 3432–3440.
[197] W. Peng, S. Liu, H. Sun, Y. Yao, L. Zhi, S. Wang, J. Mater. Chem. A 1 (2013) 5854–5859.
[198] H. Sun, S. Liu, G. Zhou, H.M. Ang, M.O. Tadé, S. Wang, ACS Appl. Mater. Interfaces 4 (2012) 5466–5471.
[199] H. Sun, Y. Wang, S. Liu, L. Ge, L. Wang, Z. Zhu, S. Wang, Chem. Commun. 49 (2013) 9914–9916.
[200] X. Duan, Z. Ao, H. Sun, L. Zhou, G. Wang, S. Wang, Chem. Commun. 51 (2015) 15249–15252.
[201] X. Duan, K. O'Donnell, H. Sun, Y. Wang, S. Wang, Small 11 (2015) 3036–3044.
[202] X. Duan, S. Indrawirawan, H. Sun, S. Wang, Catal. Today 249 (2015) 184–191.
[203] X. Duan, Z. Ao, L. Zhou, H. Sun, G. Wang, S. Wang, Appl. Catal. B: Environ. 188 (2016) 98–105.
[204] C. Wang, J. Kang, H. Sun, H.M. Ang, M.O. Tadé, S. Wang, Carbon (2016).
[205] A.M. Dimiev, L.B. Alemany, J.M. Tour, ACS Nano 7 (2013) 576–588.
[206] C. Huang, C. Li, G. Shi, Energ. Environ. Sci. 5 (2012) 8848–8868.
[207] K.I. Bolotin, K.J. Sikes, Z. Jiang, M. Klima, G. Fudenberg, J. Hone, P. Kim, H.L. Stormer, Solid State Commun. 146 (2008) 351–355.
[208] M.D. Stoller, S. Park, Z. Yanwu, J. An, R.S. Ruoff, Nano Lett. 8 (2008) 3498–3502.
[209] Z.-T. Hu, J. Liu, X. Yan, W.-D. Oh, T.-T. Lim, Chem. Eng. J. 262 (2015) 1022–1032.
[210] G. Lee, K. Cho, Phys. Rev. B 79 (2009) 165440.
[211] B.G. D.-e. Jiang, S. Sumpter, J. Dai, Chem. Phys. 126 (2007) 134701.
[212] B. Frank, J. Zhang, R. Blume, R. Schlögl, D.S. Su, Angew. Chem. Int. Ed. 48 (2009) 6913–6917.
[213] W. Qi, D. Su, ACS Catal. 4 (2014) 3212–3218.
[214] S. Liu, W. Peng, H. Sun, S. Wang, Nanoscale 6 (2014) 766–771.
[215] F. Rodríguez-Reinoso, M. Molina-Sabio, Carbon 30 (1992) 1111–1118.
[216] A. Nsabimana, X. Bo, Y. Zhang, M. Li, C. Han, L. Guo, J. Colloid Interface Sci. 428 (2014) 133–140.

[217] Y. Gao, G. Hu, J. Zhong, Z. Shi, Y. Zhu, D.S. Su, J. Wang, X. Bao, D. Ma, Angew. Chem. Int. Ed. 52 (2013) 2109–2113.
[218] N.R. Wilson, P.A. Pandey, R. Beanland, R.J. Young, I.A. Kinloch, L. Gong, Z. Liu, K. Suenaga, J.P. Rourke, S.J. York, J. Sloan, ACS Nano 3 (2009) 2547–2556.
[219] D. Yu, K. Goh, L. Wei, H. Wang, Q. Zhang, W. Jiang, R. Si, Y. Chen, J. Mater. Chem. A 1 (2013) 11061–11069.
[220] Y. Zheng, Y. Jiao, L. Ge, M. Jaroniec, S.Z. Qiao, Angew. Chem. Int. Ed. 52 (2013) 3110–3116.
[221] S. Wang, E. Iyyamperumal, A. Roy, Y. Xue, D. Yu, L. Dai, Angew. Chem. 123 (2011) 11960–11964.
[222] H. Liu, P. Sun, M. Feng, H. Liu, S. Yang, L. Wang, Z. Wang, Appl. Catal. B: Environ. 187 (2016) 1–10.
[223] B. Frank, R. Blume, A. Rinaldi, A. Trunschke, R. Schlögl, Angew. Chem. Int. Ed. 50 (2011) 10226–10230.
[224] A.M. Rao, P.C. Eklund, S. Bandow, A. Thess, R.E. Smalley, Nature 388 (1997) 257–259.
[225] L. Duclaux, Carbon 40 (2002) 1751–1764.
[226] X. Chen, W. Wang, H. Xiao, C. Hong, F. Zhu, Y. Yao, Z. Xue, Chem. Eng. J. 193–194 (2012) 290–295.
[227] S.K. Kuriechen, S. Murugesan, Water Air Soil Pollut. 224 (2013) 1–8.
[228] S.K. Kuriechen, S. Murugesan, S.P. Raj, P. Maruthamuthu, Chem. Eng. J. 174 (2011) 530–538.
[229] M. Ahmadi, F. Ghanbari, M. Moradi, Water Sci. Technol. 72 (2015) 2095–2102.
[230] Q. Chen, F. Ji, Q. Guo, J. Fan, X. Xu, J. Environ. Sci. 26 (2014) 2440–2450.
[231] P. Sathishkumar, R.V. Mangalaraja, S. Anandan, M. Ashokkumar, Chem. Eng. J. 220 (2013) 302–310.
[232] Q. Chen, F. Ji, T. Liu, P. Yan, W. Guan, X. Xu, Chem. Eng. J. 229 (2013) 57–65.
[233] Q. Chen, F. Ji, Q. Guo, W. Guan, P. Yan, L. Pei, X. Xu, Ind. Eng. Chem. Res. 52 (2013) 12540–12549.
[234] G. Zhou, H. Sun, S. Wang, H. Ming Ang, M.O. Tadé, Sep. Purif. Technol. 80 (2011) 626–634.
[235] Y. Wang, L. Zhou, X. Duan, H. Sun, E.L. Tin, W. Jin, S. Wang, Catal. Today 258 (Part 2) (2015) 576–584.
[236] G. Chen, X. Si, J. Yu, H. Bai, X. Zhang, Appl. Surf. Sci. 330 (2015) 191–199.
[237] H. Sun, S. Liu, S. Liu, S. Wang, Appl. Catal. B: Environ. 146 (2014) 162–168.
[238] P. Sathishkumar, N. Pugazhenthiran, R.V. Mangalaraja, A.M. Asiri, S. Anandan, J. Hazard. Mater. 252–253 (2013) 171–179.
[239] H. Sun, X. Feng, S. Wang, H.M. Ang, M.O. Tadé, Chem. Eng. J. 170 (2011) 270–277.
[240] F. Chi, B. Song, B. Yang, Y. Lv, S. Ran, Q. Huo, RSC Adv. 5 (2015) 67412–67417.
[241] Y. Tao, Q. Ni, M. Wei, D. Xia, X. Li, A. Xu, RSC Adv. 5 (2015) 44128–44136.
[242] K. Zhu, J. Wang, Y. Wang, C. Jin, A.S. Ganeshraja, Catal. Sci. Technol. (2016).
[243] Y. Yao, J. Qin, Y. Cai, F. Wei, F. Lu, S. Wang, Environ. Sci. Pollut. Res. 21 (2014) 7296–7306.
[244] K.-Y. Andrew Lin, Z.-Y. Zhang, RSC Adv. 6 (2016) 15027–15034.
[245] Y. Wang, Y. Xie, H. Sun, J. Xiao, H. Cao, S. Wang, J. Hazard. Mater. 301 (2016) 56–64.
[246] J. Cong, G. Wen, T. Huang, L. Deng, J. Ma, Chem. Eng. J. 264 (2015) 399–403.
[247] Y. Pang, H. Lei, Chem. Eng. J. 287 (2016) 585–592.
[248] N.N. Mahamuni, Y.G. Adewuyi, Ultrason. Sonochem. 17 (2010) 990–1003.
[249] M.J. Davies, B.C. Gilbert, J.K. Stell, A.C. Whitwood, J. Chem. Soc. Perk. T. 2 (1992) 333–335.
[250] Y. Kirino, T. Ohkuma, T. Kwan, Chem. Pharm. Bull. 29 (1981) 29–34.
[251] P.L. Zamora, F.A. Villamena, J. Phys. Chem. A 116 (2012) 7210–7218.
[252] G.S. Timmins, K.J. Liu, E.J.H. Bechara, Y. Kotake, H.M. Swartz, Free Radical Biol. Med. 27 (1999) 329–333.
[253] J.-L. Clement, B.C. Gilbert, W.F. Ho, N.D. Jackson, M.S. Newton, S. Silvester, G.S. Timmins, P. Tordo, A.C. Whitwood, J. Chem. Soc. Perk. T. 2 (1998) 1715–1718.
[254] G.-D. Fang, D.D. Dionysiou, S.R. Al-Abed, D.-M. Zhou, Appl. Catal. B: Environ. 129 (2013) 325–332.
[255] M. Zalibera, P. Rapta, A. Staško, L. Brindzová, V. Brezová, Free Radical Res. 43 (2009) 457–469.
[256] H. Niehaus, K. Hildenbrand, J. Chem. Soc. Perk. T. 2 (2000) 947–952.
[257] C.D. Jonah, B.S.M. Rao, Radiation Chemistry: Present Status and Future Trends, Elsevier Science, 2001.
[258] R.O.C. Norman, P.M. Storey, P.R. West, J. Chem. Soc. B 108 (1970) 1087–1095.
[259] O.P. Chawla, R.W. Fessenden, J. Phys. Chem. 79 (1975) 2693–2700.
[260] J. Wang, Y. Guo, B. Liu, X. Jin, L. Liu, R. Xu, Y. Kong, B. Wang, Ultrason. Sonochem. 18 (2011) 177–183.
[261] G. Sarifuddin, A. Rajakumar, Curr. Anal. Chem. 8 (2012) 143–149.
[262] C. Tai, J.F. Peng, J.F. Liu, G.B. Jiang, H. Zou, Anal. Chim. Acta 527 (2004) 73–80.
[263] E.J. Rosenfeldt, K.G. Linden, S. Canonica, U. von Gunten, Water Res. 40 (2006) 3695–3704.
[264] P. Westerhoff, H. Moon, D. Minakata, J. Crittenden, Water Res. 43 (2009) 3992–3998.
[265] Y. Pi, J. Schumacher, M. Jekel, Ozone: Sci. Eng. 27 (2005) 431–436.
[266] S.E. Page, W.A. Arnold, K. McNeill, J. Environ. Monit. 12 (2010) 1658–1665.
[267] C. Feng, N. Sugiura, S. Shimada, T. Maekawa, J. Hazard. Mater. 103 (2003) 65–78.
[268] J. Zhang, Y. Nosaka, Appl. Catal. B: Environ. 166–167 (2015) 32–36.
[269] J. Zhang, Y. Nosaka, J. Phys. Chem. C 118 (2014) 10824–10832.
[270] D. Wu, M. Liu, D. Dong, X. Zhou, Microchem. J. 85 (2007) 250–256.
[271] J.-F. Jen, M.-F. Leu, T.C. Yang, J. Chromatogr. A 796 (1998) 283–288.
[272] C. Liang, Z.-S. Wang, C.J. Bruell, Chemosphere 66 (2007) 106–113.
[273] J. Zou, J. Ma, J. Zhang, Environ. Sci. Technol. 48 (2014) 4630–4631.
[274] C. Liang, H.-W. Su, Ind. Eng. Chem. Res. 48 (2009) 5558–5562.
[275] X. He, S.P. Mezyk, I. Michael, D. Fatta-Kassinos, D.D. Dionysiou, J. Hazard. Mater. 279 (2014) 375–383.
[276] A.L. Teel, M. Ahmad, R.J. Watts, J. Hazard. Mater. 196 (2011) 153–159.
[277] X. Gu, S. Lu, X. Guo, J. Sima, Z. Qiu, Q. Sui, RSC Adv. 5 (2015) 60849–60856.
[278] I. Hussain, Y. Zhang, S. Huang, Q. Gao, RSC Adv. 5 (2015) 41079–41087.
[279] A. Ghauch, A.M. Tuqan, Chem. Eng. J. 183 (2012) 162–171.
[280] F. Qi, W. Chu, B. Xu, Appl. Catal. B: Environ. 134–135 (2013) 324–332.
[281] S. Yuan, P. Liao, A.N. Alshawabkeh, Environ. Sci. Technol. 48 (2014) 656–663.
[282] C.L. Clifton, R.E. Huie, Int. J. Chem. Kinet. 21 (1989) 677–687.
[283] X. He, A.A. de la Cruz, K.E. O'Shea, D.D. Dionysiou, Water Res. 63 (2014) 168–178.
[284] T. Zhang, W. Li, J.-P. Croué, Appl. Catal. B: Environ. 121–122 (2012) 88–94.
[285] S. Yuan, P. Liao, Environ. Sci. Technol. 48 (2014) 4632–4633.
[286] U. von Gunten, Water Res. 37 (2003) 1469–1487.
[287] L. Xu, R. Yuan, Y. Guo, D. Xiao, Y. Cao, Z. Wang, J. Liu, Chem. Eng. J. 217 (2013) 169–173.
[288] J. Lu, J. Wu, Y. Ji, D. Kong, Water Res. 78 (2015) 1–8.
[289] X.-Y. Yu, Z.-C. Bao, J.R. Barker, J. Phys. Chem. A 108 (2004) 295–308.
[290] Z. Wang, R. Yuan, Y. Guo, L. Xu, J. Liu, J. Hazard. Mater. 190 (2011) 1083–1087.
[291] R. Yuan, S.N. Ramjaun, Z. Wang, J. Liu, J. Hazard. Mater. 196 (2011) 173–179.
[292] Y. Wang, J. Le Roux, T. Zhang, J.-P. Croué, Environ. Sci. Technol. 48 (2014) 14534–14542.
[293] P. Westerhoff, P. Chao, H. Mash, Water Res. 38 (2004) 1502–1513.
[294] M.L. Bao, O. Griffini, D. Santianni, K. Barbieri, D. Burrini, F. Pantani, Water Res. 33 (1999) 2959–2970.
[295] R. Toor, M. Mohseni, Chemosphere 66 (2007) 2087–2095.
[296] M. Kavanaugh, Z. Chowdhury, Removal of MTBE with Advanced Oxidation Processes, IWA Publishing (International Water Assoc.), 2004.
[297] G.L. Amy, M.S. Siddiqui, A.R. Foundation, Strategies to Control Bromate and Bromide, AWWA Research Foundation and American Water Works Association, 1999.
[298] R. Mertens, C. von Sonntag, J. Photochem. Photobiol. A: Chem. 85 (1995) 1–9.
[299] C. Sonntag, U. von Gunten, Chemistry of Ozone in Water and Wastewater Treatment: From Basic Principles to Applications, IWA Pub., 2012.
[300] S. Liang, T.I. Yun, S.W. Krasner, R.S. Yates, Water Practice Technol. 5 (2010).
[301] Z. Li, Z. Chen, Y. Xiang, L. Ling, J. Fang, C. Shang, D.D. Dionysiou, Water Res. 83 (2015) 132–140.
[302] P.-S. Yap, T.-T. Lim, Appl. Catal. B: Environ. 101 (2011) 709–717.
[303] F. Fu, Z. Cheng, J. Lu, RSC Adv. 5 (2015) 85395–85409.
[304] D.G. Driscoll, J. Carter, J. Williamson, L. Putnam, Hydrology of the Black Hills Area, US Department of the Interior, US Geological Survey, South Dakota, 2002.
[305] R. Haghsheno, A. Mohebbi, H. Hashemipour, A. Sarrafi, J. Hazard. Mater. 166 (2009) 961–966.
[306] S. Tait, W.P. Clarke, J. Keller, D.J. Batstone, Water Res. 43 (2009) 762–772.
[307] E. Genschow, W. Hegemann, C. Maschke, Water Res. 30 (1996) 2072–2078.
[308] A.J. Silva, M.B. Varesche, E. Foresti, M. Zaiat, Process Biochem. 37 (2002) 927–935.
[309] X. Liu, T. Zhang, Y. Shao, CLEAN Soil Air Water 42 (2014) 1370–1375.
[310] P. Wang, A.G. Fane, T.-T. Lim, Chem. Eng. J. 215–216 (2013) 240–251.
[311] P. Wang, T.-T. Lim, Water Res. 46 (2012) 1825–1837.
[312] B. Hofs, J. Ogier, D. Vries, E.F. Beerendonk, E.R. Cornelissen, Sep. Purif. Technol. 79 (2011) 365–374.
[313] Y. Guo, B. Xu, F. Qi, Chem. Eng. J. 287 (2016) 381–389.
[314] B.I. Harman, H. Koseoglu, N.O. Yigit, M. Beyhan, M. Kitis, Desalination 261 (2010) 27–33.
[315] S. Byun, S.H. Davies, A.L. Alpatova, L.M. Corneal, M.J. Baumann, V.V. Tarabara, S.J. Masten, Water Res. 45 (2011) 163–170.
[316] L.M. Corneal, M.J. Baumann, S.J. Masten, S.H.R. Davies, V.V. Tarabara, S. Byun, J. Membr. Sci. 369 (2011) 182–187.
[317] R. Goei, Z. Dong, T.-T. Lim, Chem. Eng. J. 228 (2013) 1030–1039.
[318] R. Goei, T.-T. Lim, Ceram. Int. 40 (2014) 6747–6757.
[319] F. Ghanbari, M. Moradi, F. Gohari, J. Water Process Eng. 9 (2016) 22–28.
[320] C. Luo, J. Ma, J. Jiang, Y. Liu, Y. Song, Y. Yang, Y. Guan, D. Wu, Water Res. 80 (2015) 99–108.
[321] J. Criquet, N.K.V. Leitner, Chemosphere 77 (2009) 194–200.
[322] D. Zhou, L. Chen, C. Zhang, Y. Yu, L. Zhang, F. Wu, Water Res. 57 (2014) 87–95.